The Gravity Field and Crustal Structure of the Main Ethiopian Rift

by

Abera Alemu

A dissertation submitted to the Department of Geodesy
in partial fulfilment of the requirements for
the degree of Doctor of Philosophy in Geodesy

The Royal Institute of Technology
Department of Geodesy
Stockholm, Sweden

January, 1992

Denna serie utges av

Geodetiska institutionen
Kungl Tekniska högskolan
100 44 STOCKHOLM

TRITA-GEOD serien omfattar

1000-serien:	Avhandlingar Forskningsrapporter
2000-serien:	Kurslitteratur, kompendier
3000-serien:	Examensarbeten
4000-serien:	Kongress- och symposierapporter Reserapporter

This series is published by

Department of Geodesy
The Royal Institute of Technology
S-100 44 STOCKHOLM

The TRITA-GEOD series comprises:

The 1000-series:	Dissertations Research reports
The 2000-series:	Lecture notes, compendiums
The 3000-series:	Diploma theses
The 4000-series:	Congress and Symposia reports Travel reports

Abstract

All existing gravity data (1500 taken by the author and 800 reprocessed older data) in the Main Ethiopian Rift and the adjacent plateaus (between latitudes $4^0$45'N and $12^0$00'N) were reduced to Bouguer and free-air values. The resulting values are compiled into 5 mGal and 10 mGal contour interval Bouguer anomaly and free-air anomaly maps respectively. The accuracy of the Bouguer anomaly at each gravity station is estimated to ± 2.9 mGal.

The Bouguer anomaly map reveals that: both the Western and Eastern Plateaus are associated with gravity minima (e.g ≤ -265 mGal near Asasa on the Eastern Plateau and near Fiche on the Western Plateau), and these gravity minima are located in areas of maximum elevation. Within the middle of the rift floor, a trend of gravity maxima (median highs) whose locations generally coincide with the locations of various Quaternary volcanic centers runs parallel to the main escarpments. Between $7^0$30'N and $8^0$45'N, a trend of elongated gravity maxima corresponding to marginal grabens appear to run along the whole length of the west side of the rift floor. Along the rift axis gravity values generally increase north and south of the latitude of Awasa (7^0N). This increase is from -195 mGal in the Awasa district to -65 mGal in the Gewane area when going northwards and to -135 mGal in the Konso area south of Lake Chamo when going southwards along the rift axis. This trend of gravity maxima coincides with the locations of maximum crustal thinning along the youngest structural deformation of the Wonji Fault Belt.

Six profiles were extracted from the Bouguer anomaly map through the major plate tectonic systems (the Western Plateau, the Eastern Plateau, the Main Ethiopian Rift and southern Afar) of interest in the area. Two-dimensional gravity models; i.e. infinite in strike extent, were computed along these profiles. The objective was to obtain models whose gravity effect possessed the same qualitative features and approximately the same anomaly shapes and magnitudes as the observed profiles. The densities used to compute the models were constrained by the results of the deep seismic refraction sounding profiles of the region and the adjacent areas.

The results of these calculations are that: the crust in the plateaus is underlain by a normal mantle. It is 35 to 41 km thick beneath both the Western and the Eastern Plateaus and occurs at the locations of gravity minima in the region surveyed. Within the Main Ethiopian Rift, the crust thins from about 30 km in the south to 23 km in the north. The observed thinning is some 7 to 8 km and is caused by an upward progression of low density mantle material (anomalous mantle) that intrudes itself into the lower crust. The quantity of the anomalous mantle material decreases from north to south beneath the rift. It is about 22 km thick and 150 km wide in the north, whilst in its central and southern parts, it is 15 to 20 km thick over a 100 km wide zone.

To determine the degree to which the crust attained isostatic balance, the following methods were employed.

(i) computation of mass distributions along the seismically controlled 2-D gravity models for 20, 30, 40, 50 and 60 km depth levels;

(ii) compilation of an isostatic Moho-depth map according to the Airy-Heiskanen model of compensation.

The results of these calculations are that: with reference to the mass distributions, the curves show that the crust is isostatically balanced at the 30 km depth level, north of latitude 9^0N. South of this latitude, isostatic equilibrium is first reached between the 40 and 60 km depth levels. Isostatic equilibrium north of latitude 9^0N is achieved through the contribution of the anomalous upper mantle lying at shallow depths. The balance southwards is due mainly to the combined effect of the thicker crust and the normal mantle. As regards the isostatic Moho-depth map, there is a significant correlation between the Bouguer anomaly and the calculated Moho-depth maps. The steep gravity gradient, which marks the transition from the plateau areas to the rift is also reflected in the Moho-depth map. As in the 2-D crustal density models, the Moho-depth map reveals that the crust beneath the rift thins from south to north. The magnitude of the axial positive gravity anomalies observed on the compiled map increase in magnitude north and south of latitude 7^0N.

The compiled gravity maps, isostatic Moho-depth map and Geoid undulation map are found to be sensitive indicators of the tectonic and geologic structures of the region.

A two dimensional correlation analysis made between the different parameters considered in this study (Bouguer anomaly, free-air anomaly, elevation and Moho-depth) shows that there are significant correlations between some of them.

ACKNOWLEDGEMENTS

This research is financed by the Swedish Agency for Research and Educational Cooperation with Developing Countries (SAREC) and the Addis Ababa University (AAU) under the authority of agreements between the Swedish and Ethiopian governments. This work is part of the joint project between the Royal Institute of Technology, Department of Geodesy and the Geophysical Observatory of AAU under the Project **Geodesy and Gravimetry in the Ethiopian Rift**, to whom I am grateful for the research grant.

I am indebted to my supervisor **Prof. Dr. Lars E. Sjöberg** for his concern, encouragement, advice and proper guidance through out the progress of this research including his field trips to Ethiopia. I am also grateful to **Dr. Laike M. Asfaw**, Project leader, for his encouragement in the research work and for his academic advice.

I gratefully acknowledge all those members of the Geophysical Observatory of Addis Ababa University, The Ethiopian Mapping Authority and the Geothermal Division of the Geological Survey of Ethiopia for their invaluable assistance during the field work. Here I want to thank all members of the Department of Geodesy, KTH for their kindness and generous assistance which made my study profitable. Special thanks go to **Dr. Huaan Fan**, for his friendly and invaluable assistance in computing the gravimetric geoid undulations and for critically reading the manuscripts and giving valuable comments for improvement, and **Thomas Nord** and **Erick Asenjo** for their valuable technical help. I am also grateful to **Dr. Herbert Henkel** for his stimulating discussions and valuable comments in the compilation and interpretation of the gravity maps.

I owe my sincere thanks to those who, either close or at distance were concerned about me and my work particularly **Prof. Gunnar Jacks** and his family. Thanks are also due to my wife Birke Yami who helped to prepare the maps and figures and organize the notes. Without her support this thesis couldn't have come to a conclusion. I thank my parents and all other family members for their encouragement and continuous support. Last but not least I thank my little daughter Fitsum Abera for her patience to stay alone without my treatment.

TABLE OF CONTENTS

LIST OF FIGURES

List of tables

Chapter 1.

Introduction

The East African continental rift system (Cenozoic) comprises a series of rift zones (Rosendahl et al., 1986) and extends for some 3200 km from the Afar triple junction at the Red Sea - Gulf of Aden intersection to the Zambezi River in Mozambique (Fig. 1). It is normally considered to be a continental extension of the global ocean rift-ridge system (Baker and Wolhenberg, 1971; McKenzie et al., 1970) being associated with a zone of shallow seismicity continuous with the Gulf of Aden and the Carlsberg ridge. The length and width of this feature are visible, and the depth of disruption to the lithosphere and asthenosphere is estimated to be at least 100 km (Brown and Girdler, 1980).

The physiographic character of the system varies considerably along its length. Its northern end is a triple junction with two oceanic ridges: the Red Sea and the Gulf of Aden. This junction occurs in Afar (Fig. 1) which, like Iceland, is one of two regions on earth where the rocks of the present day ocean rifts are exposed above sea level (i.e tectonic and magmatic processes common in oceanic ridges can be observed at the surface within it). Further south, the Main Ethiopian Rift (MER) transects the Ethiopian dome, separating the Ethiopian Plateau (Western Plateau) to the West from the Somali Plateau (Eastern Plateau) in the east. In the vicinity of Lake Victoria this rift system bifurcates resulting in the formation of the Eastern Rift and the Western Rift of the East African Rift system. Both rifts are characterized by continuous belts of normal faulting and graben structures and the occurrence of shallow earthquakes (Maasha and Molnar, 1972). They differ from each other in important ways. The Eastern rift is associated with abundant volcanism and shallow earthquakes and is often assumed to be an extension of the ocean ridge system - Carlsberg ridge (Ewing and Heezen, 1956) whereas much of the Western Rift appears to be older and is often assumed to be unrelated to the ocean ridge system (McConnel, 1967). The Malawi Rift to the south has much in common with the western branch and is often considered to be an extension of it (Rosendahl et al., 1986).

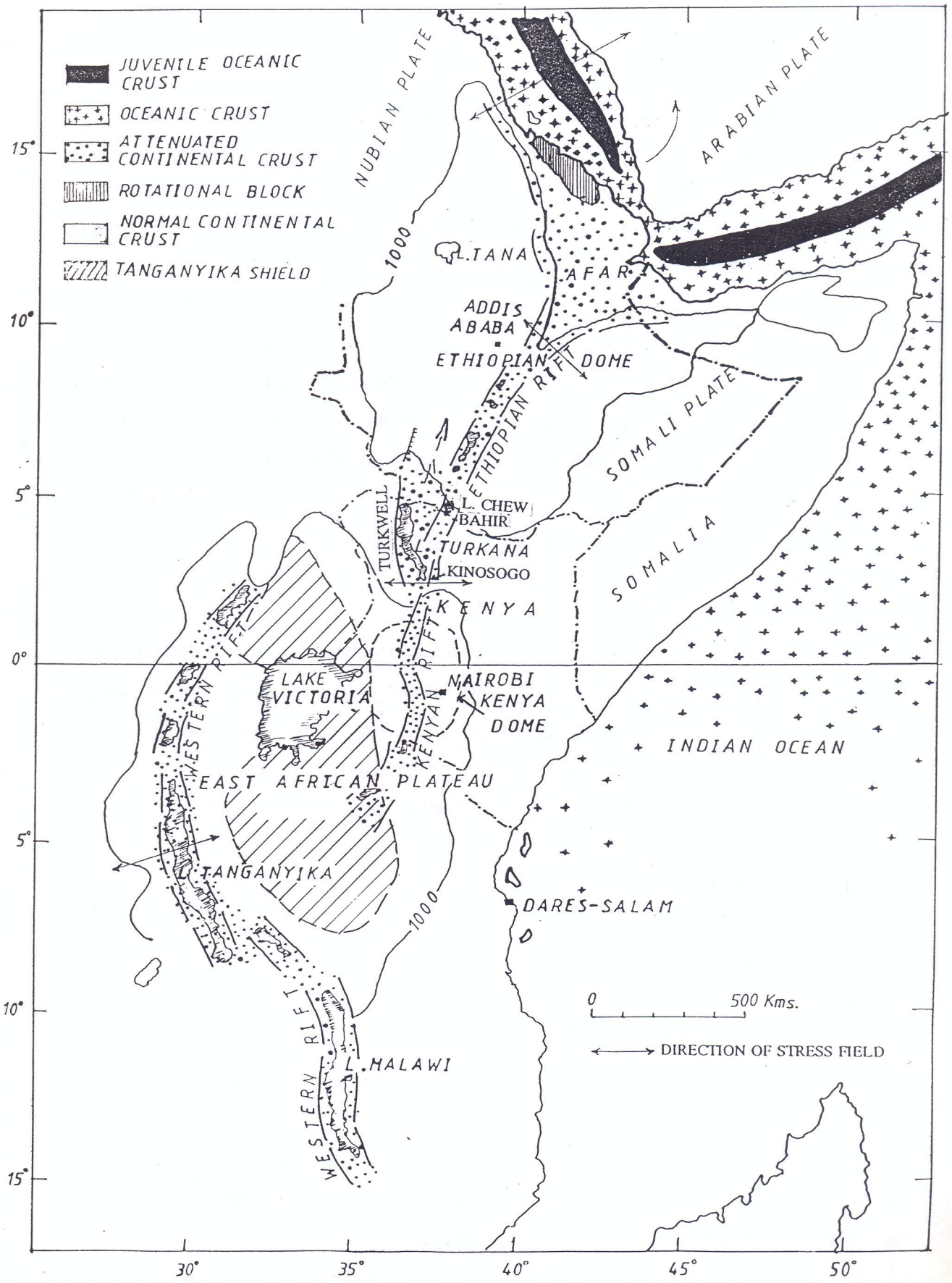

Figure 1: Regional tectonic model of the east African rift system, showing regions underlain by normal continental crust (i.e the Nubian, Arabian and the Somali plates), those underlain by attenuated continental crust (i.e the Afar depression, the Ethiopian and Kenyan sections of the East African Rift and its western arm); and finally those underlain by Juvenile or pure Oceanic crust (i.e the Red sea trough, Gulf of Aden, the Somali Basin in the Indian ocean). This is the only large scale continental rift system to have a direct connection, through the Gulf of Aden, to the oceanic rift system.

The term Ethiopian Rift is here used to designate the triangular Afar depression and the NNE striking MER (Fig. 2). The Main Ethiopian Rift (MER) extends for about 650 km from the Lake Chamo region in the south ($4^0$45'N) to the region of Ayelu Volcano in the north ($9^0$45'N) beyond which its NNE trending structures are replaced by the NNW trending structures of the Afar Depression (Wolde, 1989).

This thesis is based on the results of about 2300 gravity observations made on the floor and shoulders of the MER within 150,000 km^2 study area between latitudes $4^0$45'N and $11^0$10' N. In addition to the gravity field other studies considered in this work include the interpretation of the isostatic Moho depth and geoid undulation maps constructed for the same region. The study could indicate the locality and the scale of ongoing tectonic activities and the character and orientation of faults in the region. These parameters provide important constraints to construct rift models.

No detailed geophysical study of the subsurface of the Main Ethiopian Rift has yet been undertaken on a regional scale. Earlier gravity investigations made by Alemu, 1983, 1988; Alemu and Sjöberg, 1990; Gouin and Mohr, 1964; Searle and Gouin, 1972; Hunegnaw, 1989; Oluma, 1989 and the Ethiopian Institute of Geological Survey in the Main Ethiopian Rift were confined to local areas and are of limited regional significance.

The objectives of this study are thus:

1. To fill the gap in the regional gravity coverage between the Kenyan Rift and the Afar Depression.

2. To present reliable gravity data which will form a sound basis for further investigation of the rift system.

3. To investigate the nature of the gravity anomalies associated with the rift system and the adjacent uplifted regions bordering the MER.

4. To define the locations and magnitudes of the observed positive and negative Bouguer anomalies.

5. To investigate the continuity of the axial positive anomaly in the MER, previously mapped by Searle (1970) in the Kenyan Rift and by Makris (1975) in the northern part of the MER and the Afar Depression.

6. To generate crustal models that produce the gravity anomalies matching the observed gravity data as well as major geological and tectonic features of the region.

7. To compare the gravity results with other geophysical and geological investigations carried out to study the rift system.

Chapter 2

Geographical, Geological and Geophysical Review

2.1 The Main Geographical Features of Ethiopia

Ethiopia is situated in the horn of Africa between $3^0$24'N and 18^0N latitude, 33^0E and 48^0E longitude. It is roughly a triangular area, occupying about 1,235,000 km^2 of land. Its apex in the north reaches the Red Sea at Ras Kassar and its base rests on the borders of Kenya and Somalia. In the east, it is bounded by the Red Sea, Djibouti and Somalia and in the west by the Sudan. It is a mountainous country with tormented relief, separated by deep gorges and tectonic depressions.

The country has an elevated central plateau varying in height between 2000 and 3000 meters above sea level and constitutes the water source for East Africa; it is on the high Ethiopian Plateau that several of the largest affluents of the Nile have their source, in particular the Blue Nile. This central plateau is bisected by a 1000 km long rift system that runs in a predominantly north and northeast direction from the Kenyan border to the Red Sea shore.

The rift system divides the country into two major blocks - the Ethiopian Plateau (Western Plateau) to the west and the Somali Plateau (Eastern Plateau) to the east. The Western Plateau shows a very gentle decline westwards towards the prominent escarpment overlooking the Sudan plains. It is interspaced with huge Miocene volcanic ranges and cratered cones that decline from north to south and lying above the general plateau level; the high peaks are north of the Blue Nile (e.g Ras Dashn rises to 4550m). The Plateau is also split into individual regions by deep river valleys (e.g the Abay gorge), regions which are historic provinces, each with a relatively independent history (eg. Shoa, Gojam,...etc). The Eastern Plateau has an average elevation between 1200m and 2000m and drops gradually from south to north. It has a steeper surface tilt towards SSE than the Western Plateau resulting in a south-south easterly drainage pattern.

The highest summits of all its volcanic massifs except the ENE-WSW elongated Batu volcanic massif (4307m), which rises up within the plateau are totally confined to the crest overlooking the rift system, the highest being Kaka (4190m). In general, Half of the country's land surface rises above 1200m, more than a quarter above 1800m and about 5% reaches heights of 3500m above Sea Level.

Among the lowland regions of Ethiopia, the rift zone (Main Ethiopian Rift and Afar Depression) constitutes the most important unit (Figs. 1&2). Its southern sector abounds in lakes. To the northeast, the Afar Depression, opens in a funnel-like fashion. The floor of the rift rises about 600m from north to south, reaching a maximum elevation of 1800m south east of Addis Ababa in the Meki watershed. A combination of tectonic movements and volcanism, as well as other geologic factors are responsible for the main topographic features and drainage patterns of Ethiopia. A brief account of the geological and tectonic developments of the Main Ethiopian Rift are given in the following sections.

2.2 Physiography and Geological Structure of the Main Ethiopian Rift

The investigated region covers a 150,000 km^2 area of the Main Ethiopian Rift (MER) and its shoulders. Elevations vary from 800 meters up to heights greater than 4100 meters at the Chilalo volcano summit. In general, the area is characterized by well defined NNE-SSW structural blocks or units.

A fairly detailed summary of the geology of an area is regarded as a necessary background for a gravity interpretation and discussion. Hence, a brief discussion of the surface geology and fault structure determined from surface observations carried out in the Main Ethiopian Rift are presented.

Since the initial work of Mohr (1960), the geological history of this region has been documented by several authors (Mohr, 1960, 1962 a&b, 1967, 1972 and 1983; DI Paola, 1972; Lloyd, 1977; Baker et al., 1972). All the geological and structural descriptions that will be considered here as relevant to this study are summarized from these previous studies.

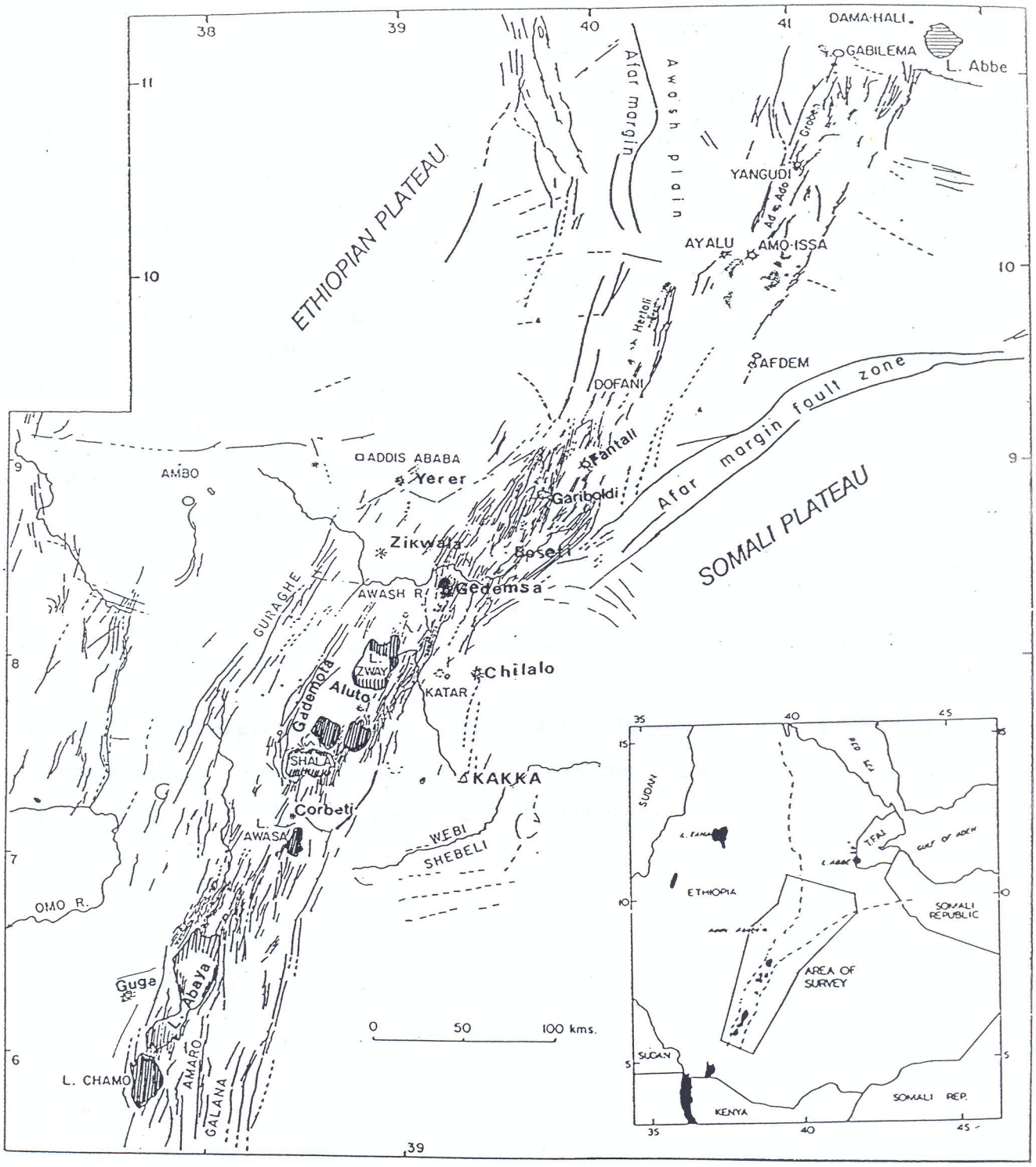

Figure 2: Structural subdivision of the Main Ethiopian Rift with major faults and Pliocene - Quaternary Volcanoes. The major marginal faults of the rift valley are shown with thicker trace. Inset shows the location of the survey area (modified from Mohr, 1976).

The development of the Main Ethiopian Rift (MER) is accepted to be due to the drifting apart of the Western Plateau to the west and the Eastern Plateau to the east through tensional normal faulting. In plan view, the structure of the MER (Fig.2) curves all along its length (i.e has a gently curvilinear plan, convex to the west) and widens out at its northern end to become identified with south western Afar beyond which its NNE trending structures are replaced by the NNW trending structures of the Afar Depression. This shape is not achieved by curvature of the main bounding faults, but rather by changes in direction of the fault trends and lineaments that are themselves essentially linear. At its southern end (4^0 45'N), crustal extensions are transposed west into the Turkana Rift (Fig.1) from which there begins a southward continuation of the Kenyan Rift (Mohr & Wood,1976).

The Turkana Rift extends north up to the lower Omo Valley. It is a tectonic depression where Precambrian rocks are locally exposed in its floor (Fig.3) and extends into the western flank of the Main Ethiopian Rift.

The Main Ethiopian Rift begins at about latitude $4^0$45'N, where the Amaro Horst separates the Lake Chamo Rift on the west from the Galana Rift to the east (Fig.2). The Amaro Horst, which is bounded by rejuvenated faults to the east, declines abruptly at its northern end, where the rift widens to about 60 km. Five large rift lakes of tectonic or volcano-tectonic origin (Ziway, Langano, Abiata, Shala and Awasa) occupy the central part of the Main Ethiopian Rift. West of the rift lakes, major faults appear, which trend to the typical NNE-NE rift direction. Between 8^0 and $8^0$30'N, the Guraghe escarpment which is 35 km long with a vertical displacement exceeding 1500m (Di Paola and Berhe, 1979), forms the western margin of the rift.

The eastern escarpment has a vertical throw between 500m and 1000m relative to the rift floor. East of Lake Awasa, a strongly denuded older fault scarp shows a late Miocene-Pliocene downwarping of the Eastern plateau into the rift. Further north, the eastern escarpment is strongly upwarped riftwards in the chain of the rift lakes (Lake Ziway and Lake Langano). This strongly stepped escarpment is formed by a complex of NNW and NNE trending Pleistocene faults. At about latitude $7^0$30'N (in the vicinity of Lakes Shalla,

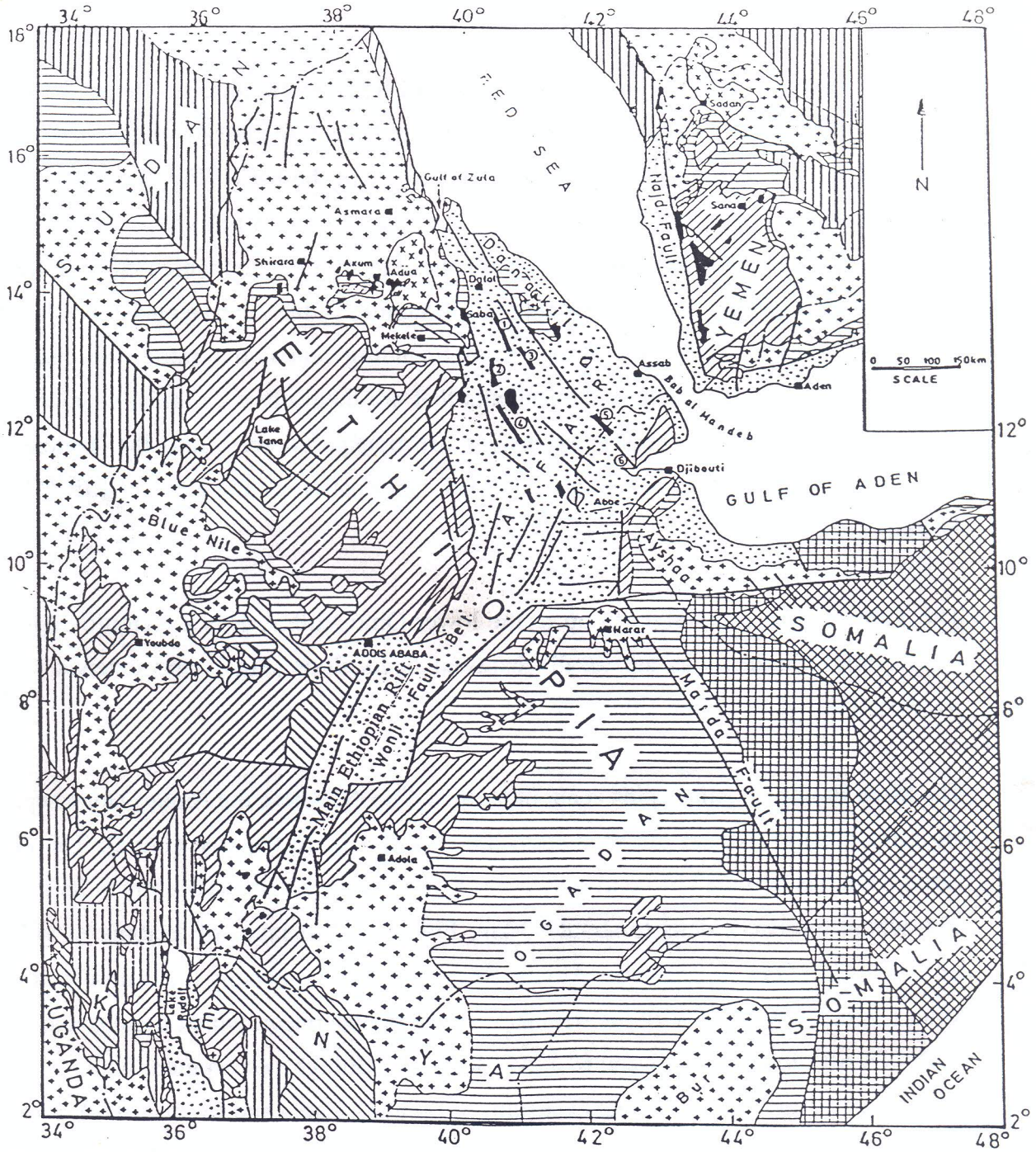

Figure 3: Geologic map of Ethiopia (Beyth, 1986).

Abiyata and Langano), these faults coincide with part of a huge craterlike feature (Fig. 2). Relative to the general trend of the Main Ethiopian Rift changes in structural orientation are observed north of Lake Ziway as compared to its southern and central parts. These are the eastward displacement of the eastern escarpment at latitude $8^0$12'N (Kazmin and Berhe, 1978) and westward displacement of the western escarpment at latitude 9^0N. The westward displacement of the western escarpment is related to the latitudinal Yerer fault (Mohr, 1966a).

Extensive basaltic plateau volcanism began in the early Miocene in Ethiopia and extended to the Turkana Rift. The first major stage of rifting was initiated somewhat later, during the mid-Miocene in Ethiopia and the early Pliocene in Kenya. This faulting was accompanied by renewed volcanism (rhyolite and trachyte volcanism) becoming more centrally located along the axes of rifting.

Major domal uplift occurred in the late Pliocene and Quaternary accompanied by the formation of deep grabens and further alkaline volcanism. The Main Ethiopian Rift is centrally located on the crest of the broad uplift of the Ethiopian dome, between the Western and Eastern Plateaus. By the Pleistocene the protorift was a topographically shallow trough (Baker & Mitchell,1976) with deep infilling of silicic volcanics erupted from volcanic centers close to the rift margins. Mohr (1966b) suggests that the marginal faults are Pleistocene in age and that the separation of the Western Plateau to the west and the Eastern Plateau to the east occurred at this time. Fragmentation of the rift floor formed the youngest structural deformation, largely concentrated within a narrow, 5-12 km wide belt of normal faults, known as the Wonji Fault Belt (Mohr et al., 1980; LIoyd,1977).

The Wonji Fault Belt (WFB) maintains a NNE orientation along the entire length of the MER and has been forced into en-echelon offsets in order to remain within the rift margin envelope (Mohr, 1980). This belt is regarded as a manifestation of incipient spreading center. In Afar such structures are designated as axial ranges. The Bouguer gravity map compiled under this study shows that the WFB is associated with a trend of gravity maxima all along its length.

The displacement lines of this fault belt are sites of maximum shallow crustal heating; this can be deduced from the present geothermal activity, the associated observed positive gravity anomalies and the quantities of volcanic products and their compositions.

2.3 Rocks flooring the rift

The tops of the rift scarps are at places exposed by trap basalts of lower Miocene age (Fig. 3). These trap basalts are supposed to underlie rhyolites, trachytes, ignimbrites, agglomerates, and basalts of the upper Miocene and younger ages in the rift floor.

A notable feature of the MER is the occurrence of young volcanic centers nearly all along its length. Volcanism in the MER is of upper Miocene to Holocene age (Mohr 1960, 1966a, 1966b ; Lloyd 1977). Rhyolite volcanism is associated with the axial zone of the rift particularly with the silicic volcanic centers of the WFB (Corbetti volcanic center, Shalla Caldera, Gademota Caldera, and Aluto volcanic center, Gademsa Caldera, etc.) (Fig.2). The rift floor is partially infilled with lacustrine sediments derived from Quaternary volcanic rocks of Pleistocene and Holocene age (Fig.3).

Contemporaneous with the volcanism the infill consists of intercalations of silt stone, clay stone, pumices, etc. Ephemeral (short-lived) lakes have also occupied the central part of the MER since the earliest stages of its development and these lakes contributed sediment to the rift floor.

Considering this complex frame of geologic and tectonic features, the gravity measurements were projected in order to obtain new structural information by the measured gravity field based on a fair distribution of gravity stations.

2.4 Structure and Geology of the Eastern Rift of East Africa.

The Eastern Rift of East Africa traverses Ethiopia and Kenya and extends to northern Tanzania. In north Tanzania, a belt of widely spaced faults of Neogene age extends

southwest to link the southern section of the Eastern Rift with the Western Rift (Fig.1). The Eastern Rift consists of normal grabens, asymmetric grabens and monoclinically flexed depressions. These depressions separate the East Kenya-Somalia crustal block from the remainder of Africa. The Eastern Rift may be divided into the following main segments:

(1) The North Tanzania divergence

(2) The Kenyan Rift

(3) The Turkana Depression

(4) The Main Ethiopian Rift

(5) The Afar Depression

2.4.1 The North Tanzania divergence

The transition from the southern part of the Kenyan dome to the less high inner-plateau of northern Tanzania occurs between latitudes 2^0 and 3^0S. It is marked by the absence of the main fault patterns of the Eastern Rift and the splitting of its western ones (Fig.1).

2.4.2 The Kenyan Rift.

The Kenyan Rift is a complex graben bisecting the Kenya dome. It extends from the Natron-Magadi basin in the south to Lake Turkana in the north (Fig. 1). The adjacent plateaus stand at heights of 1600 to 3200m (neglecting high volcanic cones). The rift floor descends from 2000m in the central part to 650m in the south. The main fault scarps range from 300 to 1600m in height. They are en-echelon in plan and form a complex graben 60 to 70 km wide. The eastern side of the graben is stepped, producing step-fault platforms. These marginal structures reduce the width of the inner graben floor to between 17 and

35 km. The fault fractures are normal and rarely exposed. Escarpment heights and measurable displacements of stratigraphic units indicate minimum fault throws of 1600 to 2200m on the west side of the rift, and about 1000m on the east side. The volcanic succession along its flanks is over 2000m thick, and is thicker within the rift floor.

The graben floor and the step-fault platforms are composed of Plio-Pleistocene volcanics, which are cut by swarms of closely spaced young faults. The faults of the rift floor are locally obscured by late quaternary volcanic plies (McCall, 1968), while the depressions are partly filled by lower and middle Pleistocene sediments (McCall et al., 1967).

2.4.3 The Turkana Depression.

The Kenya Rift gradually widens north of latitude 1^0N, where its structure resembles that in northern Tanzania. The axial graben extends north to the southern part of Lake Turkana (Fig. 1). The rift here is about 20 km wide, with escarpments rarely exceeding 400m in height (Dodson, 1963). Its northern continuation is the Kinu Sogo Fault belt east of Lake Turkana. At north end of this belt a distinct graben is again developed on the Ethiopian border and is occupied by Lake Chew Bahir. The remainder of the Turkana depression is a triangular lowland, 300 to 1000m in elevation. It is bordered on the west by the Turkwell and Uganda escarpments.

The Turkwell escarpment is the highest, oldest and most dissected of the rift fault escarpments in Kenya. Development of the Turkwell and the Uganda escarpment is thought to have stated during the early Miocene. It formed a depression over much of the Turkana within which the Miocene basalts were erupted. In early Pliocene times, major faults cut the floor of the Turkana Depression. The rapture divided the depression into west-tilted blocks, thus extending the Turkwell fault southwards.

The Turkana depression is thus a triangular lowland between the Kenyan and Ethiopian domal uplifts. It is 200 km wide in the north and narrows southwards. Its margins become more strongly faulted until it merges into the Kenyan Rift.

Chapter 3

Seismic Refraction Experiments in the Region.

The seismic refraction experiments carried out in the rift zone of the Eastern Rift of the East African Rift system so far are shown in Fig.4. These include the deep seismic sounding (DSS) experiments of Berckhemer et al. (1975) in Ethiopia, the deep seismic sounding experiments of Lepine et al. (1972) and Ruegg (1975) in the Djibouti republic and the Kenyan Rift International Seismic Project (KRISP) experiments of Griffiths et al. (1972) Khan et al. (1987).

The experiments were carried out mainly to test the hypothesis of crustal thinning by investigating the crustal structure of the rift system and the adjacent plateaus.

Unfortunately, there is no refraction seismic experiment performed in the region of the Main Ethiopian Rift between latitudes 4^0 and 8^0N. The results of seismic refraction experiments in the northern sector of the MER and those of the Kenyan rift were used to constrain the crustal density models computed for the region of the MER between 4^0N and 8^0N.

3.1 Deep Seismic Sounding Experiment in the Afar Depression and the Western Plateau

In March 1972 the crustal structure underlying the Afar Depression and the Ethiopian Plateau was investigated by a (DSS) experiment (Berckhemer et al., 1975). The experiment consisted of five seismic profiles (120-300 km long) along the main trends of crustal thinning in Afar and one profile on the Western Plateau west of Addis Ababa (Fig.5) in order to compare the results within the northern part of MER and the Afar areas with that of the unattenuated continental crust of the Western Plateau. A brief description of the individual seismic profiles relevant to this study is presented below. The

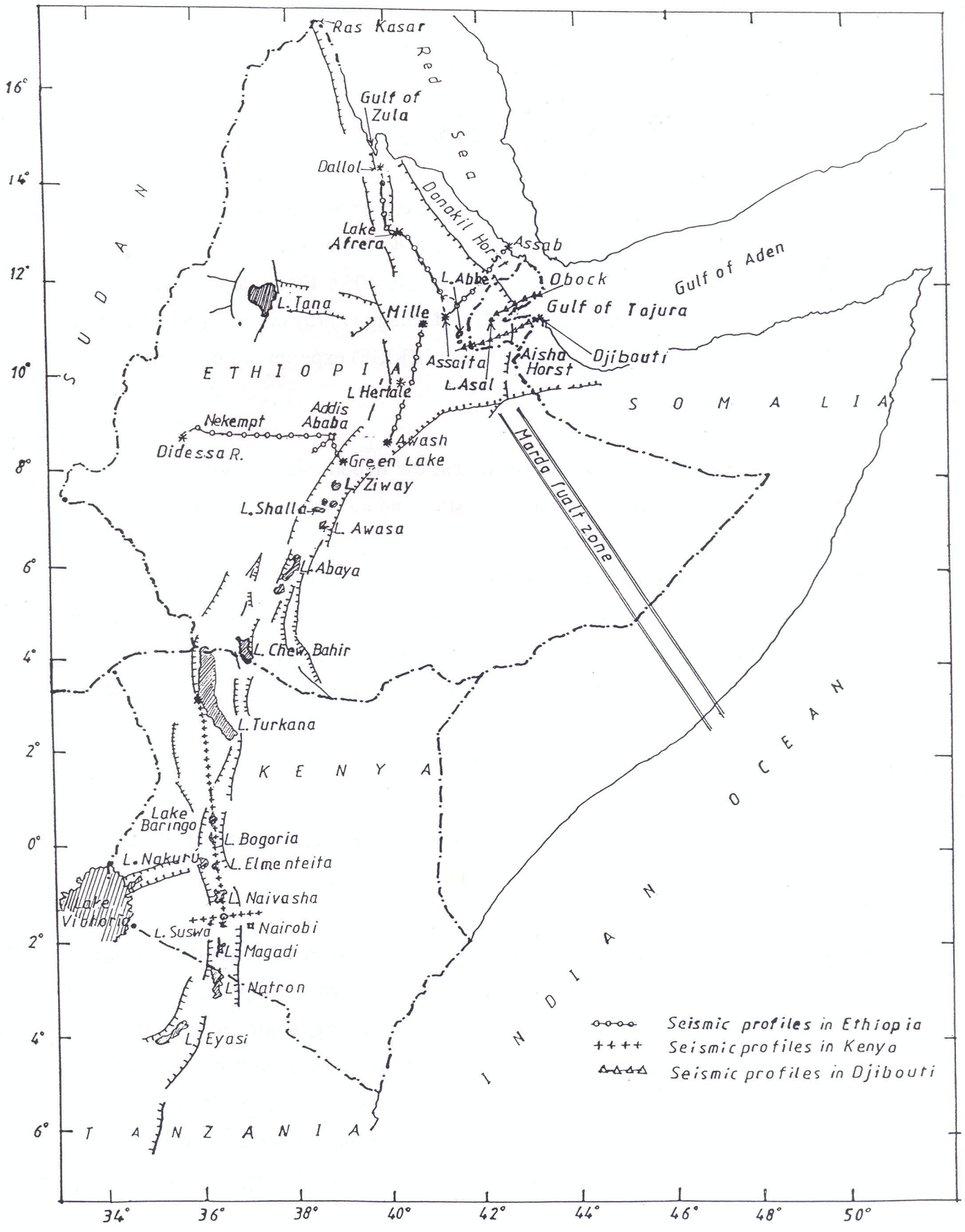

Figure 4: Location map of the seismic refraction profiles in Ethiopia, Kenya and the Djibouti republic.

evaluation discussed is presented in Makris and Ginzburg (1987). The data and models for the individual shot-points are reproduced here.

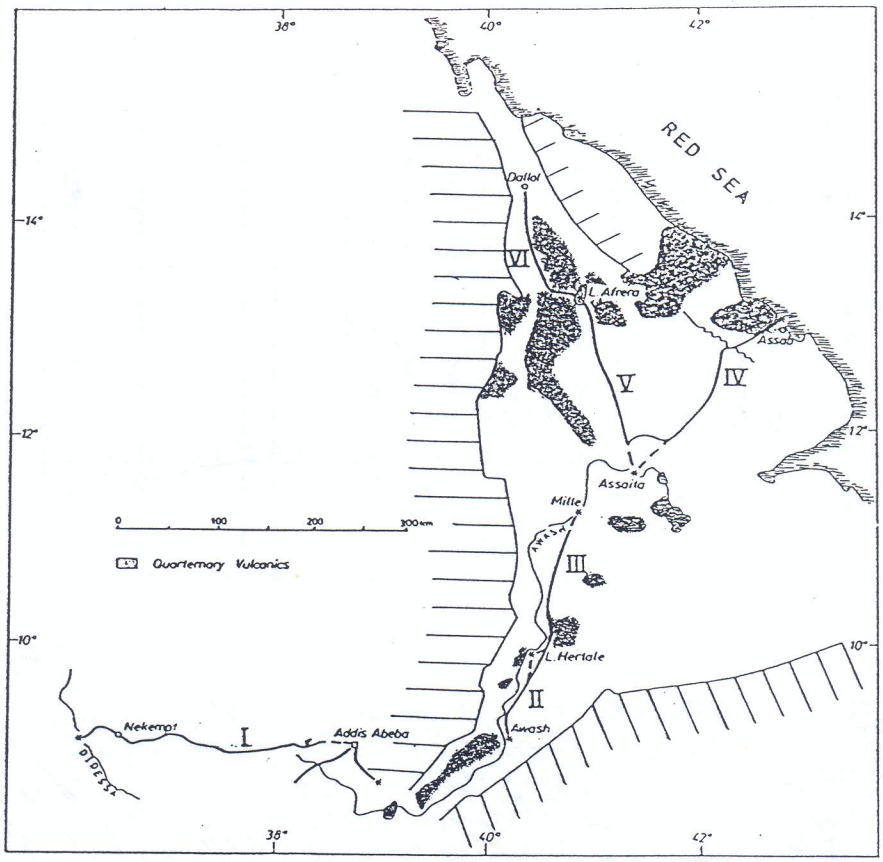

Figure 5: Location of the seismic refraction profiles on the Western Ethiopian plateau, the northern part of the Main Ethiopian Rift and the Afar depression (from Berckhemer, et al. 1975)

3.1.1 Profile I: Didessa - Green Lake (Debrezeit)

This is an east-west reversed profile extending from 36^0E - 39^0E along the latitude of Addis Ababa (9^0N) on the Western Plateau (Fig.6). The velocity sequence obtained along this profile was 3.75 Km/sec, corresponding to the basalt and sedimentary cover, 6.10 Km/sec for the upper crust 6.65 Km/sec for the lower crust and 8.00 Km/sec for the normal mantle. The basalt and sediments are a maximum of 2.5 Km thick from west to east. There is an upper and lower crustal thickening towards the east. The upper crust

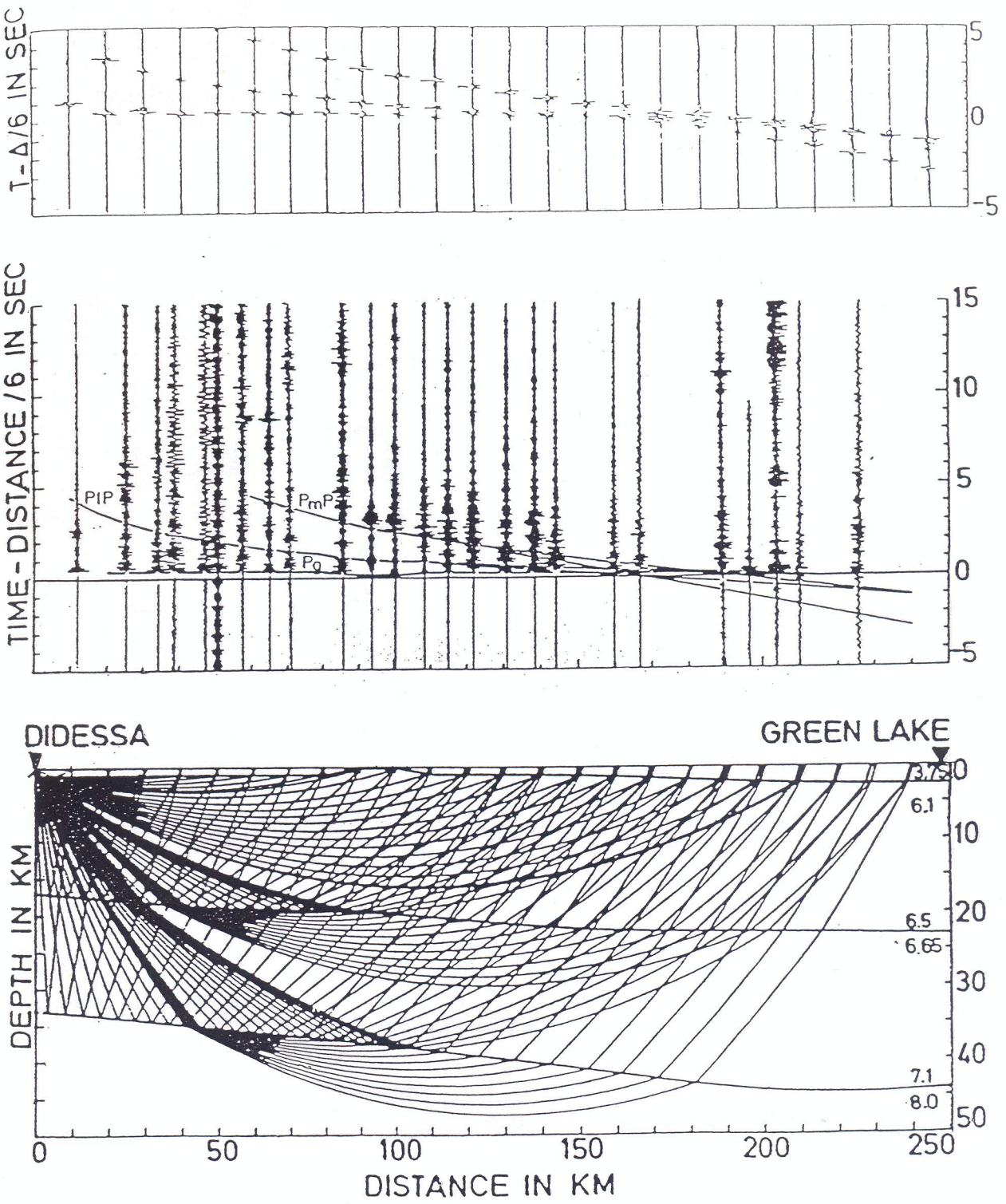

Figure 6: Proposed velocity - depth structure, record section and synthetic seismogram of profile 1, located on the western plateau. Velocities shown are in km/sec. This profile was measured in order to compare results within the Afar depression with that of unattenuated continental crust of the western plateau. The profile is reversed with shots at Didesa and Green lake. The top layer is composed of sediments and basalts (Makris, J. and Ginzburg, A., 1987).

reaches a maximum thickness of 23 km; while the depth to the normal mantle increases from 33 to 44 km which indicates that there is an eastward thickening of the upper crust. The model obtained suggests a normal continental crust, with a thinning towards the Western Plateau.

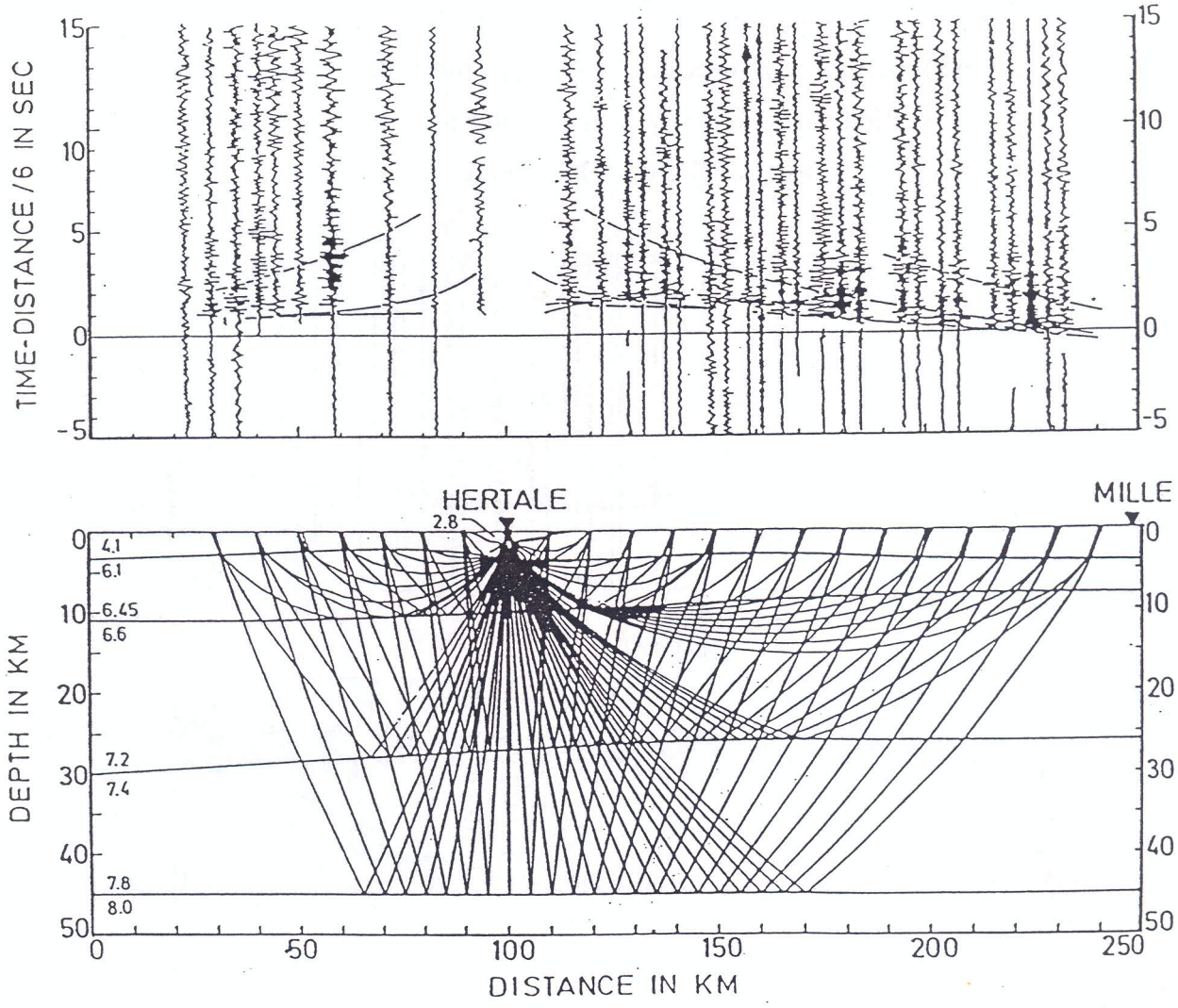

Figure 7: Velocity depth structure and record section of profiles 2 and 3: Shot point Hertale (Makris, J. and Ginzberg, A., 1987).

3.1.2 Profile II and III: Mille - Hertale - Awash

This profile is reversed and extends in a SSW direction from the south-eastern corner of the Afar Depression ($11^0 25'$N) down to the Main Ethiopian Rift to about the latitude of

Addis Ababa (9^0N). The data and models for the Mille and Hertale shot-points are reproduced here (Figs.7 & 8). The velocity sequence obtained along this profile is 2.80 Km/sec (for the Pleistocene sediments in Lake Hertale), 4.10 Km/sec (basalts), 6.10 Km/sec (upper crust), 6.70 Km/sec (lower crust) and a very low P_n velocity of 7.40 Km/sec corresponding to an anomalous mantle. The upper crust along this profile abnormally thins from 11 km in the south to 7 km in the north. Correspondingly, the seismic Moho depth along this profile changes from 30 Km in the south to 26 km in the north. A strong reflection can be seen at the end of the Mille record and at the end of the Hertale record section. This event was interpreted as a reflection from the top of the normal mantle (8.00 Km/sec) at about 45 km depth.

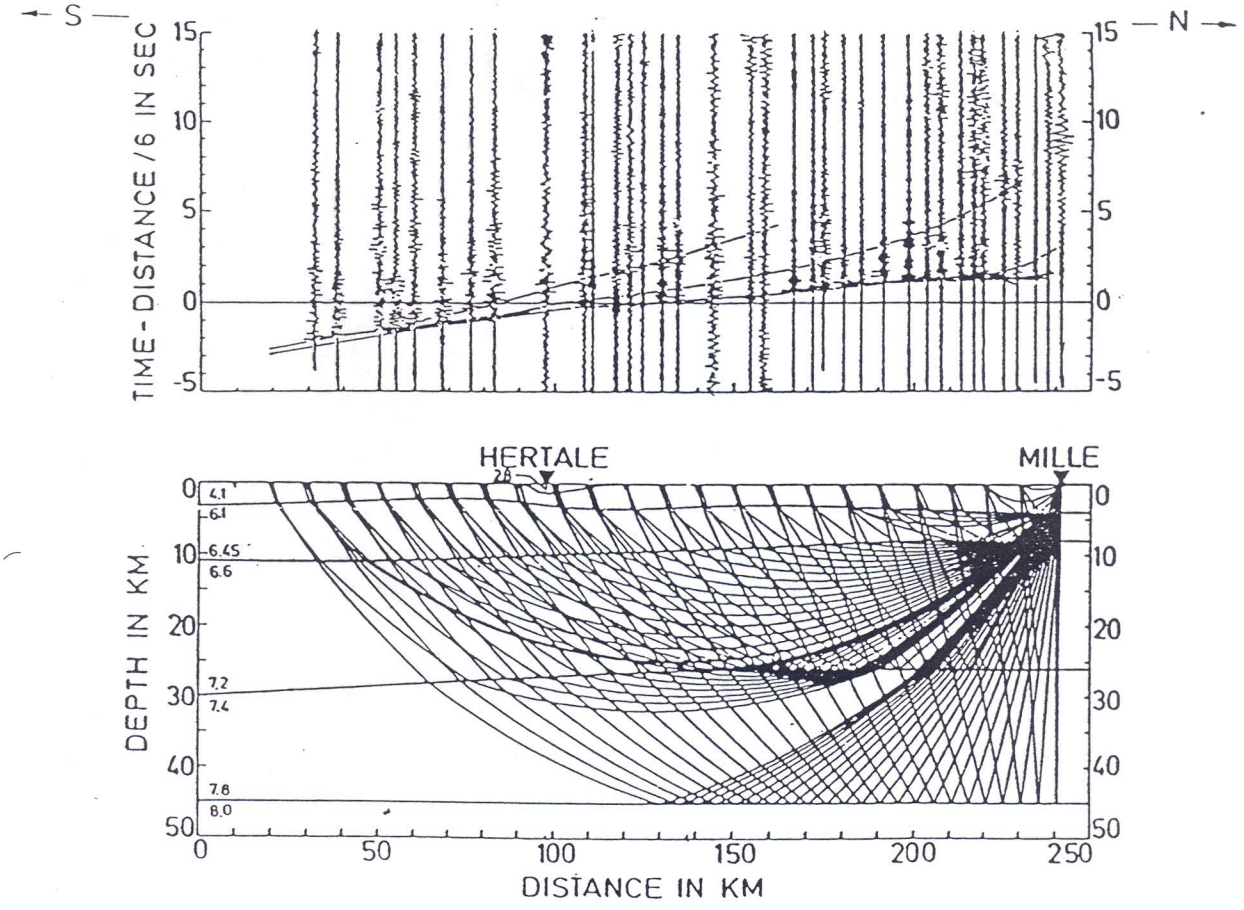

Figure 8: Velocity - depth structure and record station of profiles 2 and 3. Shot point Mille. This reversed profile is located in the south eastern corner of the Afar depression. Fig. 7a and b are the model and record sections of the Mille and Hertale shot- points respectively. The 2.8km/sec velocity layer at lake Hertale corresponds to the Pleistocene sediments in this area. The strong reflection observable at the ends of the Mille and Hertale record sections was interpreted as a reflection from the top of the normal mantle (velocity: 8.00 km/sec) at a depth of about 45 km (Makris, J. and Ginzburg, A., 1987).

3.1.3 Profile IV (Assaita - Assab)

This profile runs from Assaita towards the Red Sea. It can be considered to form a continuation of the Djibouti seismic profiles towards central Afar. At the south-western end of the profile (corresponding to the Tendaho Cotton Plantation Area), a 2.5 km thick layer of young sediments with a velocity of 2.20 km/s overlies the basalt cover and wedges out to the north-east. The top of the crystalline basement (upper crust) with a velocity of 6.20 km/s shows strong relief. This layer is 11 km thick (Fig.9). The lower crust has a velocity of 6.60 km/s; its upper boundary produces an excellent PiP reflection, while its lower boundary is at a depth of 26 to 23 km. The anomalous mantle has a velocity of 7.50 km/s. The total crustal thickness decreases gradually towards the Red Sea. The record section also shows a good later reflection coming from below the anomalous mantle. This reflection is thought to probably represent the top of the 8.00 km/s velocity discontinuity in the lithosphere, which is estimated to occur at a depth of 35 km. This is similar in depth to other reflectors found in other locations of the Red Sea (30 to 40 km), Makris et al. (1985).

3.1.4 Profile V and VI (Assaita - Lake Afrera - Dallol)

Profiles V and VI run in approximately N-S direction, starting at the central part of the Afar Depression and ending at the salt domes of Dallol. They show the most dramatic changes in crustal structure. A 3.95 km/s velocity sedimentary cover occurs near Assaita and disappears to the north. Near Dallol another thick accumulation of low velocity (3.35 km/s) material, which represents sediments and evaporites (Behle et al., 1975), overlies the basalt series (4.50 km/s). A thin 6.10 km/s velocity upper crust underlies this layer, whose thickness is determined to be only about 6 km (Fig. 10).

The upper lower crust boundary is at a depth of 10 km in the south and about 5 km in the north. The lower crust-anomalous mantle boundary shows remarkable depth variations. The anomalous mantle (7.40 km/s) is located at a depth of about 26 km in the southern

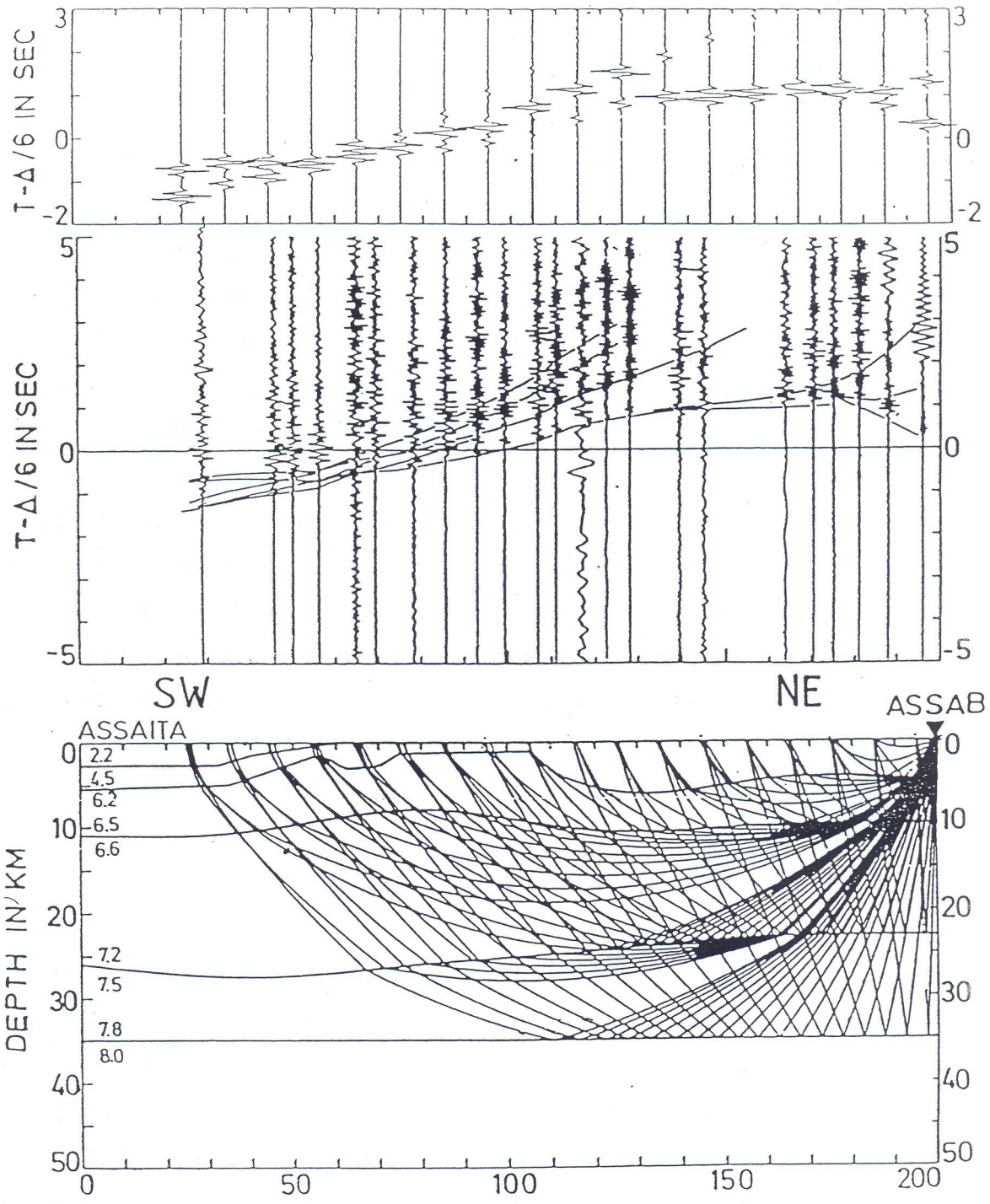

Figure 9: Model, record section and synthetic seismogram of profile 4. The profile runs from central Afar towards the Red Sea. The top of the crystalline basement shows strong relief. The upper boundary of the lower crust produces excellent PIP reflections. In the record, a good later reflection coming from below the anomalous mantle, similar to the reflections noted in profiles 2 and 3 is present. This probably corresponds to the top of the 8.00 km/s velocity discontinuity in the lithosphere estimated at the depth of 35kms. It is similar to other reflectors found in other locations of the Red Sea at the depths of 30 to 40kms (Makris et al, 1985, Makris, J.; Ginzberg, A,; 1987).

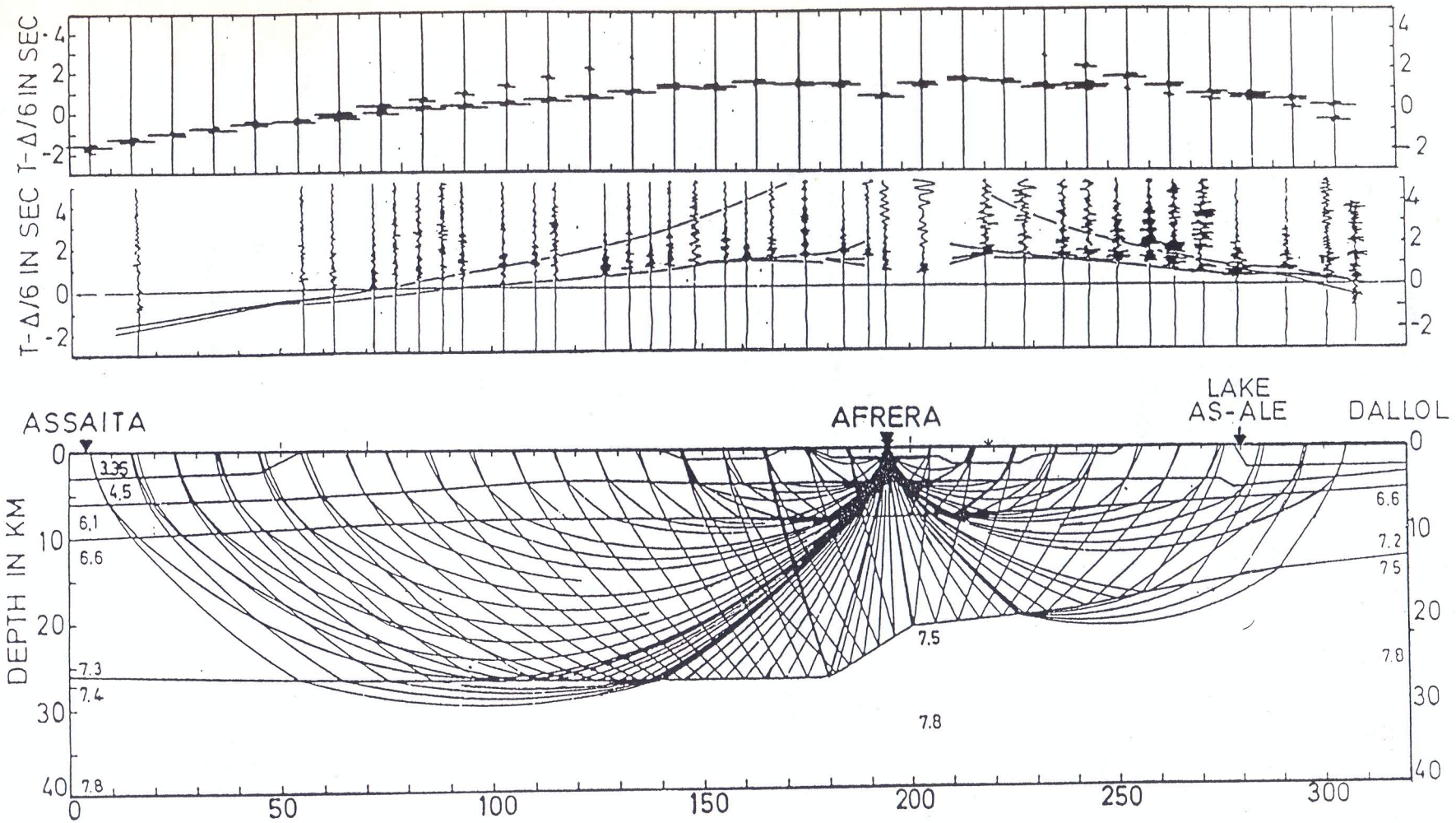

Figure 10: Velocity - depth structure, record section and synthetic seismogram of profile 5 and 6. The profile starts in central Afar and ends at the salt domes of Dallol, in an almost northerly direction. The model shows the most dramatic changes in the crustal structure. A 2.50km thick, 3.95 km/s velocity sedimentary layer is present at Assaita and disappears to the north. Near Dallol, another thick accumulation of sediments and evaporites, of low - velocity 3.35km/s overlies the basalt series. A thin 6kms thick, 6km/s velocity upper crust is present. There a drastic change of depth of the lower crust - anomalous mantle boundary from 20kms in north Afar to only 14kms at Dallol. (Makris, J,; Ginzburg, A,; 1987).

end of this profile. The top of the anomalous mantle is only about 20 km deep in north Afrera and decreases rapidly towards Dallol, where its depth is only 14 km.

The most important conclusions to be drawn from the DSS study in the northern part of MER, the Afar depression and the Western Plateau are: (i) The crust beneath the rift zone is an uttenuated and is underlain by an abnormally thin and anomalously low velocity mantle material of varying thicknesses. (ii) The Western Plateau is underlain by a normal mantle and the thickness of the crust here is determined between 38-40 km.

3.2 Deep Seismic Soundings in Djibouti

This seismic experiment was performed in March-April 1971 mainly in the Gulf of Tadjura region (south eastern Afar). The Gulf of Tadjura forms the link between the Gulf of Aden and the Afar axial ranges. The Afar axial ranges are reckoned to be situated upon lines of active crustal spreading along which most of the volcanoes in Afar occur characteristically.

One of the major objectives of the seismic experiment was to determine the nature of the crust and the upper mantle structure (Lithosphere) in this region;i.e. whether it is attenuated continental lithosphere or oceanic lithosphere in nature. For this purpose, several seismic refraction profiles were run parallel to the axis of the Gulf (Fig. 11a). Details of the experiment and their evaluation are discussed in Lepine et al. (1972) and Ruegg (1975).

A brief description of a few profiles thought to be continuous with the Afar seismic profiles of Berckhemer et al. (1975) is presented below. Profiles 02 and 05 run between Djibouti and Lake Abbe, while profile 04 runs between Obock and Lake Asal. Profile 01

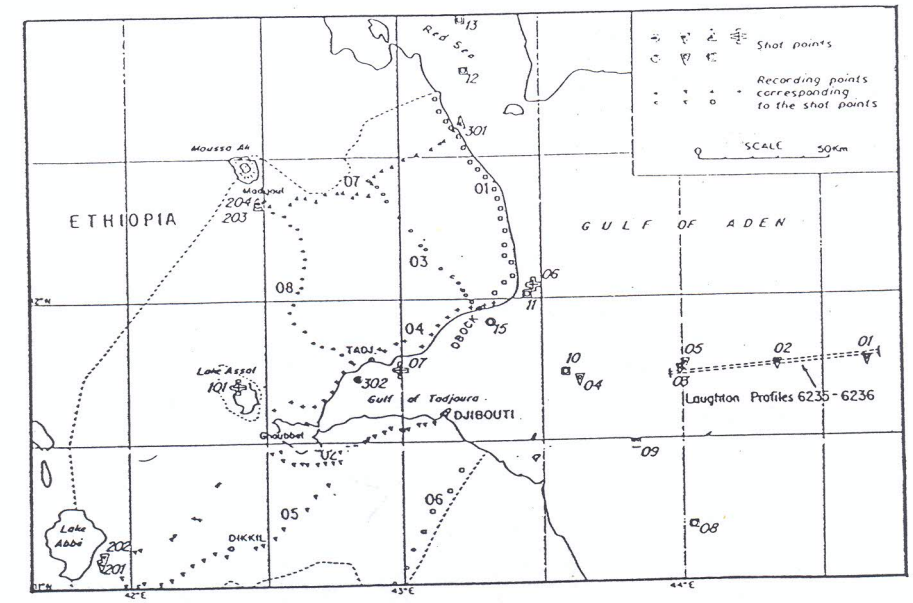

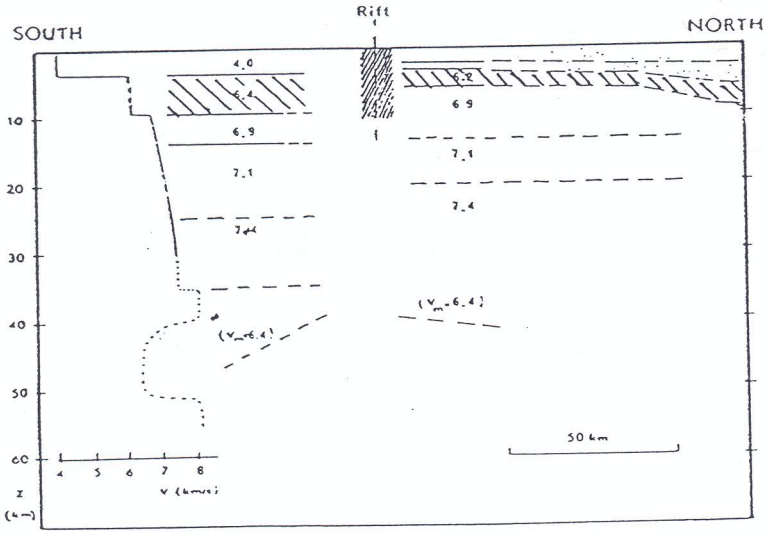

Figure 11: (a) Location of seismic profiles in the Djibouti area
(b) Mean north - south velocity - depth model for the Djibouti region. (Ruegg, 1975).

runs in a NS direction along the straits of Bab-el-Mandeb. Furthermore, recordings were made along four additional short profiles in the area (Fig.11a) to study the variation in the crustal structure.

3.2.1 Profile 01 (Obock - Doumeira)

Seven shots were recorded on this reversed profile. The travel-time curves and depth model for this profile are reproduced here (Fig. 12). In an attempt to determine the true velocities of the layers, the following results were obtained: P wave velocities of 3.40 - 4.00 Km/s were computed for the sediments, 4.00 - 4.60 Km/s for the lava flows, 6.00 - 6.50 Km/s for the crystalline basement and 6.70 - 6.90 Km/s for the lower crust. An increase in V_p from 7.10 Km/s at 13 Km depth to between 7.40 and 7.50 Km/s at 20 Km depth was observed.

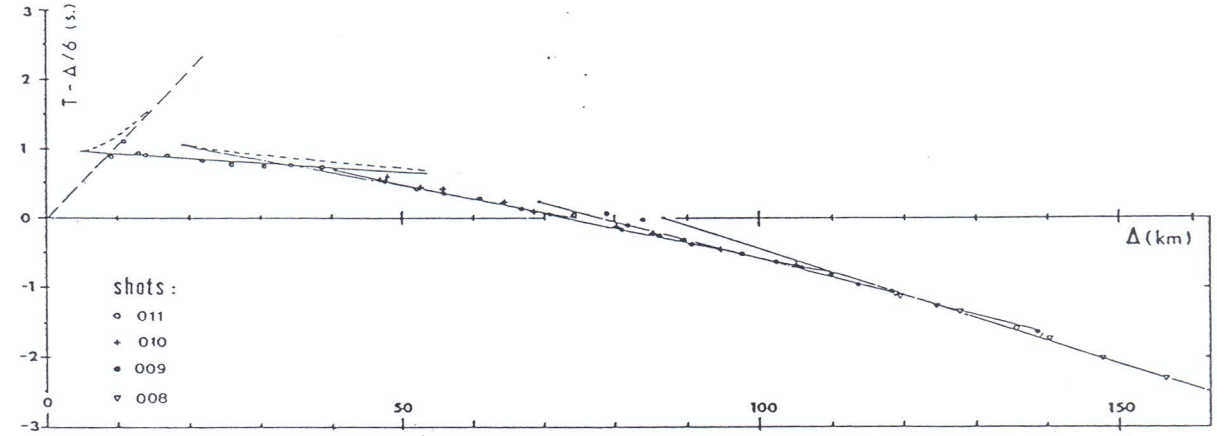

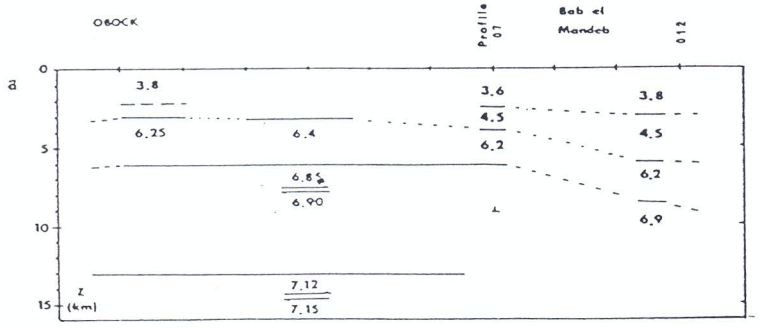

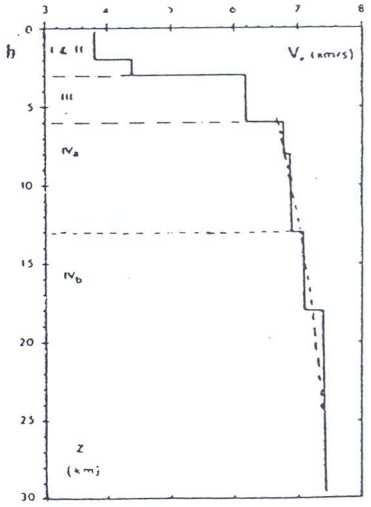

Figure 12: (a) Travel - time curve b) Velocity - depth model (c) Velocity - depth function of profile 01: Obock - Doumeira (Ruegg,1975).

This velocity range is thought to correspond to the updoming anomalous mantle beneath the surrounding crust. S wave velocities V_s were also computed for some profiles. This enabled the computation of Poisson's ratio ($\sigma = V_p/V_s$) every time P and S velocities were obtained in the same range of distance. High values of 0.26 to 0.33 were obtained, which in conjunction with a low S velocity corresponding to the upper mantle are attributed to partially melted mantle material and high heat flow near the axis of the ridge. Poisson's ratios, which are considered to be characteristic for continental and old oceanic crusts as well as the normal mantle, range from 0.25 - 0.26. The high values (i.e 0.26 - 0.33) obtained are thus due to a slower propagation of S waves, which are caused by changes in the elastic parameters (due to a partially melted material) in the upper lithosphere.

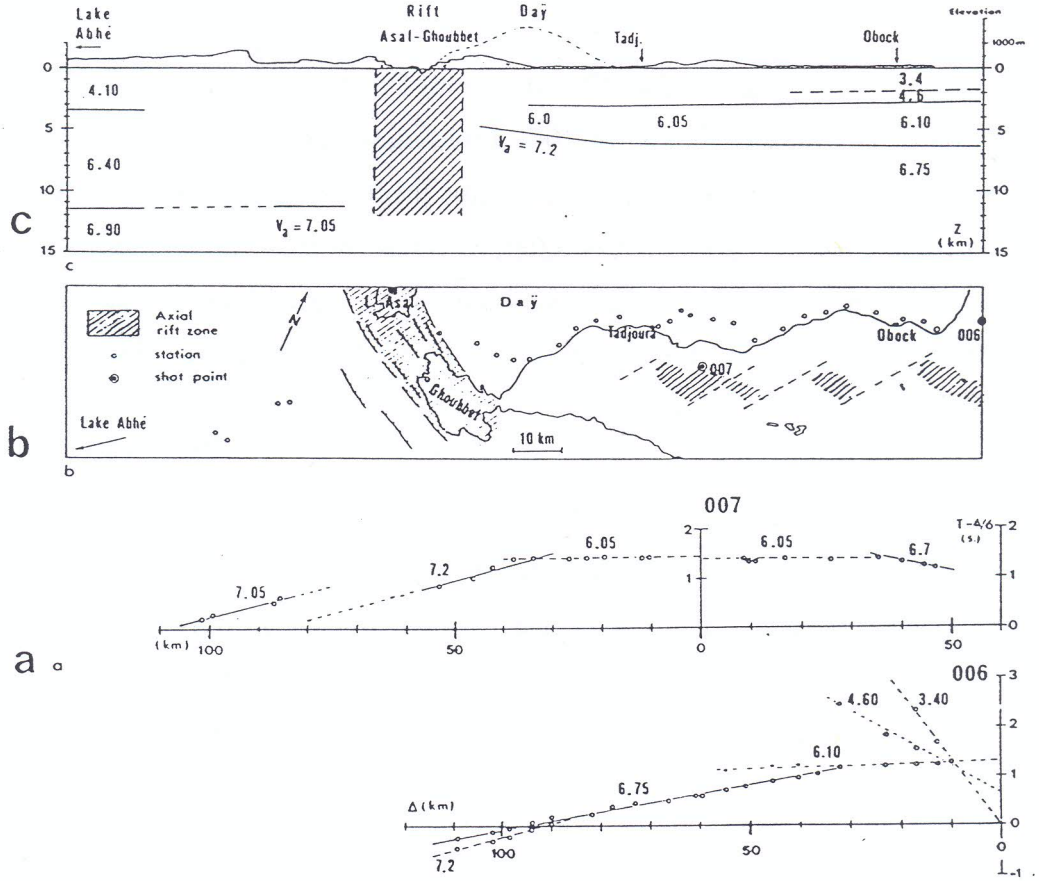

Figure 13: (a) Travel -Time curves (b) Locations of recording stations and tectonic sketch map (c) Velocity - depth model of profile 04 (Ruegg, 1975).

3.2.2 Profile 04 (Obock - Tadjoura - Lake Asal)

This profile runs parallel to rift of the Gulf of Tadjoura. The travel-time curve for shots

006 and 007, location of stations and the tectonic sketch map and the velocity-depth model along profile 04 are given in Fig. 13. The same order of velocities were computed in the profile: i.e V_p =3.40 - 4.60 km/s for the sediments and basalt cover, 6.00 - 6.40 km/s for the upper crust and 6.75 - 7.00 km/s for the lower crust.

A P wave-velocity of 7.23 km/s is found for first arrivals at a distance of 90 km from shot 006, i.e beneath the Asal-Ghoubbet rift, whilst from shot 007, this wave begins at only 40 km. This velocity structure suggests an updoming of the crust in this area.

3.2.3 Profile 02 and 05 (Djibouti - Lake Abbe)

Two shots were recorded on Profile 02 and five on Profile 05. The mean velocity depth-function is given in Fig. 14. A crust of 10 km thickness is composed by a 4.10 km/s and a 6.40 km/s layers. Velocities computed along this profile were V_p = 4.1 - 6.4 km/s layers. As in Profile 01 the mantle layer is characterized by an increase of apparent velocity with distance between shot points and recording stations. An anomalous increase of velocities (6.80 - 7.20 km/s) is observed for the shots near lake Abbe, which was interpreted as due to updoming of the mantle layers.

Strong second arrivals were identified and interpreted as deep reflected waves. Their mean velocity (i.e computed between the deep reflecting layer and the surface) is estimated at 6.60 km/s, where the depth of the reflector is estimated to lie between 34 and 42 km. Later low frequency arrivals were also recognized along this profile. Their interpretation suggests that these reflections are coming from the lower interface of a possibly low velocity zone, at a depth between 40 and 60 km.

The main results and tectonic implications of the seismic experiment in Djibouti were analyzed by constructing a mean north-south tectonic cross-section in the territory (Fig. 11b). This was based on the results of the Djibouti seismic refraction experiment carried

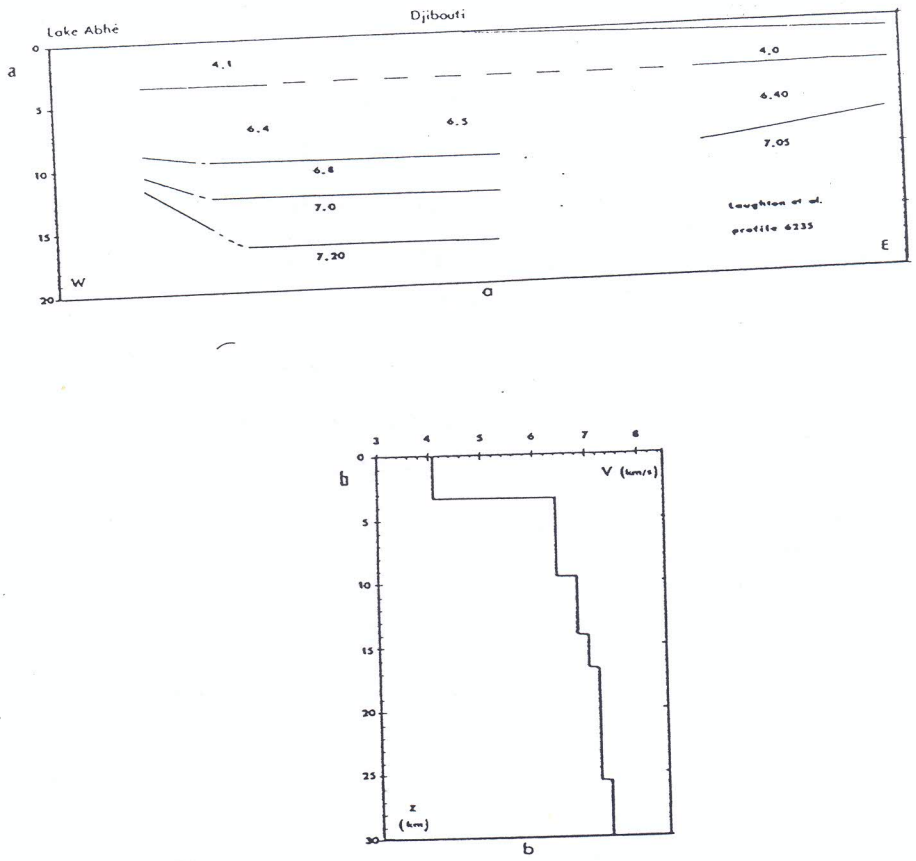

Figure 14: (a) Velocity - depth model (b) Mean velocity depth for profiles 02 and 05 (ruegg, 1975)

out in the region (Fig. 11). The investigation showed that the crust is thinner in the northern part than in the southern part. The anomalous mantle lies at shallower depths as compared to those determined along the seismic profile in southern Afar. The top of the anomalous mantle deepens as one goes away from the rift (Asal-Ghoubbet rift).

3.3 The Kenyan Rift International Seismic Project (KRISP)

Two N-S and one E-W oriented seismic refraction experiments (KRISP68 and KRISP85) carried out beneath the Kenyan Rift (Fig. 15) are considered. One of the major aims of the experiments was to investigate the crustal and upper mantle velocity-depth structure beneath the Kenyan Rift and the adjacent plateaus in order to provide some control for the interpretation of the available gravity data and to test the hypothesis of crustal thinning.

The KRISP68 seismic refraction investigation was performed between Lake Turkana and Lake Bogoria (Fig. 15) and indicated the presence of a 20 km thick layer of high velocity (6.38 km/s) material within 3 km of the rift floor overlying a 7.5 km/s layer presumed to be anomalous mantle material (Griffiths et al. 1972).

The KRISP85 seismic experiment (Fig. 15) consisted of two seismic refraction lines: A NS profile along the rift axis (NS-line) and the other across the rift (EW-line). The NS-line was performed with shot points at Lake Baringo (BAR), Chepkererat (CHE), Solai (SOL), Elmenteita (ELM), Naivasha (NAI), Susua (SUS) and Magadi (MAG) following the trend of the positive axial Bouguer anomaly mapped along the rift axis. The EW-line (Fig. 15) ran from Ntulelei on the western flank to Mount Margaret, on the rift floor near eastern escarpment with shot-points at Ewaso Nagiro (EWA), Ntulelei (NTU), Susua (SUS), Mount Margaret (MAR). A P-wave record section of the NS-line is shown in Fig. 16, for two shots at Lake Baringo with phase correlations and velocity-depth function.

The main features of the velocity-depth model along the rift axis are shown in Fig. 17. It shows that the depth to the basement (i.e. material of P-wave velocity of about 6.05 km/s observed beneath both the axis of the rift and the rift flanks) within the rift axis has variations of about 4 km. The KRISP85 experiment data has also indicated that the Moho discontinuity (assumed here to be where the P-wave velocity increases to about 7.5 km/s) is about 35 km (below sea level) beneath the central sector of the rift. A 7.60 km/s velocity layer occurs at approximately 35 km depth. It is overlain by a 10 km thick lens which includes anomalous low velocity material. This lens is said to represent the base of the crust. It thickens beneath the Kenyan dome

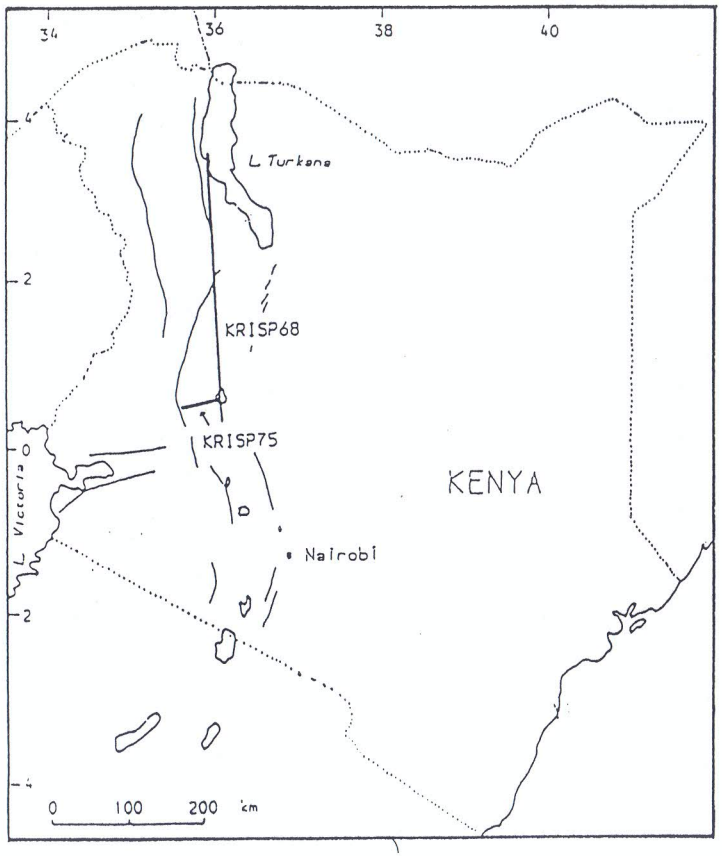

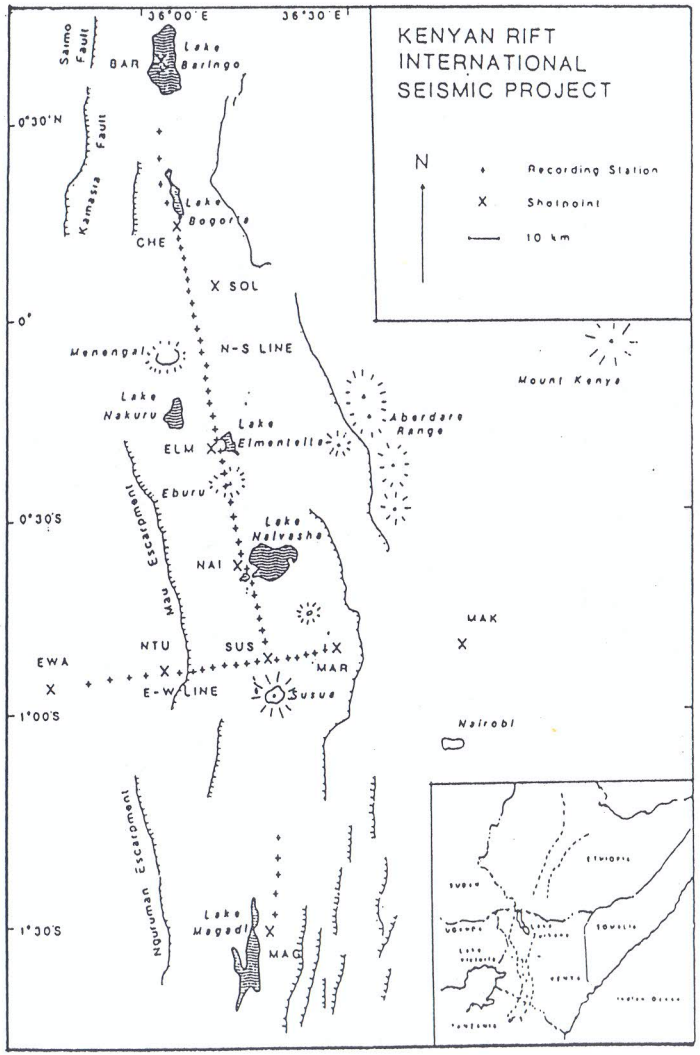

Figure 15: Locations of the KRISP seismic profiles in the Kenyan Rift (Griffiths et. al., 1971; Khan et al. 1987).

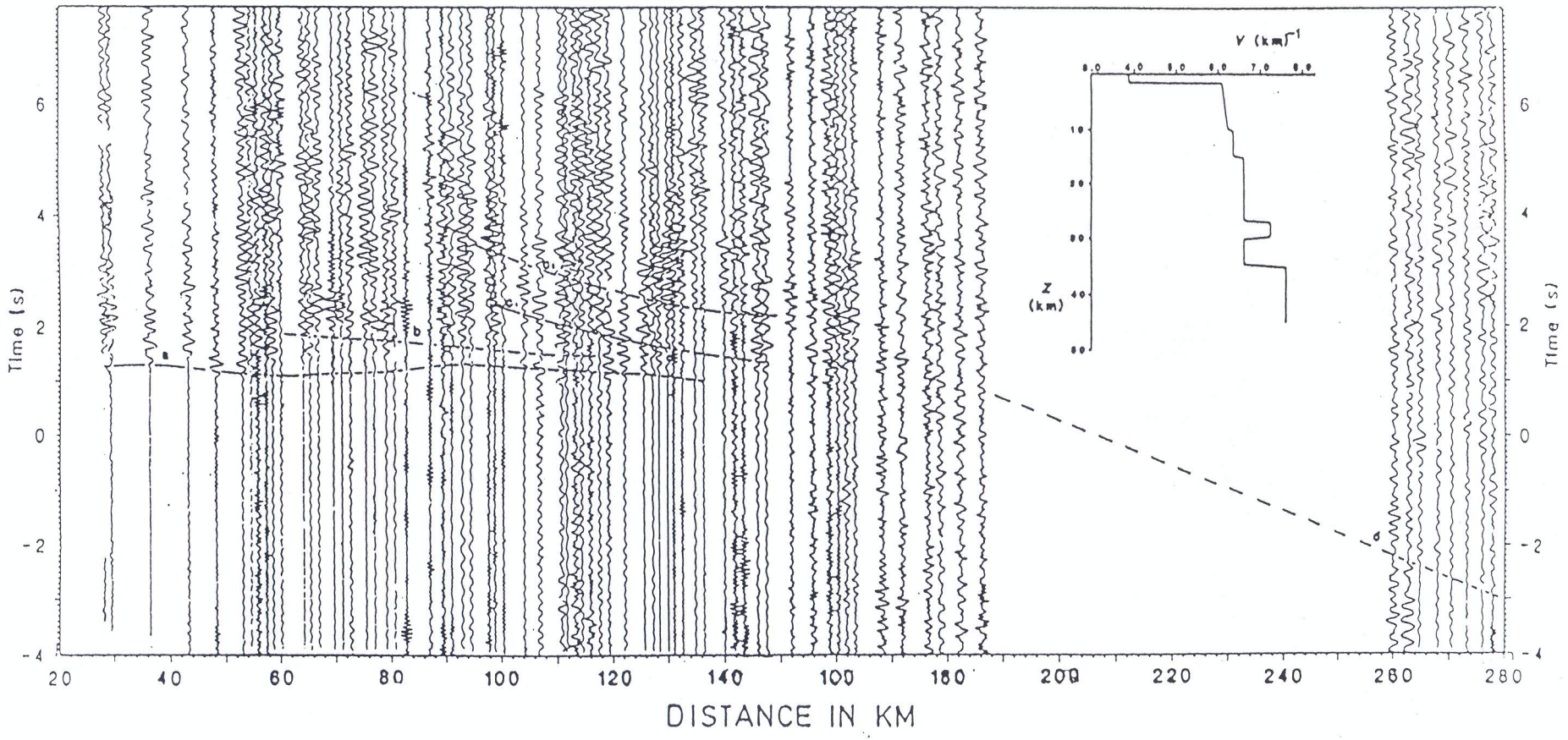

Figure 16: Record section of the KRISP85 NS profile (along the rift axis) for the shots at lake Baringo with correlations and velocity-depth function. Reducing velocity is 6.00km/sec. Phase "a" corresponds to P_g with an apparent velocity of 6.00 km/sec. It has apparent velocity from the reverse shot, which indicates that the basement dips southwards between lakes Elmenteita and Naivasha. The P-wave velocities increase from 6.10 km/sec to 6.25 km/sec at 10 km depth. Phase "b" is reflection from an intercrustal discontinuity at about 15 km depth. Phase c_1 represents a reflection from a discontinuity at 27 km depth, with a velocity of approximately 7.25 km/sec. Phase c_2 in a reflection from the normal mantle at 35 km depth. Phase "d" are diving waves from the normal mantle (Khan et.al., 1987).

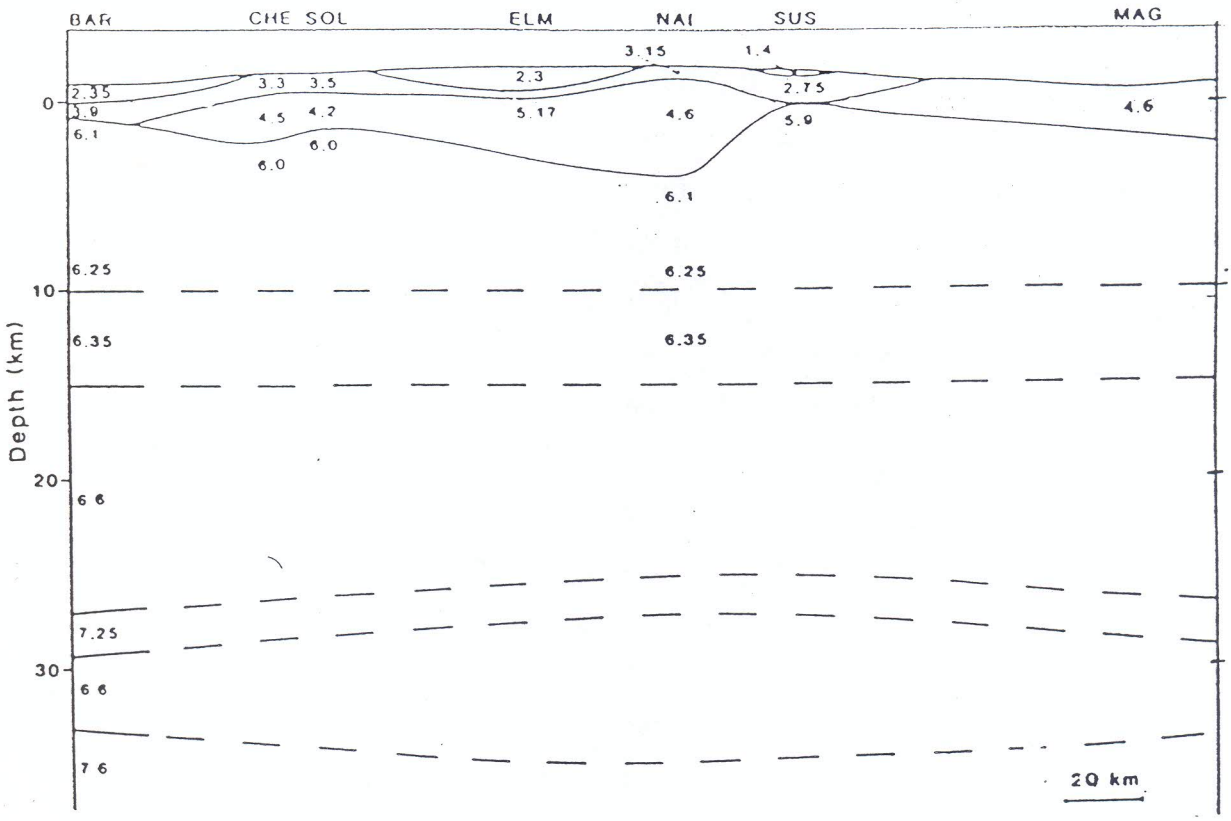

Figure 17: Two-dimensional velocity depth model along the rift axis from lake Baringo to lake Magadi. Velocities shown are in km/sec. The rift infill has velocities ranging from 1.40 to 4.60 km/sec and thickness of 2.00 km beneath lake Baringo & Suswa and a maximum thickness of 6.00 km below lake Naivasha. The basement thickness varies upto 4 km. An anomalous mantle occurs at about 27 km depth with a velocity of around 7.25 km/sec. It is about 10 km thick and dips beneath the Kenyan dome. a normal mantle velocity of 7.60 km/sec was calculated at 35 km depth (Khan et.al.,1987)

3.4 Other Seismic investigations in the Kenyan Rift.

Rykounov et al. (1972) determined a two layer crustal model (35-37 km thick) through the analysis of microearthquakes recorded in the southern part of the rift between Kenya and Tanzania.

Bonjer et al. (1970) investigated the crustal structure of the eastern flank of the rift under Nairobi by spectral analysis of long period body waves and determined a 42 km thick 2 layer crust.

The crustal structure below Nairobi and Addis Ababa was investigated by Herbert and Langston (1985) using teleseisms. This investigation indicated a similar crustal thickness of 41 km below both stations. This agreed with previous estimates. For instance, spectral response ratios of long-period body waves at Addis Ababa yielded a 40 km thick crust (Bonjer et al. 1970), and 43 km at Nairobi. Analysis of first arrivals of regional and local earthquakes recorded by a seismic array on the western flank of the rift provided a crustal model that varies in thickness between 42 and 46 km (Maguire and Long, 1976).

3.5 Conclusions drawn from the seismic refraction experiments

The rift zones (Main Ethiopian Rift, the Afar Depression and the Kenyan Rift) is characterized by the presence of a velocity transition zone just above the crust-upper mantle discontinuity. The crust beneath the rift in Ethiopia thins considerably from the central part of MER to Afar. The observed thinning is about 16 km, The crust reaching 30 km in the central part of MER and 14 km in north Afar. Further south the crust thins from the MER to Turkana north Kenya. The observed thinning is about 10 km the crust reaching 20 km in Turkana. On the other hand the crust thickens as one goes south from Turkana to the central part of the Kenya rift. The observed thinning here is about 15 km, the crust reaching 35 km in the central and southern sectors of the Kenya rift.

A comparison of the observed crustal thicknesses indicate that the Turkana rift has a major crustal thinning (20 km) comparable to that of the Afar Depression (20-14 km). In contrast to the Turkana thinned crust the southern sector of the Kenyan rift has a thick crust (35 km) comparable with that of the MER. On the basis of crustal thinning as indicating the amount of crustal attenuation, it may be argued that there is a more advanced rifting stage in the Turkana rift and the Afar Depression relative to the MER and the Kenyan rift.

Chapter 4.

The Gravity Field of the MER: Field Studies and Results

4.1 The Gravity Data

The simple Bouguer gravity anomaly map (Fig. 18) and the free-air anomaly map (Fig.19) were compiled from approximately 2300 gravity observations.

The data sources include:

1. 1500 gravity values collected by the author in the Ethiopian Rift since 1982 using the Canadian Sharp Gravimeter No. 128 (Worden type gravimeter) and the Lacoste and Romberg, Model G gravimeter.

2. About 800 reprocessed gravity data of Gouin and Mohr (1964,1968), Mohr and Rogers (1966), Mohr and Gouin (1967), Mohr and Rogers (1972), Makris et al. (1972). All the stations occupied have been referred to the IGSN71 (Morelli et al. 1971) gravity datum. The primary gravity base of the Geophysical Observatory (977452.16 mGal) of Addis Ababa University which is referred to the IGSN71 Datum by the US DMA Aerospace Center in 1973, was used. The station spacing is quite variable, but the average spacing is between 2-10 km. The gravity station network in the rift is adequate to provide good detail. However, over the plateaus, the coverage is fairly sparse. The compiled maps (Bouguer and free-air anomaly maps) cover the whole of the Main Ethiopian Rift. The accuracy of the Bouguer anomaly at each station lies in the order of ±2.5 mGal, the errors depending mainly on inaccuracies in the elevation determinations. Furthermore the free-air anomaly map of the same region was compiled by using data derived from OSU91A geopotential model (Rapp et al., 1991)

4.2 Data reduction

As a rule, the earth's gravity (g) is measured at points on its surface. On the other hand, since the earth's surface doesn't represent a regularized equilibrium surface g varies because of variations in latitude, elevation, topography of the surrounding terrain, earth tides and subsurface density variations. g is not directly comparable with the normal sea level gravity (γ) referring to the surface of the ellipsoid. Hence, a reduction of g to an equipotential sea level surface (geoid) is necessary. These reductions must attempt to produce the value of g that would have occurred if it were possible to observe on the geoid surface. The manner in which g is reduced to the geoid to compute the different gravity anomalies is known as gravity reduction.

All the stations occupied in the study area have been referred to the IGSN71 (Morelli et al. 1971) gravity datum. The primary gravity base of the Geophysical Observatory (977452.16 mGal) of Addis Ababa University which is referred to the IGSN71 Datum by the US DMA Aerospace Center in 1973 was used. The theoretical gravity , γ, at latitude φ, has been calculated from the 1967 gravity formula (Geodetic Reference system 1967, Moritz, 1971).

The approximation :

$$\gamma = 978031.85\ (1 + 0.0053024\ \sin^2\varphi + 0.0000059\ \sin^2 2\varphi)\ \text{mGal}, \qquad (1)$$

which is accurate to ± 0.4 mGal, has been used.

As gravity measurements are not made on the ellipsoid but usually on the earth's surface at some height h above a reference equipotential surface (geoid), reductions must be applied to the observed values before any anomaly may be obtained. Different types of anomalies are possible depending upon the manner in which this correction is computed.

In general the corrections brought to an accurate gravimetric survey are of many natures, but they can be classified under corrections for:

1. Instrumental drift (drift correction)

2. Fluctuations due to the superposition of an exterior gravity field (tidal correction)

3. Variations of the earth's gravity field due to the location of a gravity station on the earth's surface.

4. Terrain (terrain correction)

4.2.1 **Instrumental correction** (drift or time variation of gravimeters)

In practice, all gravimeters have a certain amount of drift. This time variation may be due to many causes (e.g slight temperature and/or pressure variation even if the instrument is self- compensated) but more commonly due to the fact that the quartez springs are not perfectly elastic and are subject to creep over a certain period of time. The drift in the gravimeter reading at a station may be from a few hundredths of a mGal to four tenths of a mGal per hour.

In order to correct for drift, one or more stations were reoccupied at intervals of one to three hours. Assuming the drift of the gravimeter is linear, the differences between two readings at a station were plotted against time. Corrections were read off and applied to the intermediate stations readings. The calibration constant of the Canadian gravimeter was checked before and after the execution of the field campaigns.

4.2.2 Tidal correction

The combined attraction of the sun and the moon may change the gravity at a station cyclically with a maximum daily amplitude of 0.3 mGal. Appropriate corrections can be made by referring to special tables (e.g tables regularly published in advance for each year in Geophysical Prospecting, the Journal of the European Association of Exploration Geophysicists). Since tidal variations are rather slow, it is assumed that their effects will fully be incorporated in the instrumental drift correction.

4.2.3 Elevation reduction

The elevation reduction to the geoid, through the height h, neglecting the matter contained between the geoid and the earth's surface (free-air correction) is obtained by the inverse square law, and this variation of gravity with height is expressed by:

$$\delta g_F = - (\partial g/\partial h)h \approx -(\partial \gamma/\partial h)h = 0.3086h \text{ mGal} \quad (2)$$

where h is height above sea level in metres. This constant factor (0.3086 mGal/m) has been used throughout our computation of the free-air correction.

4.2.4 Bouguer reduction

In order to account for the effect of masses between the geoid and the observation point, the gravitational attraction of an infinite horizontal slab of rock material of thickness equal to the station height h and density ρ (normally 2.67 g/cm^3) was computed using the known slab (Bouguer slab) correction formula:

$$\delta g_B = -2\pi G\rho h = -0.0419\rho h = -0.1119h \text{ mGal} \quad (3)$$

4.2.5 Terrain correction

Terrain corrections were determined out to 15 km only for stations in the Aluto-Shashemene area using the zone chart method (Hammer, 1939). The mean terrain effect computed at points along two profiles which traverse the summit of Aluto volcano (this volcano has a peak elevation of 2335m above sea level and rises by about 700 meters above the rift floor) in an E-W and N-S direction amounts to about 2.0 mGal. Neglecting the terrain effect for the rest of the stations in the survey area is thus assumed to cause an error not greater than 2.0 mGal in the Bouguer anomalies. This 2.0 mGal is therefore treated as a systematic error in computing the overall mean square error of the gravity anomaly Δg.

For each station, where terrain correction is taken care of, the Bouguer anomaly Δg_B (most frequently applied to study the internal structure of the earth's crust and to applied geophysics) was determined by means of the formula,

$$\Delta g_B = g - \gamma + \delta g_F + \delta g_B + \delta g_T \qquad (4)$$

where g = observed gravity; γ = normal gravity; δg_F = free - air correction; δg_B = Bouguer correction and δg_T = terrain correction.

The Bouguer anomaly computed by neglecting the terrain correction is known as the simple Bouguer anomaly (S.B.A) and takes the simplified form

$$\Delta g_B = g - \gamma + (0.3086 - 0.0419\rho)h \qquad (5$$

If $\rho = 2.67$ g/cm^3 is introduced,

$$\Delta g_B = g - \gamma + 0.1967h \qquad (6)$$

4.3 Elevation and coordinates of the gravity stations

In the Langano-Aluto area station positions and absolute altitudes were determined by tacheometry. For stations outside of Langano-Aluto area elevations were determined using barometers: Trigonometric points, bench marks, height points of railways, and spot heights established by the Ethiopian Mapping Authority (EMA) in the study area were used as base stations for elevation control. The Paulin System surveying altimeters were used. The scales of these instruments have been calibrated on control points with an altitude difference of about 2000m. An accuracy of ± 1m for the tacheometric observations and ± 5m -10m for the altimetric observations giving an error in the Bouguer anomaly of 1.12 mGal may be guaranteed.

A uniform determination of the geographic coordinates was not possible everywhere, because a unique set of maps did not exist, for example of scale 1: 50,000, covering the entire area. At worst, we had to use maps of a scale 1: 250,000. In such cases, the positioning error amounts to about 0.5 km, which corresponds to about 0.15 mGal, caused by the effect of imprecise latitude.
Simple Bouguer anomalies were computed for the conventional density 2.67 g cm^{-3}. The normal gravity was calculated according to IGSN71 using the international gravity formula of 1967.

4.4 Assessment of errors

In analyzing the accuracy of gravity anomalies Δg it is necessary to appraise the accuracy of the method used in computing them, i.e., the completeness of the formula used and the correctness of the numerical values of the constants occurring in it. Terms neglected in simplified formulae may cause systematic errors in the computed anomalies Δg . A systematic error is introduced in Bouguer anomalies, for example by neglecting the correction for irregularities in the terrain.

It is also necessary to assess the effect of random and systematic errors of the parameters of the formula, the values of which are determined separately for each gravity point. These include the observed value of gravity, the geographic latitude and the elevation of the observation point.

The overall mean square error $\sigma_{\Delta g}$ of the gravity anomaly Δg is defined by

$$\sigma^2_{\Delta g} = m^2_{\Delta g} + s^2_{\Delta g} \qquad (7)$$

where $m_{\Delta g}$ is the standard error (due to random errors) and $s_{\Delta g}$ is the terrain effect (bias) (Sjöberg, 1990) of the gravity anomaly.

The variance $m^2_{\Delta g}$, can be computed from the law of propagation of errors:

$$m^2_{\Delta g} = m^2_g + (\partial\Delta g/\partial\varphi)^2 m^2_\varphi + (\partial\Delta g/\partial h)^2 m^2_h \quad (8)$$

where m_g, m_φ and m_h are the standard errors in determining the gravity (observation error), the geographic latitude and the elevation of the gravity point respectively;

The standard error m_g, can usually be obtained by checking the gravity measurements. To accomplish this task, 10 check points (S1,S2,S3,...,S10) were considered. 3 independent observations (relative gravity values) made on each check point making a total of 30 independent observations were considered. The mean value of gravity and residuals V were determined at each check point for the individual observations.

The internal variance (Bjerhammer, 1973) of these observations was computed following the scheme outlined in Table 4.1 and the formula:

$$m^2_g = \{\sum_{S1}(VV) + \sum_{S2}(VV) + \ldots + \sum_{S10}(VV)\}/(n-s) \quad (9)$$

where n is the total number of independent observations and s is the number of gravity check points. The computed standard error m_g amounts to ±0.85 mGal.

Table 4.1

Table of gravimeter readings for computing the internal variance (for 10 check points)

y	$\hat{y}$	V	VV	
1067.40	1068.46	1.06	1.1236	
1069.80	1068.46	-1.34	1.7956	
1068.20	1068.46	0.26	0.0676	$\hat{y}_1$=1068.46
1144.03	1145.36	1.33	1.7689	
1146.12	1145.36	-0.76	0.5776	
1145.93	1145.36	-0.76	0.3249	$\hat{y}_2$=1145.36
1136.49	1136.34	-0.15	0.0255	
1135.05	1136.34	1.29	1.6641	
1137.50	1136.34	-1.16	1.3456	$\hat{y}_3$=1136.34
1256.59	1255.89	-0.70	0.4900	
1256.29	1255.89	-0.40	0.1600	
1254.79	1255.89	1.10	1.2100	$\hat{y}_4$=1255.89
1448.71	1447.93	-0.78	0.6084	
1447.57	1447.93	0.36	0.1296	
1447.52	1447.93	0.41	0.1681	$\hat{y}_5$=1447.93
1604.84	1604.27	-0.57	0.3249	
1603.84	1604.27	0.43	0.1849	
1604.15	1604.27	0.12	0.0144	$\hat{y}_6$=1604.27
1687.49	1687.09	-0.40	0.1600	
1686.68	1687.09	0.41	0.1681	
1687.09	1687.09	0.00	0.0000	$\hat{y}_7$=1687.09
1206.80	1206.19	-0.61	0.3721	
1205.59	1206.19	0.60	0.3600	
1206.20	1206.19	-0.01	0.0001	$\hat{y}_8$=1206.19
1735.79	1735.62	-0.17	0.0289	
1735.99	1735.62	-0.37	0.1369	
1735.10	1735.62	0.52	0.2704	$\hat{y}_9$=1735.62
1457.78	1457.64	-0.14	0.0196	
1457.49	1457.64	0.15	0.0225	
1457.64	1457.64	0.00	0.0000	$\hat{y}_{10}$=1457.64

By differentiating the expression for the normal gravity γ with respect to φ, the rate of change of gravity with latitude is estimated by

$$1/R(\partial g/\partial\varphi) = 1/R(\partial\gamma/\partial\varphi) = 0.812 \sin 2\varphi \text{ mGal/km} \quad (10)$$

where R = 6371229 m is the mean radius of the earth.

For the mean latitude, $\varphi < 10^0$ of the study area, the gravity variation is about 0.03 mGal for each 120 meters travelled in a N-S direction. This means that in order to obtain an anomaly accuracy of 1 mGal, the position must be known to at least 4000 meters. For the positional error $m_\varphi = \pm 500$m ($\approx 0.27'$ of arc) we adopted in fixing the latitude φ from the available topomap of the region, the error estimate in the normal gravity amounts to $1/R(\partial\gamma/\partial\varphi)m_\varphi = \pm 0.14$ mGal for $\varphi = 10^0$

By differentiating the expression for the Bouguer anomaly formula (5) with respect to station height h, the rate of change of the combined free-air and Bouguer correction with elevation at a station may be expressed by

$$\partial\Delta g/\partial h \doteq 0.3086 - 0.0419\rho \quad (11)$$

or with the standard density 2.67 g/cm^3

$$\partial\Delta g/\partial h \approx 0.1967 \text{ mGal/m} \quad (12)$$

The maximum error estimate in the Bouguer anomaly corresponding to our adopted maximum elevation error $m_h = \pm 10$m of a gravity station therefore amounts to $(\partial\Delta g/\partial h)m_h = \pm 1.97$ mGal.

Using the formula (7) the total standard error $\sigma_{\Delta g}$ of the gravity anomaly Δg is therefore estimated to ± 2.9 mGal. The overall accuracy of the Bouguer anomaly values (assuming the correct density has been chosen) is therefore expected to be around ± 2.9 mGal.

Figure 18 shows the derived Bouguer anomaly map of the study area contoured at 5 mGal intervals. The contouring of the gravity map was carried out by hand, with the advantage that in areas of poor control it would be possible to draw 'sensible' contours that conform to the geological data of the area (or to ones preconception of it). As the magnitude of a

contour interval used to produce gravity anomaly maps depends on the uncertainty of the gravity anomalies, the contour interval chosen here can be reasonably accepted.

4.5 The gravity field of the Main Ethiopian Rift and the adjacent areas

The available gravity data considered under this study are presented as Bouguer anomaly (Fig. 18) and free-air anomaly (Figs. 19 and 20) maps to study the nature of the gravity field in the Main Ethiopian Rift. In the analysis more emphasis is put on the nature of the Bouguer anomaly field.

4.6 The Bouguer Anomalies

The analysis of the Bouguer gravity anomalies will concentrate on the Main Ethiopian Rift and the associated highlands but also will mention prominent gravity anomalies in the surrounding areas.

The Bouguer anomaly map (Fig.18), reveals that the intensity of gravity field and its regional pattern are closely connected to the topographic features of the area. The anomaly contours have a typical N-S to NNE-SSW trend which is similar to the structural trend of the region. The map displays several pockets and belts of gravity highs and lows of varying dimensions. Moreover, numerous previously unknown anomalies appear, for example, the positive anomaly belt along the western margin of the rift between latitudes $7^0$30'N and $8^0$45'N. A comparison of the negative anomalies associated with the Eastern and Western Plateaus shows that both plateaus are associated with gravity minima of the same order of magnitude (-260 mGal). The gravity minimum on the Western plateau

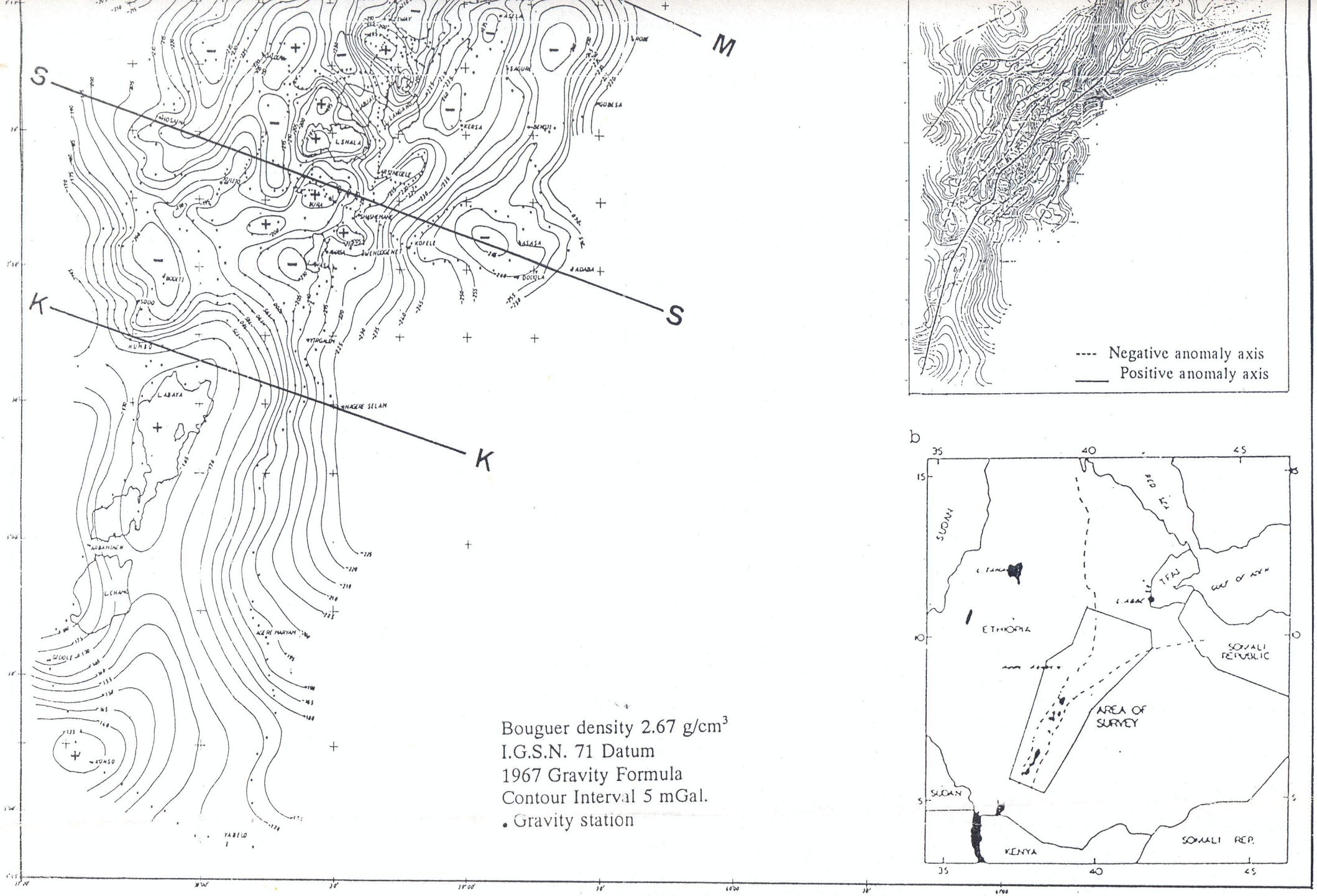

Figure 18: Bouguer anomaly map of The Main Ethiopian Rift and the adjacent plateaus. Insets show (a) gravity trends over the study area and (b) location map of the study area.

Figure 21: P-wave Velocity-Density curves used to convert the seismic velocities to density models. The curves have been taken from Nafe and Drake, 1974, Brich 1961, Woolard 1968 and Henkel et al. 1990.

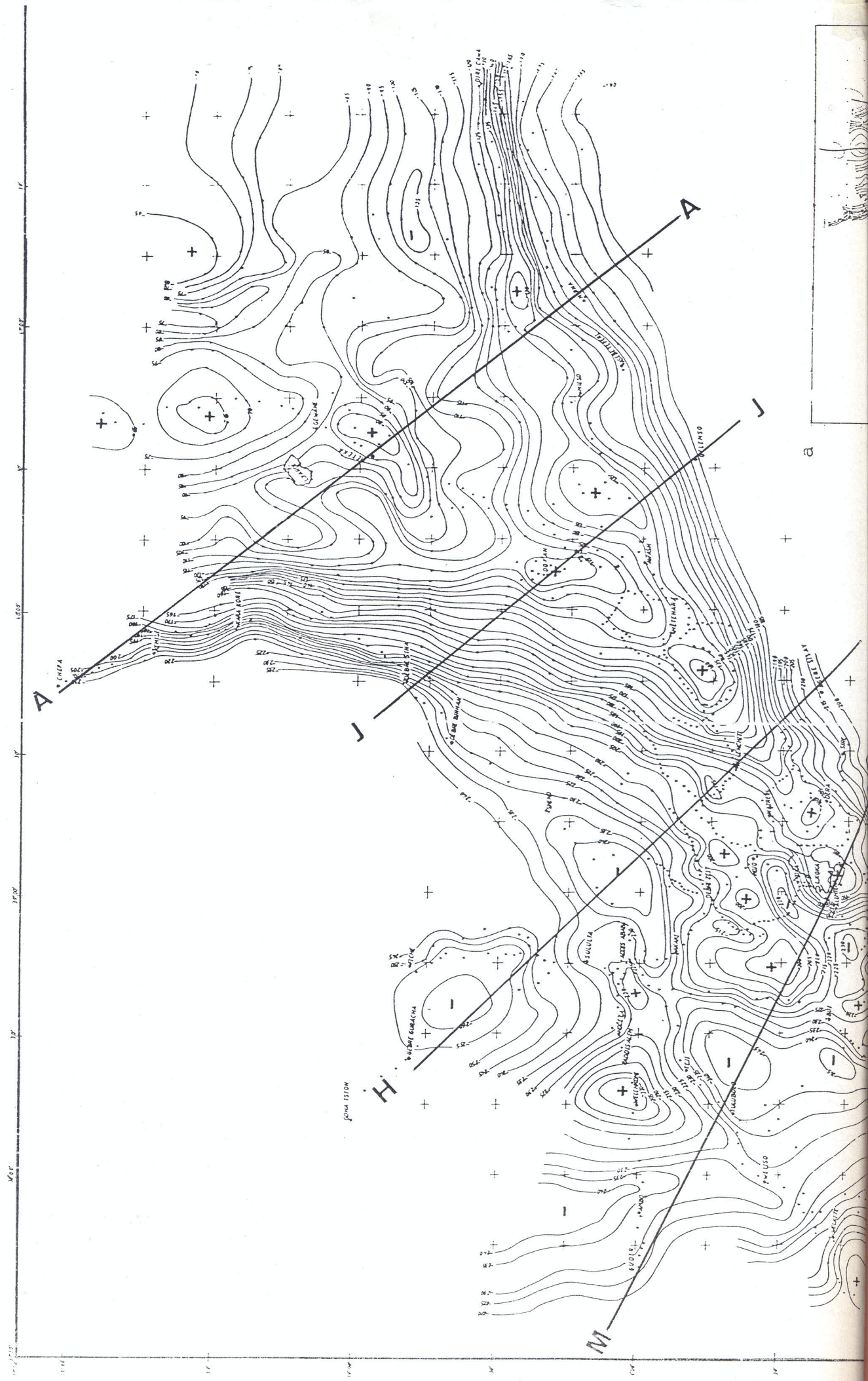

occurs north of Addis Ababa ($9^0$37'N, $38^0$37'E) and that of the Eastern Plateau occurs east of Shashemene ($7^0$07'N, $39^0$05'E).

Within the rift system, the most prominent gravity anomalies are a series of local gravity maxima trending NNE-SSW approximately along the rift axis. These gravity maxima are central to the rift floor and their values increase northwards and southwards from -195 mGal west of Shasemene to -65 mGal north of Gewane village and to -165 mGal in the Lake Abaya area, respectively. These gravity maxima beneath the central zone of the rift floor generally seem to be situated along the displacement lines of the WFB. Between latitudes 7^0 N and $9^0$15'N, the gravity maxima generally coincide with various volcanic centers, especially the Corbetti Caldera and Shalla caldera near Shashemene, the Aluto volcano and Gademota Caldera near Adamitulu, the Tulu Moye volcano near Alemtena, the Gedemsa Caldera near Dera, the Gariboldi Caldera and Fantale volcano near Metehara, the Dofan volcano, the Ayelu volcano (Fig.2).

Makris et al. (1972) have found a trend of gravity maxima extending from Metehara down to Lake Abbe over a distance of 400 Km along the Wonji Fault Belt. This study reveals that this trend of gravity maxima also extends southwards along the axis of the rift until the Konso area south of Lake Chamo, where the Main Ethiopian Rift terminates or is displaced west into the Turkana Depression of northern Kenya.

An interesting feature to be noted on the Bouguer anomaly map is that when the axes of the positive and negative anomalies are joined the gravity trends so obtained seem to extend from a few tens to several hundreds of kilometres in a NNE-SSW direction as shown in the inset (a) in Fig.18. A prominent feature of the inset map (a) is the manner in which the positive and the negative anomaly axes alternate with each other. In almost all cases the positive axes are aligned over the rift floor and the marginal grabens located adjacent to the plateau escarpments while the negative axes are associated with the elevated regions of the plateaus. Thus the present structures delineated by these gravity trends appear to be alternating bands of synclines and anticlines.

4.7 The Free-air Anomalies

The free-air anomaly map of the Main Ethiopian Rift is compiled using two data sets:

- Data set obtained by computing free-air anomalies from the observed point values using the standard free-air reduction formula.

- Data set obtained by computing the free-air anomalies using the OSU91A geopotential model at each observation point. In contrast to the previous models, this model is based on the geodetic reference system 1980. It is complete through degree and order 360^0 (Rapp et al., 1991) and combines satellite potential coefficient information, terrestrial gravity data, satellite altimeter information and topographic information. This model is claimed to define improved representations of the earth's gravitational potential beyond that available from just satellite data or just terrestrial data (Rapp et al., 1991)

The free-air anomaly maps (Figs. 19 & 20) show some fluctuations. The anomalies range from less than -40 mGal in the central part of the Main Ethiopian Rift to more than 100 mGal over the Western Plateau north of Addis Ababa. Over the plateau-rift transition zones gentle variations in topography are reflected by mild fluctuations in the free-air anomalies (between -10 to + 30 mGal) and rapid variations in topography are reflected by strong variations in the free-air anomalies (between -20 to + 80 mgal) and high gradients. The high gradients displayed on the free- air anomaly also mark the important tectonic units (the plateaus and the rift), where this is evident on the Bouguer anomaly map also.

Two prominent features of the gravity field are apparent on the free-air anomaly map: (1) large positive Free-air anomalies reaching a maximum of 90 - 100 mGal over the plateaus, which correlate with the topography, (2) negative belts of free-air anomalies of about -30 mGal beneath the rift axis. The map also shows steep gradients of free-air anomalies which appear to mark the plateau-rift transition zones on either side of the rift axis.
The free-air anomaly map computed using the OSU91A geopotential model (Fig. 20) also shows identical features as that of Fig. 19. On this map the anomaly contours are smooth and regular. The magnitudes of the anomalies are lower as compared to those revealed on Fig. 19.

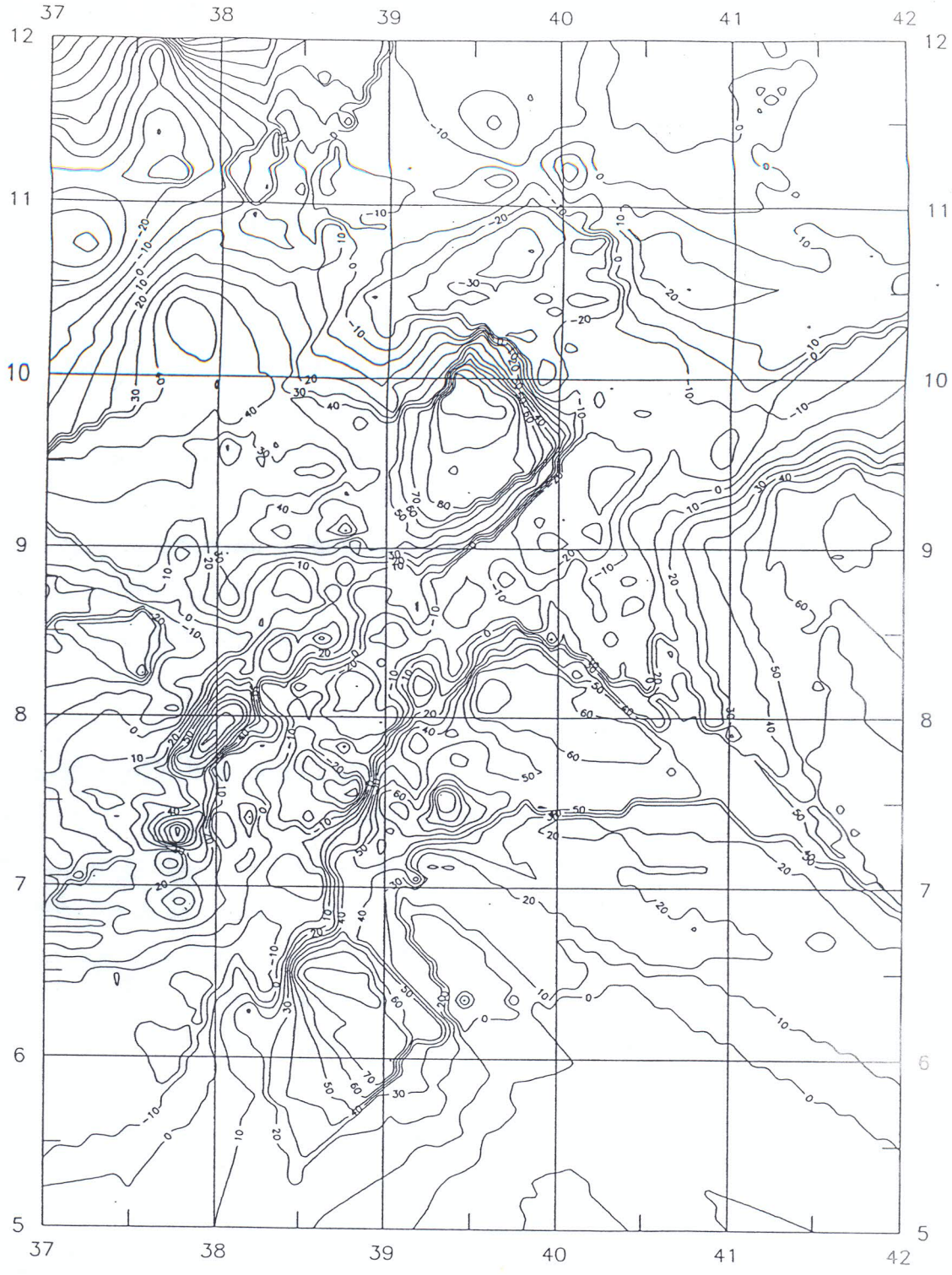

Figure 19: Free-air anomaly map of the Main Ethiopian Rift. The map is compiled by interpolating the point free-air anomalies computed at each gravity observation point on to a square grid (4'x4'). Contouring of the data at a suitable scale is done using the standard plotting software package at a contour interval of 10mGals.

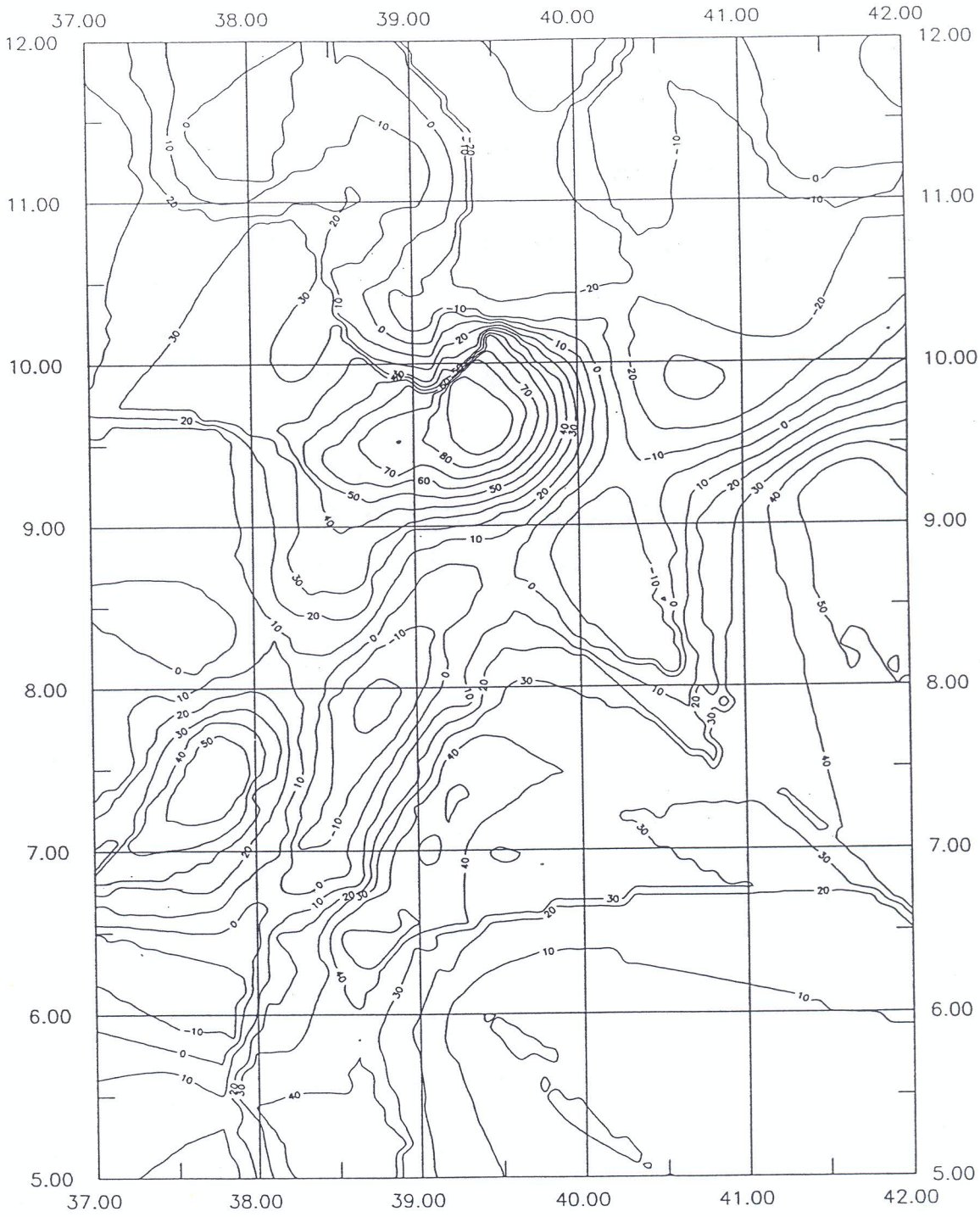

Figure 20: Free-air anomaly map of the Main Ethiopian Rift derived from OSU91A geopotential model. The free-air anomalies computed at each gravity observation point using the model (OSU91A) are interpolated on to a square grid (4'x4') and contoured at a suitable scale with a contour interval of 10mGals.

Chapter 5.

The Crustal structure of the MER from gravity and refraction seismic data

To quantitatively interpret gravity anomalies the choice of a two dimensional (2-D) or three dimensional (3-D) approach is of prime importance.

For the purpose of fitting models to the data, six profiles crossing the rift were extracted from the simple Bouguer anomaly map. The lines of the profiles are marked AA, JJ, HH, MM, SS and KK in Fig.18. Values of the Bouguer anomalies extracted from the contours of Fig.18 at a 5 km spacing, and the corresponding elevation profiles are shown in Figs. 22-27. The profiles run through the major tectonic units (the plateaus and the rift) of the region. These units are comprised of tectonic dislocations (regions of crustal attenuation) along the axis of the rift and the bounding plateaus. Gravity maxima and minima define the structures associated with the rift floor and the plateaus respectively. A glance at all the profiles shows, that the gravity anomalies contain a broad negative, 1st order regional field component with a wave length of > 100 km. Superimposed on this broad negative there is a broad (60-80 km wide) positive anomaly centered over the rift. This broad positive anomaly is modulated by smaller local gravity highs, which form well defined axial gravity highs trending approximately NNE-SSW (Fig.18).

The axial gravity highs occur usually near the center of the rift and could also be referred to as median gravity highs. Furthermore, the median gravity highs are flanked by small negative anomalies with relatively high gradients. These relatively small negative anomalies on the rift floor could be explained by the fact that the stations producing these anomalies are situated either over large thickness of lake sediments and low density rift volcanics or are affected laterally by the low density asthenosphere, which underlies the rift and its shoulders. The relatively high gradients indicate a shallow origin for the causative bodies producing these negative anomalies, and are probably the lacustrine sediments derived from quaternary volcanic rocks of Pleistocene and Holocene age that partially infill the rift floor.

To obtain a better understanding of the sources of the gravity field in the region, crustal density models were computed along the six profiles. These models are an attempt to explain the crustal structure of the area and not necessarily to explain the detailed near surface geology.

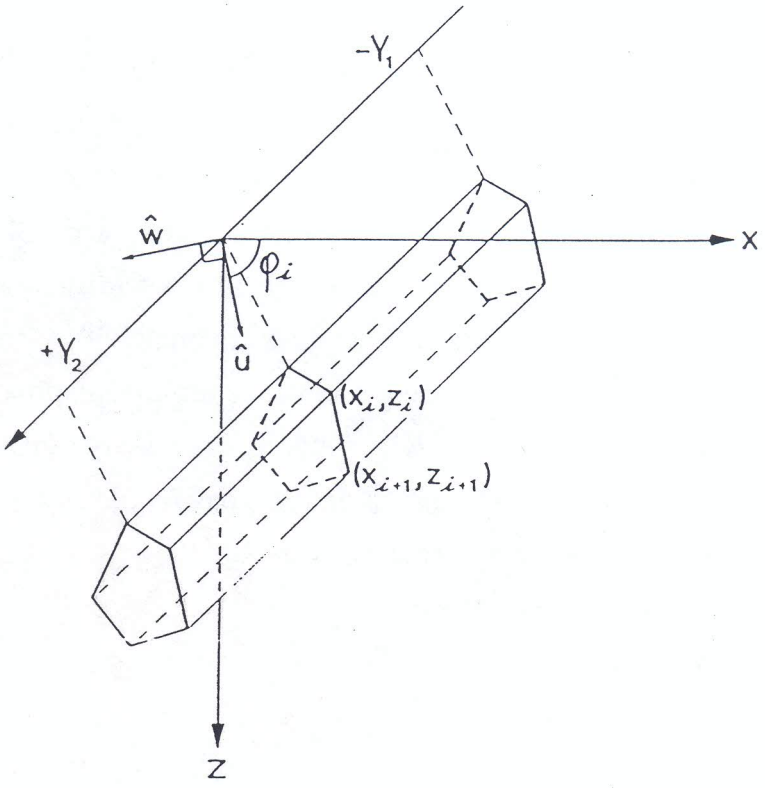

Figure 21b: 2½-D body. Strike direction is the y-direction. The 2½-D body is asymmetrical for Y_1 and Y_2 and symmetrical for $Y_1 = Y_2$. The end faces have their normals in the y-direction, and the other faces have their normals in the x-z plane (after Rasmussen and Pederson, 1979).

5.1 The gravity model

The gravity model used for the interpretation is shown in Fig. 21b. The model uses a 2½-D gravity forward modelling algorithm of Rasmussen and Pederson (1979) given below.

$$\frac{\partial g_z(\mathbf{r}_0)}{\partial z_0} = -2G\rho \sum_i \frac{\Delta x_i}{\Delta x_i^2 + \Delta z_i^2} \left\{ \Delta z_i \log \frac{r_i(R_{i+1} + Y)}{r_{i+1}(R_i + Y)} - \Delta x_i \left(\tan^{-1} \frac{u_{i+1} Y}{w_i R_{i+1}} - \tan^{-1} \frac{u_i Y}{w_i R_i} \right) \right\} \tag{13}$$

A full account on the derivation of the above formula is given in Rasmussen and Pederson (1979). This algorithm employs the well known 2-D formulae of Talwani (1973) and

Talwani and Heirtzler (1964) but slightly changed to represent a 2½-D body, i.e a body of polygonal cross section with the tails in the strike direction cut off.

The observed Bouguer anomaly values taken from the contour map along each of the six profiles are used in the computations.
The gravity model is a function of densities (ρ) and depths (z) of the different crustal layers. The densities are fixed prior to modelling while depths are varied. The computations is carried out by comparing the calculated gravity effect of the polygonal layers with the observed gravity at several points along a profile until the best fit was obtained. The objective of the calculations was to obtain models whose gravity effect possessed the same qualitative features and approximately the same anomaly shapes and magnitudes as the profiles. Since there exist an infinite number of mass distributions, which give rise to any observed gravity field, it is necessary to use all available geologic, topographic and geophysical data to define constraints and suggest and justify the assumptions necessary to construct a viable model.

In this work the constraining data are principally those of:

- The re-evaluation of the Deep Refraction Sounding Profiles of Makris and Ginzburg (1987) in the Western Plateau, the northern sector of the Main Ethiopian Rift and the Afar Depression,

- The results of the Kenyan Rift International Seismic Project (KRISP68 and KRISP85) deep seismic refraction experiments along the axis of the Kenyan rift from Lake Magadi ($1^0$30'S) to Lake Turkana ($3^0$30'N),

- The results of other seismic investigations (teleseisms and microearthquake surveys) made in Ethiopia and Kenya.

- The geological evidences available in the area and some density determinations made on rocks, which were sampled from the central part of the Main Ethiopian Rift and its escarpments especially on samples from the deep geothermal wells of Aluto Volcano by Belayneh (1983) (Appendix B).

The principal assumptions in the computations of each of the models considered here are:

- There are no lateral changes in the average density of material in a layer.

- The densities and relative thicknesses of the various layers can be changed to alter the gravity effect so long as the total thickness and average density of the column are kept constant.

- The average density of rocks increases with depth.

Once a set of crustal layers of given density and thickness are assigned to a column, the average density and thickness of the upper mantle layer can be determined. Where, however, refraction seismic data are available, the densities of individual layers are converted from the P-wave velocities using the Nafe-Drake (1963) curves for the shallow rocks and the Birch (1961) and Herbert et al. (1990) relationship for the deeper crustal and upper mantle rocks (Fig. 21). This relation is based on many measurements on different rock types and shows considerable spread so that any conversion is subject to a substantial error. The rms error in this density determination is 0.10 g/cm^3.

The following table summarizes the estimated densities for the computation of the 2-dimensional gravity models.

Table 5.1 estimated densities of crustal and upper mantle layers in the Main Ethiopian Rift.

Density interval (g/cm^3)	Velocity interval (km/s)	Layer Type
2.40-2.45	3.40-4.50	sedimentary basin
2.78	6.00-6.4	upper crust
2.95	6.60-7.20	lower crust
3.00-3.20	7.30-7.60	anomalous mantle
3.35	8.00	normal mantle

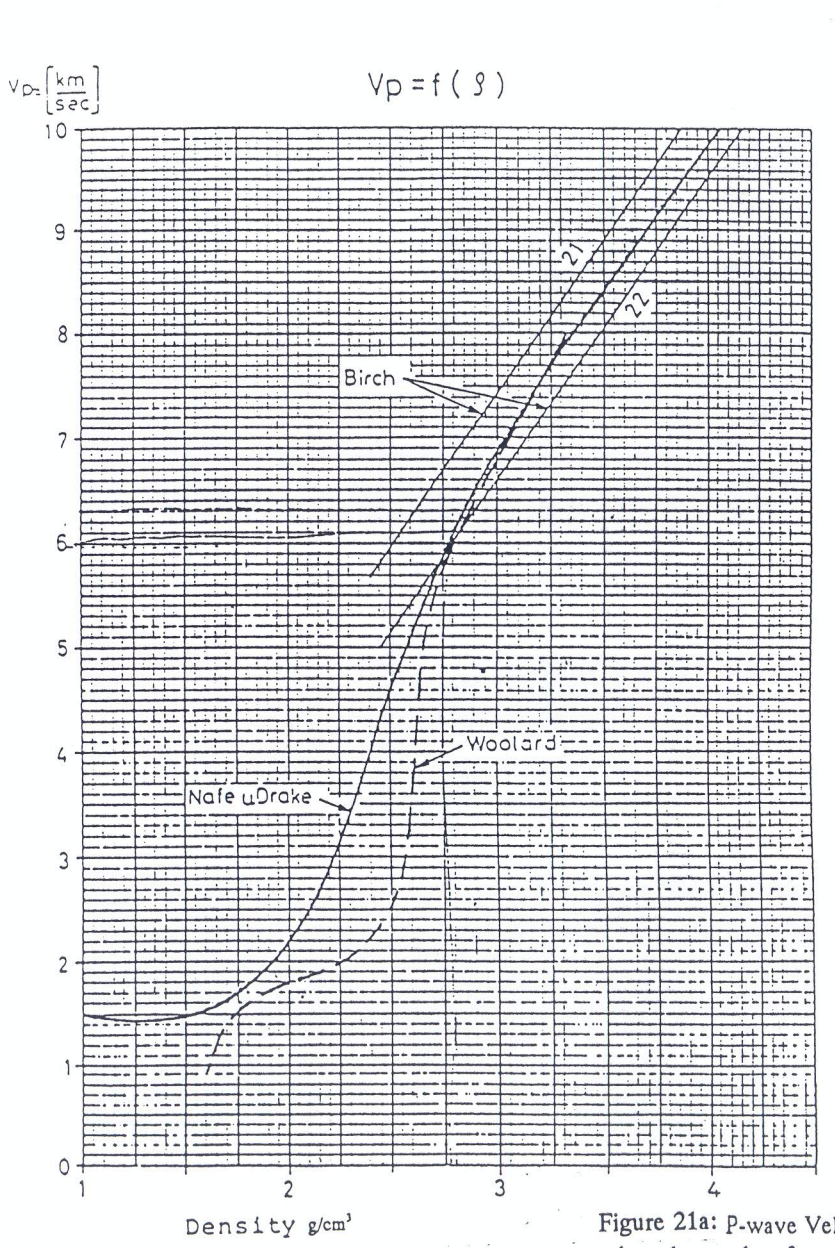

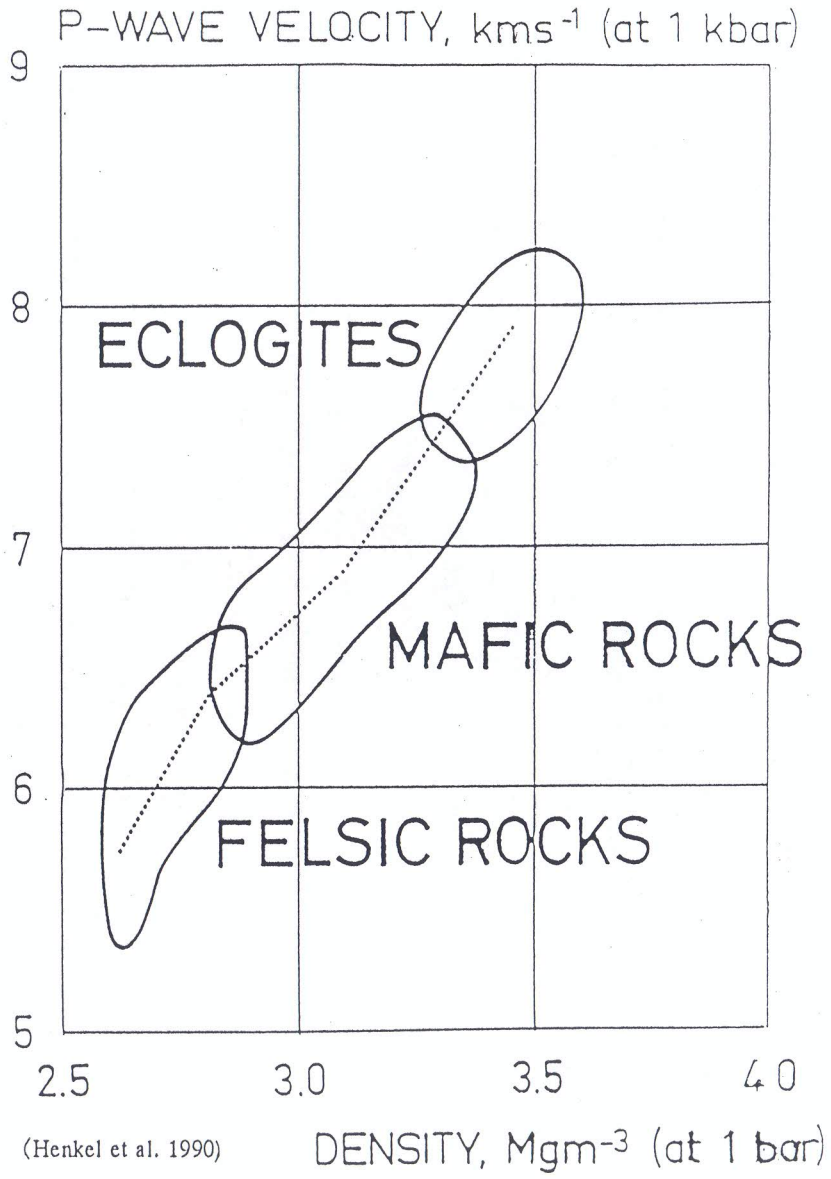

Figure 21a: P-wave Velocity-Density curves used to convert the seismic velocities to density models. The curves have been taken from Nafe and Drake, 1974, Brich 1961, Woolard 1968 and Henkel et al. 1990.

Refraction seismic data in southern Afar and the Western Plateau indicate that the crust below the Western Plateau has a typical shield type structure. It has a mean thickness of 38 km and rests on a normal mantle.

An anomalous mantle with V_p = 7.30-7.60 km/s is found beneath all the seismic refraction profiles carried out in the rift zone in Ethiopia and Kenya. The spatial variation of the depth to this layer is:

- 14 km in the salt plains of north Afar (results of profiles 5 and 6).

- 26 km in south Afar (results of profiles 3, 4 and 5).

- 30 km in the Main Ethiopian Rift (results of profile 2 and 3).

- 23 km in northern Kenya along the rift axis between the center of the Kenyan Dome and Lake Turkana (results of KRISP68 NS profile by Griffiths et al., 1972).

- 36 km along the rift axis south of Lake Bogoria (results of KRISP85 NS profile by Khan et al., 1987)

- 36 km in the southern part of the rift between Kenya and Tanzania (results of microearthquake studies by Rykounov et al. 1972).

The average thickness of the anomalous mantle layer is about 15-40 km. Most of the crust consists of material with V_p = 6.60-6.80 km/s. There also exists on all the seismic profiles in Ethiopia and Kenya a thin layer with V_p = 6.00-6.30 km/s, which is a typical velocity for an attenuated sialic upper crust.

5.2 Two-Dimensional crustal models along the selected gravity profiles

The six gravity profiles shown in Figure 18 are drawn perpendicular to a generalized axis of the Main Ethiopian Rift. The three northern profiles (AA, JJ and HH) are parallel to each other, and cross the northern sector of the rift. The remaining three profiles (MM, SS and KK), also being parallel to each other cross its southern sector. Along all the profiles the crustal density models with observed and calculated Bouguer gravity, the corresponding elevation values and the geologic sections that reflect the local geologic features are shown in Fig. 22-27. The mean density of the surface rocks exposed along each profile as estimated from density determinations given in Appendix B amounts to 2.55 g/cm^3.

The density models computed along each profile are constructed in such a way that they consist of three crustal (sedimentary basin with ρ = 2.50 g/cm^3, upper crust (crystalline basement) with ρ = 2.78 g/cm^3, lower crust with ρ =2.95 g/cm^3) layers , an anomalous mantle layer with ρ = 3.20 g/cm^3 and a normal mantle with ρ = 3.35 g/cm^3). An initial crustal thickness of 40 km, whose value is derived from the seismic refraction results of Makris and Ginzburg (1987) and results of crustal investigations by Herbert and Langston (1985) using teleseisms on the Western Plateau was used in constructing the density models.

5.2.1 Profile AA (Chefa - Meteka - Hirna)

This profile (Fig. 22) is 265 km long and starts from the Western Plateau. It crosses the northern termination of the Main Ethiopian Rift, where the gravity contours associated with the Western Plateau tend to change their orientation from NNE to N and those associated with the Eastern Plateau from NNE to E. It extends well into the Eastern Plateau across the rift and ends at 9^{0}N, 41^{0}15'E. This profile thus crosses the three major tectonic units (the plateaus and the rift) in a NNW-SSE direction in this region.

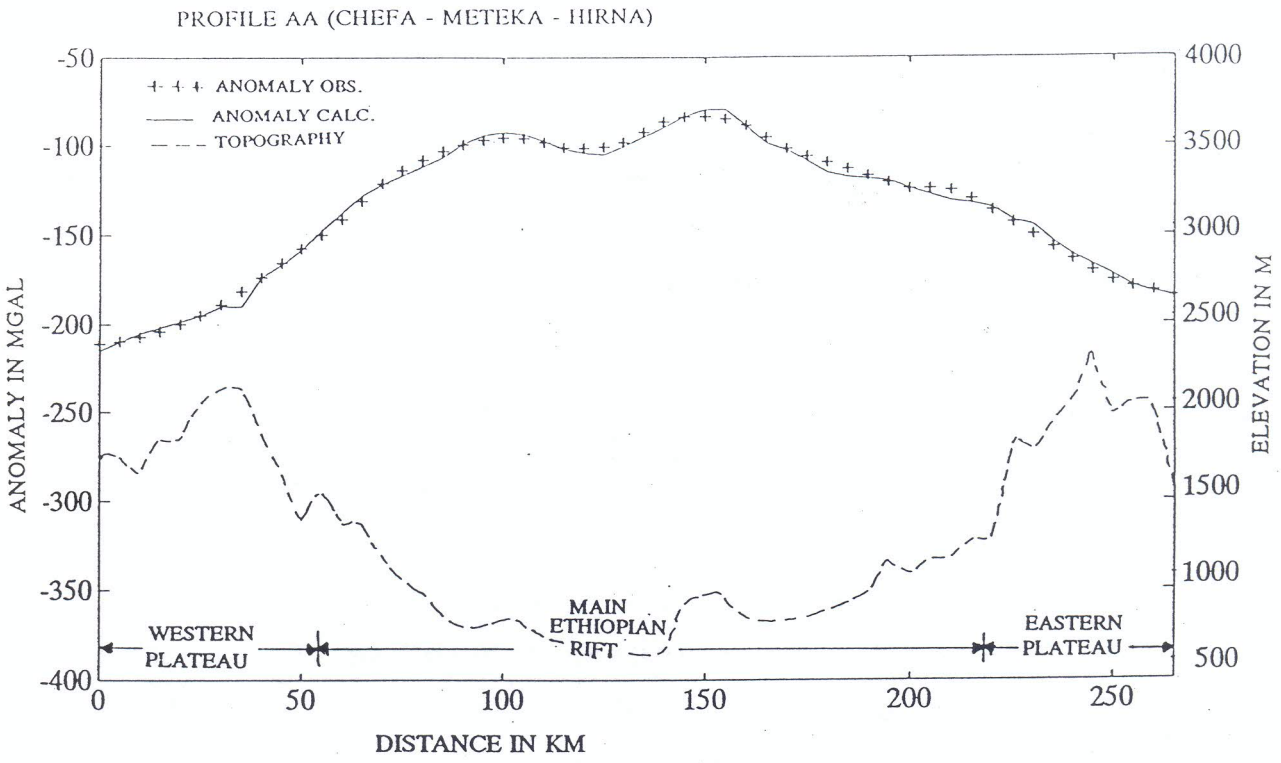

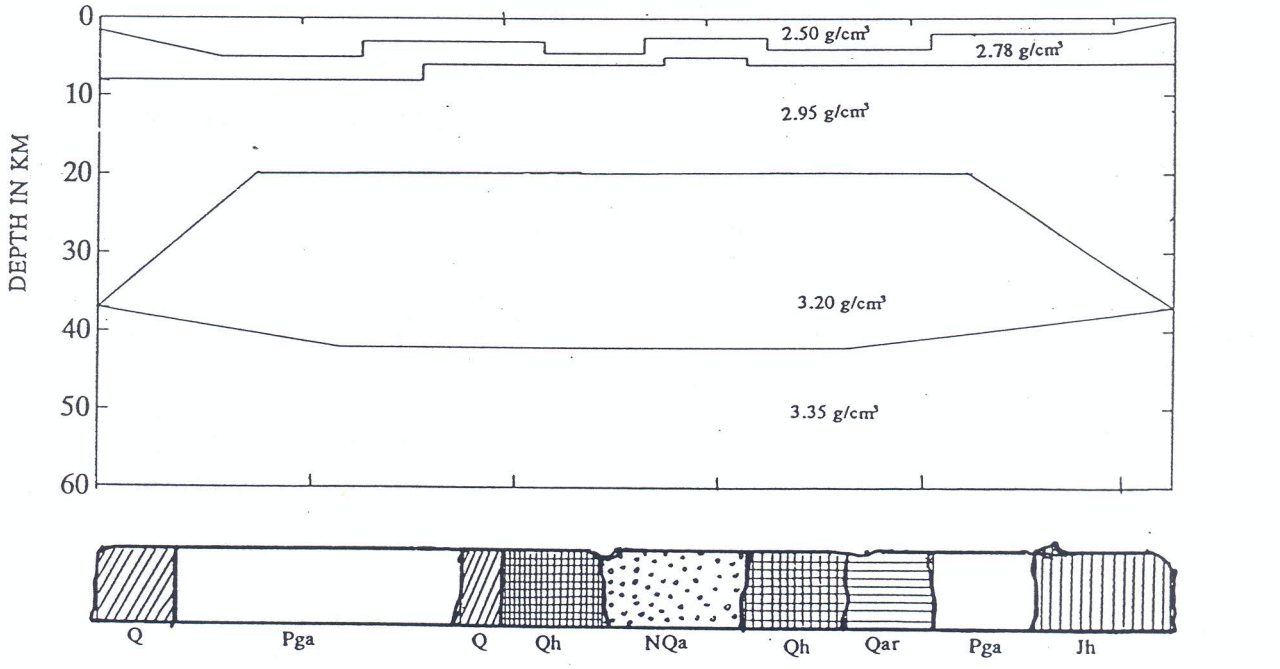

EXPLANATION

Q	Undifferentiated.	Qar	Siliceous domes and flows. Pantellerites obsidians. Complex volcanoes of andesite-trachyte-rhyolite composition.
Pga	Ashangi group (Paleocene-Oligocene-Miocene)		
Qb	Alkaline olivine basaltic flows and related spatter cones.	Jh	Lower-upper Jururassic: limestone, oolitic lime stone.
NQa	Afar group (Miocene-Pleistocene): basalts, subordinate acid lavas, ignimberites.		

Figure 22: (a) Gravity and the corresponding elevation profiles (b) Crustal density model obtained from gravity data constrained by seismic observations and (c) Geologic section that reflects the local surface geologic features along profile AA. Goodness of fit for the anomalies i.e the amount by which the calculated anomaly matches the observed one is ± 2.6 mGal. The model shows the crust beneath the rift is attenuated as compared to the normal crust beneath the plateaus due to the upward progression of the anomalous mantle to a shallow depth. Note in particular the steep gravity gradients marking the transition of the crust from one type to the other (i.e plateau-rift transition). The geologic section along this profile reveals that the central maximum positive anomaly is underlain by basalts, subordinate acidic lavas and ignimbrites. The mean dry density of the surface rocks along this profile is about 2.50 g/cm^3.

The transition of the crustal structure from one type to the other is clearly marked by steep gravity gradients (1.31 mGal/km for the western plateau-rift transition zone and 1.12 mGal/km for the eastern one). The Bouguer anomaly values increase from a minimum of -215 mGal on the Western Plateau to about +80 mGal over a 10 km wide zone at the center of the rift. Along this profile the rift widens by several km due to the tilting of the plateau blocks on either side of the rift. This tilting has resulted in the distortion of the trend of the smooth Bouguer gradients apparent on the plateau-rift transition zones to the south of this profile along the rift axis. The local geologic features along this profile are shown in the geologic section taken from the geologic map of Kazmin (1972). As mentioned earlier the average density of the whole upper mantle layer beneath the rift zone in East Africa is anomalously lower than that of a normal mantle of density 3.35 g/cm^3. It is determined to lie within the density interval estimated from the P-wave velocity /density conversion curves of Nafe-Drake, Brich and Herbert et al. (1990) The seismic refraction results (profiles II and III) in the region (Makris and Ginzburg, 1987) give a low velocity of 7.20 - 7.80 km/s for this anomalous mantle layer, suggesting a density interval of 3.00-3.20 g/cm^3. The upper limit of this density interval (3.20 g/cm^3) was used in modelling the anomalous mantle all throughout the model calculations.

Figure 22 (b) shows the results of the computed model. The model demonstrates the following main tectonic features. Starting from the eastern edge of the Western Plateau, the crust is 38 km thick. It thins to 20 km over a distance of 150 km in the rift zone and thereby increasing to 38 km at the western edge of the Eastern Plateau. The model consists of three crustal layers and two mantle layers: the top layer (sedimentary basin) consists of sediments and low density volcanics with its thickness varying from 2 to 5 km, the second layer (upper crust) with its thickness varying from 2 to 6 km, the third layer (lower crust) with its thickness varying from 7 to 30 km, the forth layer (anomalous mantle) having a maximum thickness of 27 km and the normal mantle which lies at a depth of 42 km beneath the rift and 38 km beneath the plateaus.

5.2.2 Profile JJ (Debrebirhan - Dofan - Gelemso)

This NW-SE oriented profile is 150 km long and starts from the Western Plateau near Debre Sina (Fig. 23) It crosses the northern sector of the Main Ethiopian Rift where the rift starts to funnel out into Afar. It extends well into the Western Plateau across the rift and ends at $8^0$45'N, $40^0$30'E near Gelmso. The rift floor along this profile is marked by two local maxima (-115 and -135 mGal) whose locations correspond to the location of the Dofan and Asebot volcanic centers. The transition of the crust from one type to another, like that of profile AA, is marked by steep gravity gradients. The gravity gradients on each of the plateau-rift transitions along this profile are smooth when compared with those observed along profile AA.

Figure 23 (b) shows the computed model. It demonstrates the following main tectonic features. Starting from the eastern edge of the Western Plateau, the crust is 40 km thick. It thins to 23 km over a distance of 35 km beneath the rift and thereby increasing to 40 km beneath the Eastern Plateau. The transition from the attenuated to the unattenuated normal crust (40 km thick on the plateaus) occurs within a very narrow zone on either side of the rift. This is evident from the high gravity gradients observed on the plateau-rift transition. The same density sequence as in profile AA has been used in modelling the crust and the anomalous mantle in this profile.

5.2.3 Profile HH (Gebreguracha - Welenchiti - Ageresisay)

This profile is 205 km long and starts from the Western Plateau at about the location of the minimum gravity (-265 mGal) observed on the Western Plateau in the Bouguer map of Fig. 18. It extends into the Eastern Plateau across the rift and ends at Ageresisay. Two local gravity minima located well on the Western Plateau are traversed by this profile. The transition of the crust from one type to another, like that of the previous profiles is marked by relatively less steep gradients.

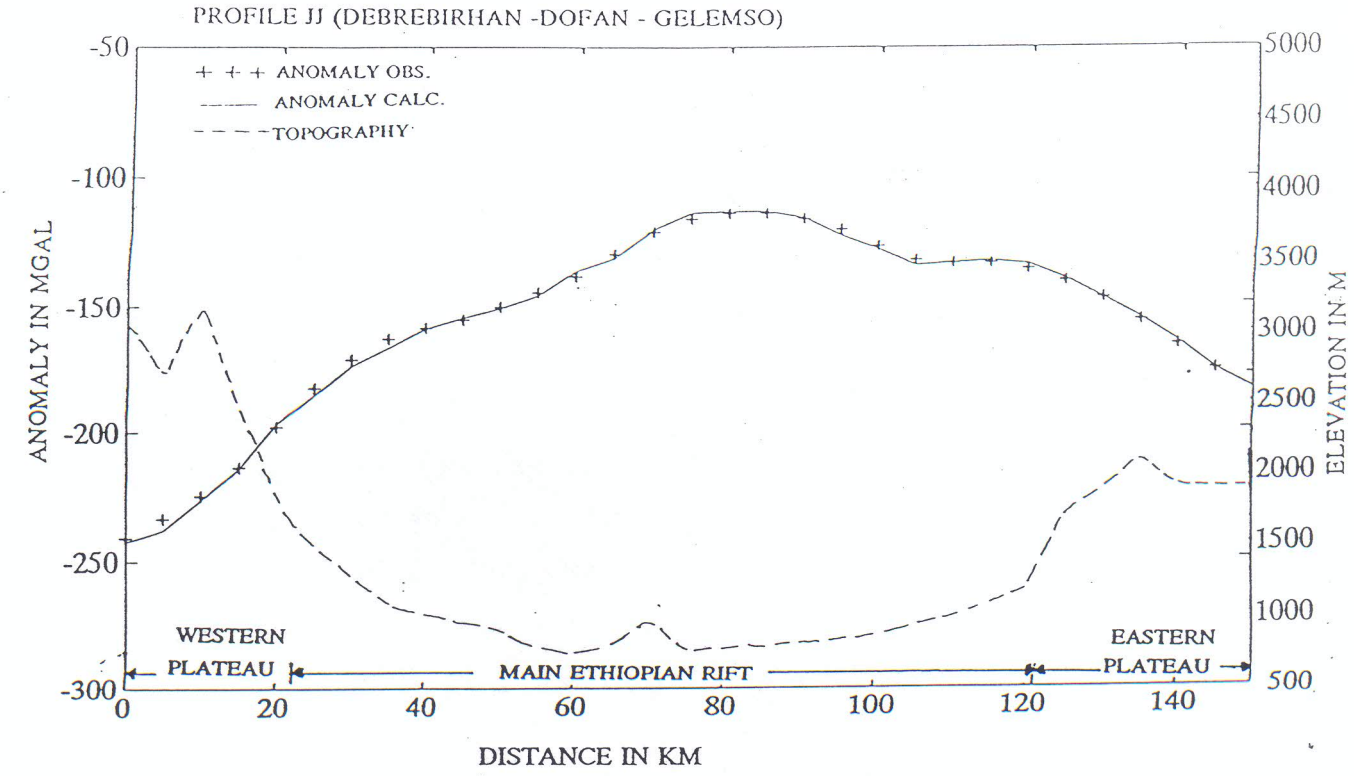

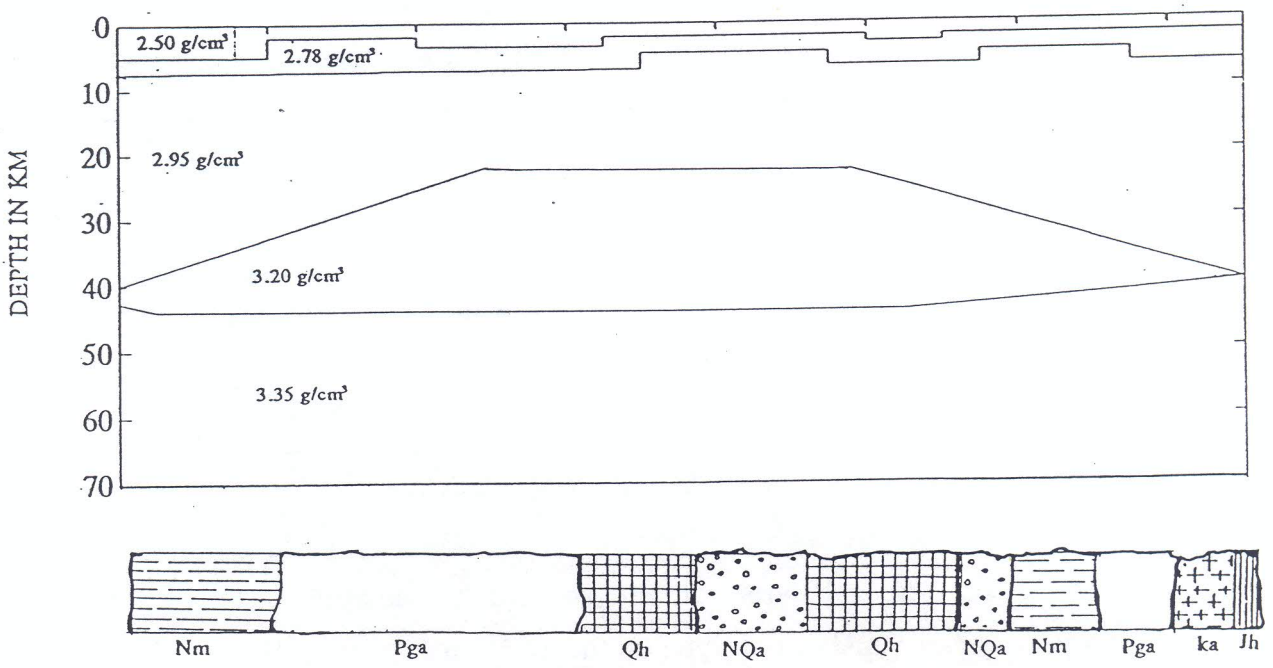

EXPLANATION

Nm	Magdala group (Upper Miocene-Pleistocene). Rhyolites, Trachytes, rhyolitis and trachytic tuffs; ignimbrites, agglomerates, basalts.	NQa	Afar group (Miocene-Pleistocene): basalts, subordinate acid lavas, ignimberites.
		Qb	Alkaline olivine basaltic flows and related spatter cones.
Pga	Ashangi group (Paleocene-Oligocene-Miocene)	Ka	Clay, silt, sandstone conglomerate (Lower Cretaceous)
Qh	Conglomerates, sands, silts, clays, reef limestone (Holocen	Jh	Limestone, oolitic lime stone (Lower-Upper Jururassic)

Figure 23: (a) Gravity and the corresponding elevation profiles (b) Crustal density model obtained from gravity data constrained by seismic observations and (c) Geologic section that reflects the local surface geologic features along profile JJ. The amount by which the calculated gravity anomaly for the model along this profile matches the observed anomaly is ± 2.5 mGal. The steep gravity gradients observed along profile AA are also evident along this profile. The regional gravity trend along this profile is similar to that of profile AA and appears to increase from the Western Plateau towards the Eastern Plateau. The geologic section displays that the surface rocks underlying this profile are also similar to that of profile AA.

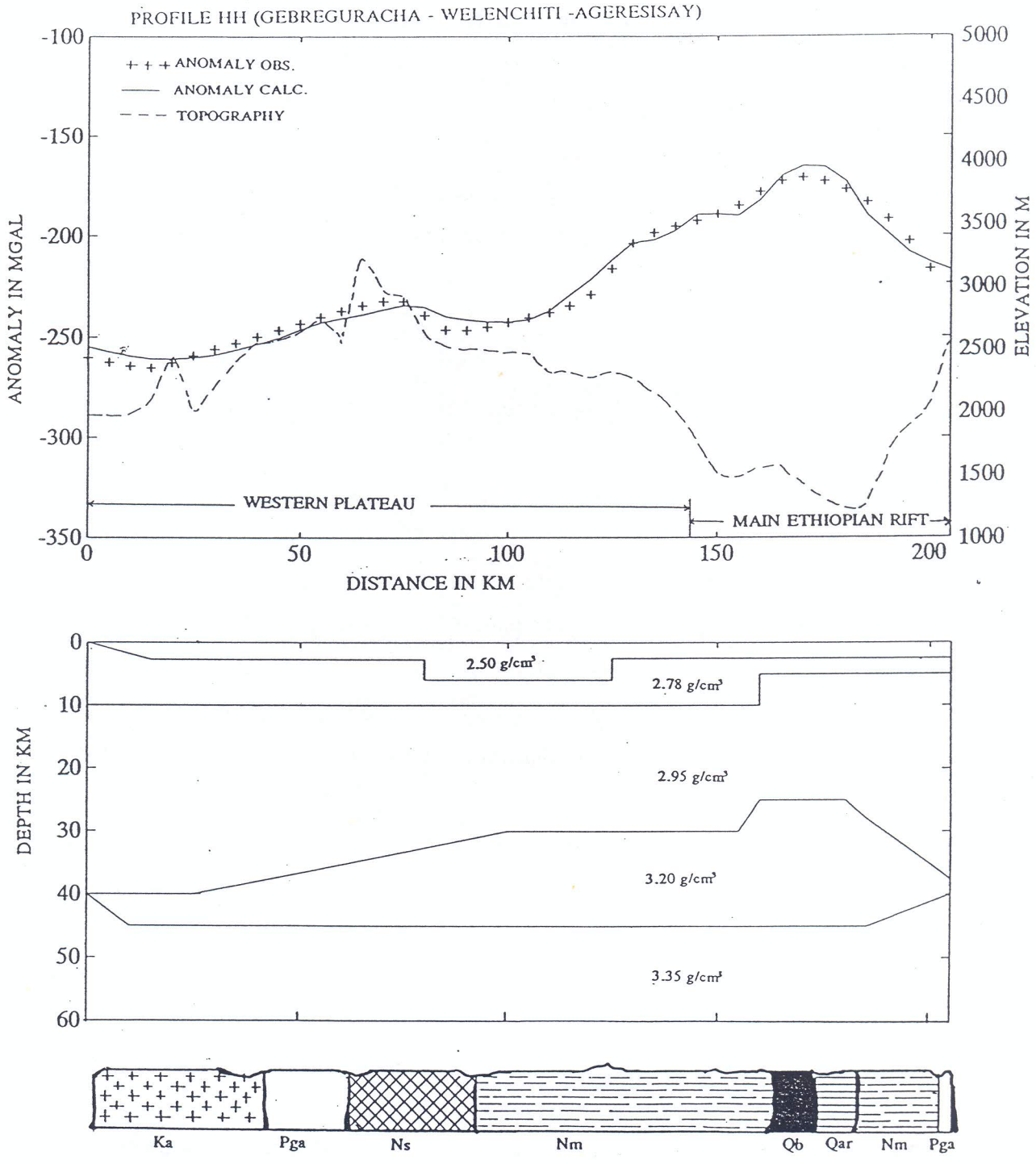

EXPLANATION

Ka	Clay, silt, sandstone conglomerate (Lower Cretaceous)	Qb	Alkaline olivine basaltic flows and related spatter cones.
Pga	Ashangi group (Paleocene-Oligocene-Miocene)	Qar	Siliceous domes and flows. Pantellerites obsidians. Complex volcanoes of andesite-trachyte-rhyolite composition.
Ns	Shield group (Miocene) alkali basalts, tuffs and agglomerates.		
Nm	Magdala group. (Upper Miocene-pleistocene). Rhyolites, Trachytes, rhyolitis and trachytic tuffs; ignimbrites, agglomerates, basalts.		

Figure 24: (a) Gravity and the corresponding elevation profiles (b) Crustal density model obtained from gravity data constrained by seismic observations and (c) Geologic section that reflects the local surface geologic features along profile HH. The amount by which the calculated gravity anomaly matches the observed one is ± 2.9 mGal. The model shows that the anomalous mantle reaches a depth of 26km indicating a moderate crustal attenuation beneath the rift zone.

Figure 24 (b) shows the computed model. It shows that the crust below the Western plateau is 40 km thick. It thins to 25km over a distance of 20 km and thereby increasing to 40 km beneath the Eastern Plateau. The velocity-depth distribution of Makris and Ginzburg (1987) for this region (profiles I, II and III) reveals crustal depth estimates of 38-40 km for the Western Plateau and 26 km for the rift. The crustal density model agrees well with this result. The anomalous mantle lies at a depth of 25 km and has a maximum thickness of 20 km.

5.2.4 Profile MM (Guder - Koka - Diksis)

This profile starts from the Western Plateau. It crosses the central part of the Main Ethiopian Rift and extends well into the Eastern Plateau. This zone is indicated on the profile by a 'zig-zag' shape of the bouguer anomaly indicating the existence of en-echelon fault patterns in the region. Such fault patterns are typical of rift zones of platforms (Appendix A). The profile also runs along a section of the Main Ethiopian rift where changes in its structural orientation (Fig. 2) are observed relative to the general trend of its southern parts. This change in orientation is due to the eastward displacement of the Eastern Plateau at $8^0$12'N and the westward displacement of the Western Plateau at 9^0N. The western plateau-rift transition zone along this profile is not clearly marked by steep gravity gradients. Two local positive anomalies in the rift floor whose locations coincide with the location of the Gedemsa and Zikwala volcanic centers (Figs. 2 and 18) are traversed by this profile. The regional gravity trend of this profile is similar to that of profile HH: i.e an increase of the gravity values from the Western plateau towards the Eastern plateau.

Figure 25 (b) shows the computed model. It reveals the following main crustal features. The crust beneath the Western Plateau is 41 km. It thins to 31 km beneath the rift and thereby increasing to 40 km beneath the Eastern Plateau. The anomalous mantle lying beneath the rift occurs at a depth of 31 km and has a maximum thickness of 14 km. It thins beneath the Western Plateau. Note that the results of the model are in good agreement with the seismic refraction and teleseisms study results of the region.

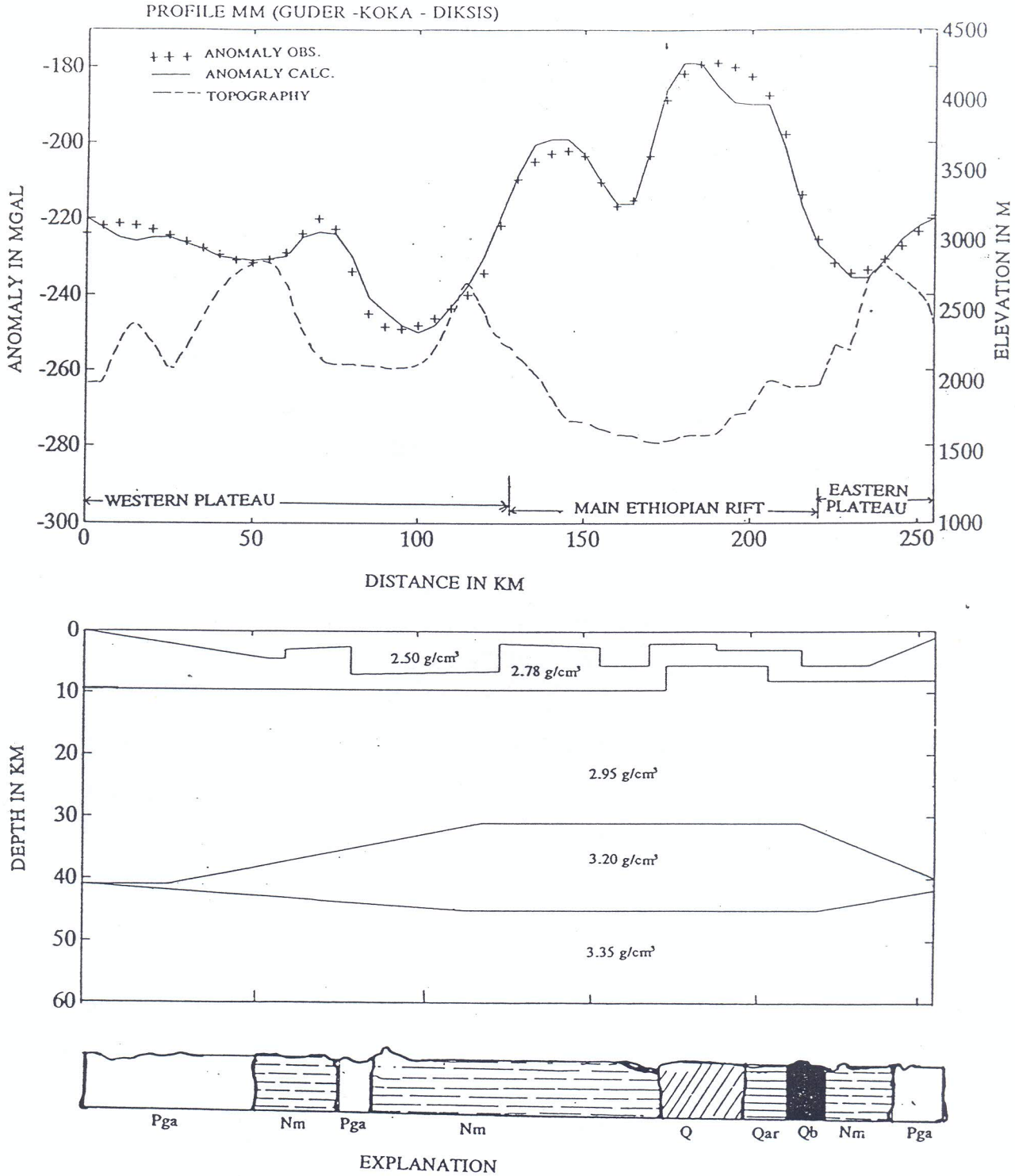

Figure 25: (a) Gravity and the corresponding elevation profiles (b) Crustal density model obtained from gravity data constrained by seismic observations and (c) Geologic section that reflects the local surface geologic features along profile MM. The amount by which the calculated gravity anomaly matches the observed one is ± 2.3 mGal. The regional gravity trend is similar to that of profile HH and appears to increase from the Western Plateau across the rift to the Eastern Plateau. The model shows a minimum crustal attenuation in the Main Ethiopian Rift as compared to the results of the previous models. The anomalous mantle here reaches a depth of 30 Km.

5.2.5 Profile SS (Hossaina - Bura - Adaba)

This profile is about 200 km long and starts from well inside the Western Plateau ($\varphi=7^0 30'N$, $\lambda=37^0 45'E$) near the village of Hossaina. It forms a traverse which is perpendicular to the Main Ethiopian Rift axis at latitude $7^0 15'N$, extends well into the Eastern Plateau across the rift and ends at $7^0 00'N$, $39^0 20'E$. The profile crosses the gravity minimum (-265 mGal) observed on the Eastern plateau in the study area. The magnitude of the local gravity maximum (-195 mGal) observed beneath the rift along this profile is the minimum as compared to the magnitude of other local maxima observed along the rift axis in the study area. The regional gravity trend of this profile is similar to that of profile KK: i.e. a decrease of the gravity values from the Western Plateau towards the Eastern Plateau.

Figure 26 (b) depicts the calculated model. It demonstrates the following main features. The crustal thickness beneath the Western Plateau is 40 km. It thins to 30 km beneath the rift thereby increasing to 40 km beneath the Eastern Plateau. The calculated model is consistent with the results of profile MM discussed above. The anomalous mantle beneath the rift is defined over a 100 km zone and is 20 km thick with its top surface lying at 30 km depth.

5.2.6 Profile KK (Humbo - Abaya - Hagereselam)

This last approximately E-W and 105 km long profile also extends from the eastern margin of the Western Plateau and extends to the western margin of the Eastern Plateau. It crosses the gravity maximum associated with the tectonic depression of Lake Abaya. The local gravity maximum (-165 mGal) observed along this profile is greater than that of along profile SS, indicating that the level of the positive gravity field along the rift axis increases southwards beginning from the latitude of profile SS ($7^0 30'N$).
The regional gravity trend of this profile is similar to that of profile SS, i.e. a decrease of the gravity values from the west to east along the profile.

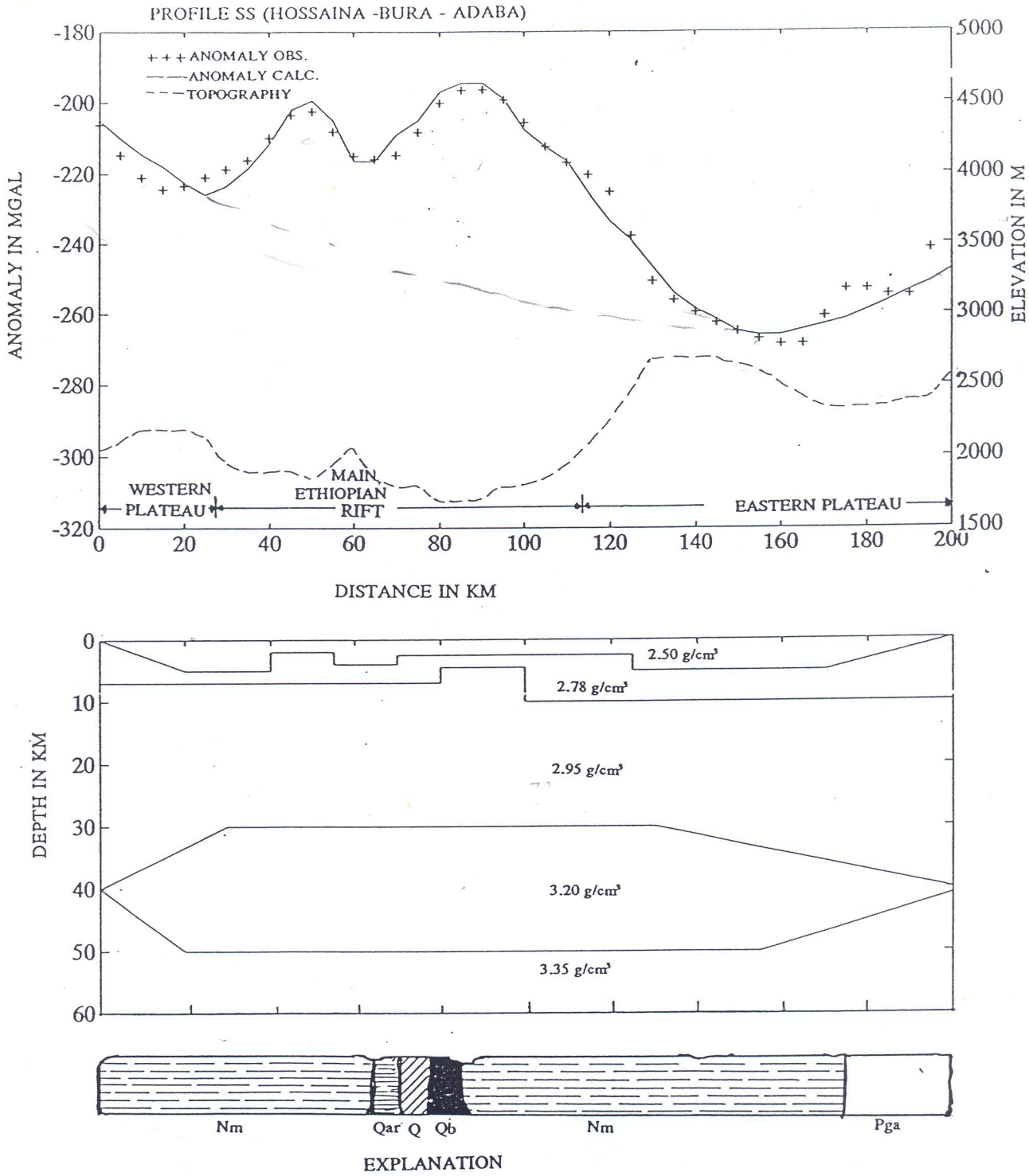

Nm Magdala group. (upper Miocene-Pleistocene). Rhyolites, Trachytes, rhyolitis and trachytic tuffs; ignimbrites, agglomerates, basalts.

Qar Siliceous domes and flows. Pantellerites obsidians. Complex volcanoes of andesite-trachyte-rhyolite composition.

Q Undifferentiated.

Qb Alkaline olivine basaltic flows and related spatter cones.

Pga Ashangi group (Paleocene-Oligocene-Miocene)

Figure 26: (a) Gravity and the corresponding elevation profiles (b) Crustal density model obtained from gravity data constrained by seismic observations and (c) Geologic section that reflects the local surface geologic features along profile SS. The amount by which the calculated gravity anomaly matches the observed one is ± 2.2 mGal. The model shows the results obtained here are very much identical to those of profile MM. The regional Bouguer anomaly trend along this profile decreases from the Western Plateau to the Eastern Plateau.

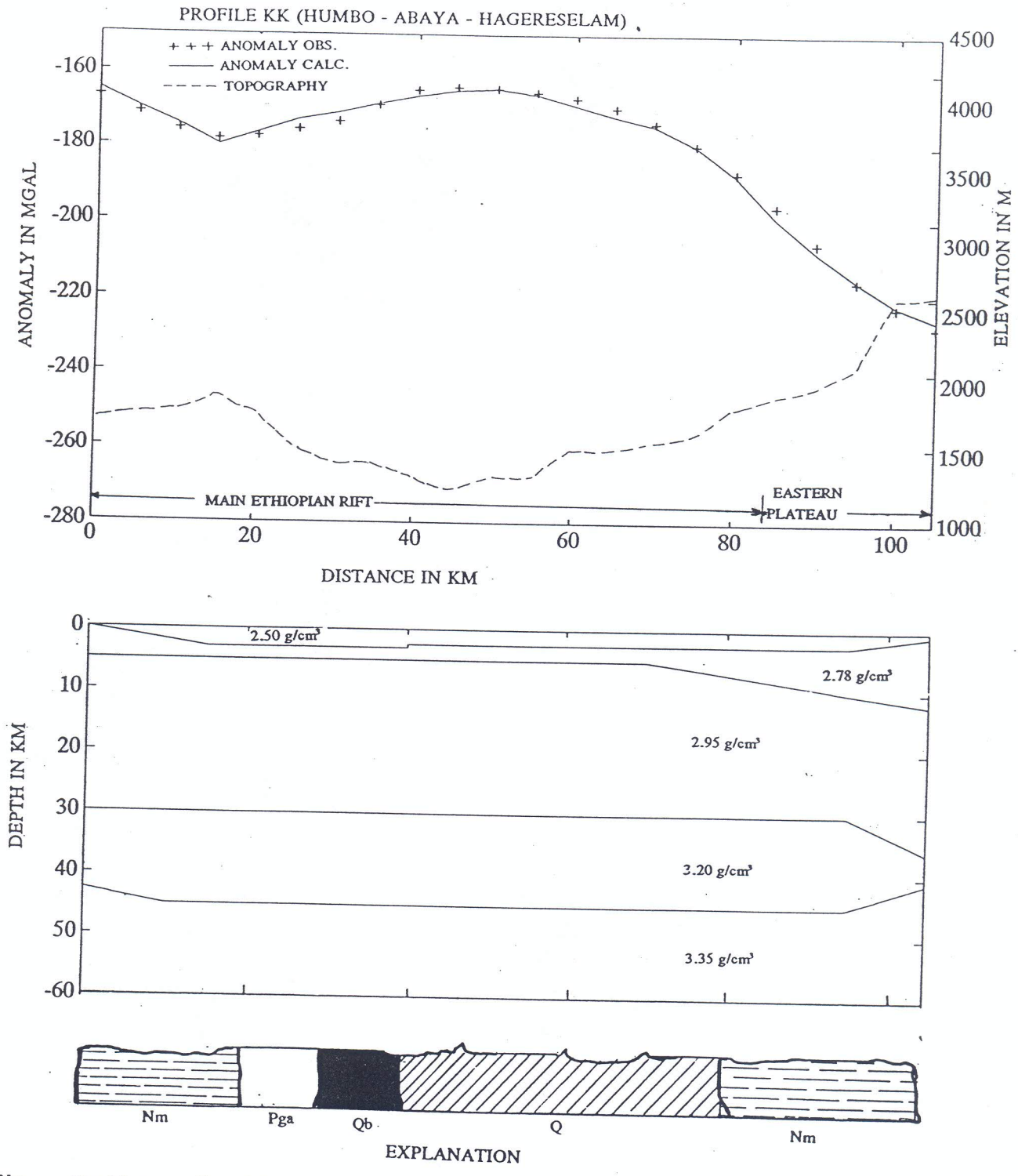

Figure 27: (a) Gravity and the corresponding elevation profiles (b) Crustal density model obtained from gravity data constrained by seismic observations and (c) Geologic section that reflects the local surface geologic features along profile KK. The amount by which the calculated anomaly matches the observed one is ± 1.3 mGal. The regional anomaly trend along this profile is similar to that of profile SS i.e decreasing from west to east.

Figure 27 (b) shows the calculated model. It shows that the crust below this profile is 30 Km thick. The anomalous mantle lies at a depth of 30 km and has a thickness of 15 km. The results of the crustal density model calculations are found to be identical with the results of the seismic observations.

5.3 Gravity profile across the East African Rift

Regional gravity field investigations across the rift zone in East Africa have shown long wave length (broad) negative Bouguer anomalies with superimposed short wave length (narrow) positive anomalies over the rift axis. The regional negative anomalies are interpreted by Girdler et al.(1969), Girdler and Sowerbutts (1970), and Baker and Wohlenberg (1971) in terms of an upward thinning of the lithosphere and replacement by lower density asthenosphere beneath the East African uplifted regions. The axial short wave length positive anomalies are interpreted by Searle, (1970) as being due to intrusive zones in continuity with the lower density asthenosphere (i.e extreme thinning of the lithosphere beneath the rift floor in East Africa).

For the interpretation of the long wave negative Bouguer anomaly three gravity profiles crossing the African continent in an E-W direction across the East African Rift zone were analyzed by Brown and Girdler (1980). In their interpretation of the long wave-length negative Bouguer anomalies they assumed that the lower part of the lithosphere has been replaced by a slightly less dense asthenosphere. This involves thinning of the lithosphere under large regions of the plateaus. The main results are that there is a large variation in lithospheric structure associated with the East African Rift system. The lithosphere is thinnest beneath the Eastern rift as compared to the Western one, and the thinning increases from south to north.

Crustal models shown in Fig. 28a were constructed for the three profiles A, B and C. The figure shows that the long wave-length Bouguer anomalies associated with the East African Rift System is evident along all the three profiles. Furthermore, the central zone

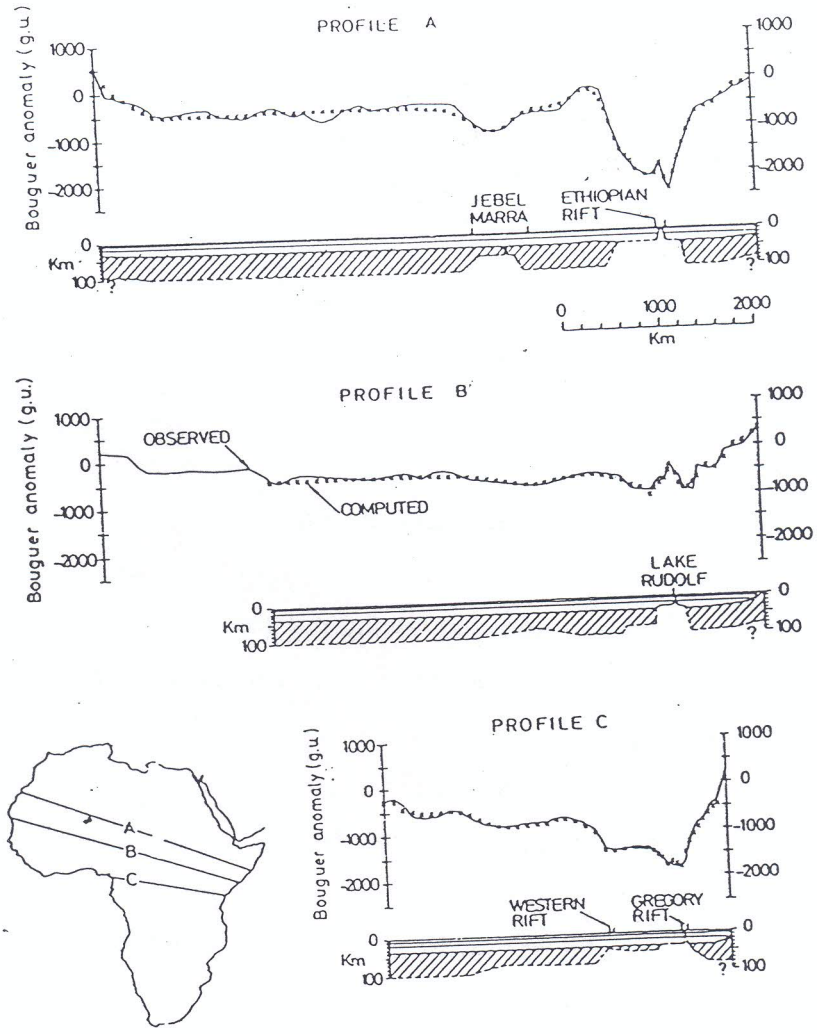

Figure 28a: Models of the structure of the lithosphere satisfying the Bouguer gravity anomalies along profiles A, B and C projected across the axis of the East African rift system (after Brown and Girdler, 1980). The models have shown; (1) a wide variation in the crustal structure of the East African rift system, (2) the crust is thinner beneath the Eastern rift and (3) the thinning increases from south to north along the rift axis.

of the rift is marked by a short wave-length positive Bouguer anomaly superimposed on the long wave-length negative one. The interpreted models indicate thinning of the lithosphere due to the existence of a low density (3.20 g/cm^3) asthenospheric material (anomalous mantle) below the rift zone. The subsequent upward expansion of this anomalous mantle material gives a negative density contrast (3.20 - 3.35 = -0.15 g/cm^3) with respect to the normal mantle causing the long wave-length negative Bouguer anomaly. The further upward expansion of the low density material into the lower crust (ρ = 2.95 g/ cm^3) gives the positive density contrast (3.20 - 2.95 = 0.25 g/cm^3) causing the superimposed short wave-length positive anomaly beneath the rift.

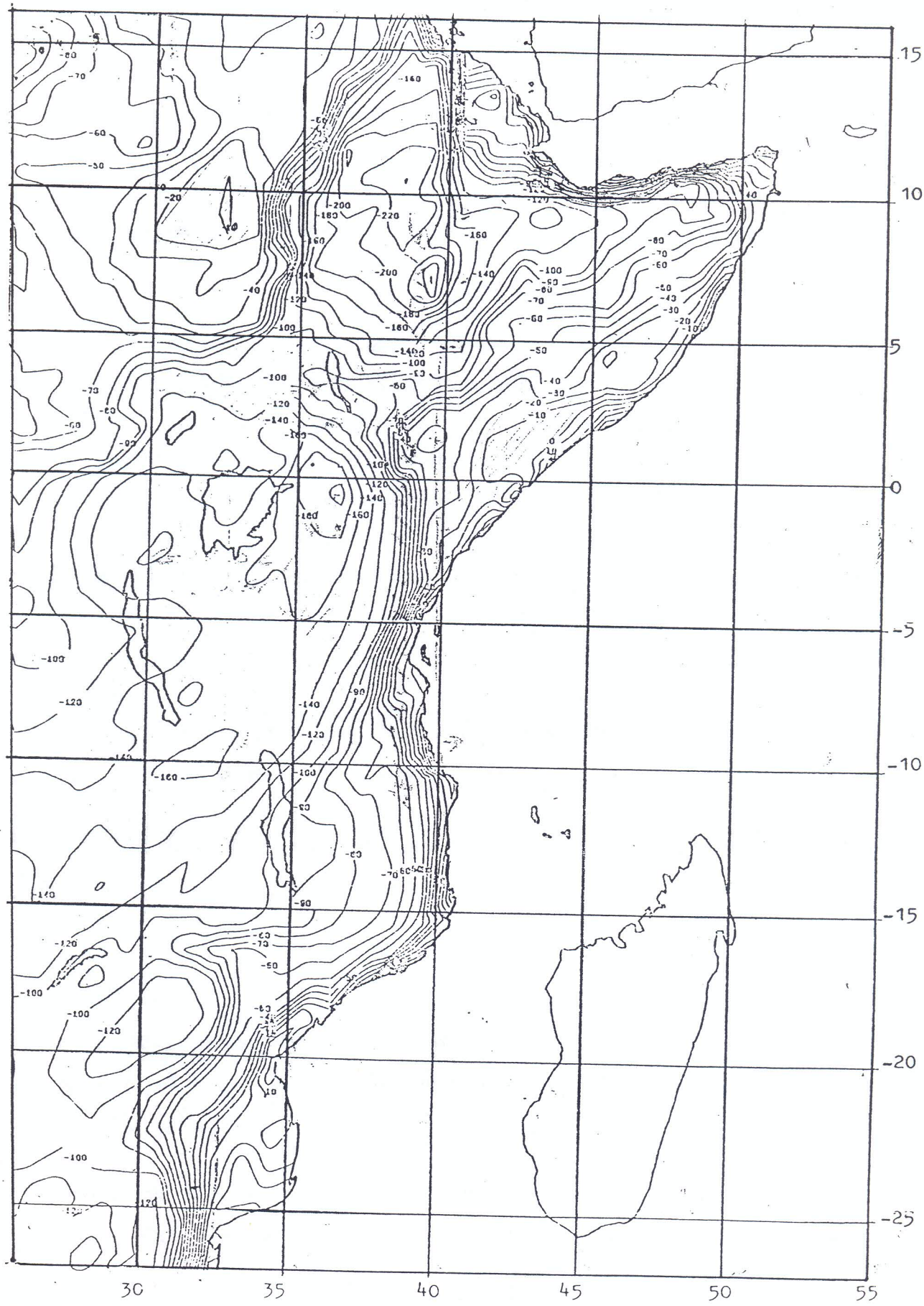

Figure 28b. NASA gravity map of eastern Africa drawn at 20 mGal interval.

Chapter 6.

Isostatic balance and the crustal structure of the Main Ethiopian Rift and the adjacent plateaus

6.1 Regional variations in Bouguer anomalies with respect to topography: General principles

Gravity anomalies indicate irregularities in the distribution of mass within the earth. Topography is a measure of irregularities in shape of the outer surface of the solid part of the earth. The relationship between gravity anomalies and topography is dependent on the distribution and magnitude of mass anomalies at depth within the earth as well as the mass due to the topography. This distribution of mass anomalies at depth in turn depends upon the tectonic processes that created the features and the physical properties of the crust. G.P. Woolard, 1969, studied the regional variations in gravity using data from USA, Canada, Alaska, Mexico, Central America, South America and India. Woolard's study revealed the following:

1. There is a strong correlation between gravity values and topographic relief, changes in geology, changes in crustal composition and anomalous thickness of the earth's crust.

2. The relationship between free-air anomalies and elevation is governed by the width (wavelength) of the anomalies associated with the topographic blocks making the overall relief pattern of a region (a continent).

3. Since there is a +300 mGal change in Bouguer anomaly value for a 3000m change in elevation, which significantly exceeds that attributable to unknown geological effects (±10 to 30 mGal), Bouguer anomalies usually describe the best relation between gravity anomaly and elevation.

4. Gravity anomalies over a crust at isostatic equilibrium are caused by changes in the crustal density and thickness. If the gravity anomaly changes positively with a change in

elevation then the anomaly gradient is always positive and vice versa.

5. For a crust, which is not isostatically balanced, due to tectonic displacements, the anomaly is caused by the tectonic displacement. The gravity gradient, in this case, is positive with a change in elevation, when the anomaly is over a graben.

The sign and gradient of a gravity anomaly is therefore a function of the width (wavelength) of the mass disturbance. The shorter the wavelength, the more pronounced the anomaly. The anomaly can however be produced by a combination of the above two (4. and 5.) effects. For example, a graben which is intruded by high density basic rocks, that may or may not have surface expression as basalt flows, may account for the above anomalies. These are characterized by positive gravity values (example Red Sea).

6.2 Isostatic balance and crustal structure: General principles

Calculations based on gravity measurements, and correlated with seismic experiments reveal that isostatic balance is approximately maintained over extensive areas of the earth's crust. the distribution of Bouguer anomalies over the world correlates with the topography. Free-air anomalies are in general near zero. This means the earth's crust is essentially in isostatic equilibrium. Visual analysis of the gravitational field and relief features give little indication about the structure of the earth's crust and upper mantle. Only in regions like transitional zones (i.e from oceans to continents), oceanic troughs, etc are gravity anomalies sufficiently clear to give visual evidence of sharp changes of mass distributions in the crust and upper mantle, as well as disturbances of isostatic balance. For great land masses (continents), isostasy is actively valid according to the Airy-Heiskanen's model (Heiskanen and Moritz, 1967) that is, mountain ranges are associated with roots below, whereas oceanic regions are floating over antiroots (Fig. 29).

The degree of isostatic compensation and also the position of the Moho surface will therefore depend on different factors including the morphology of the physical surface of the earth. Consequently, both Bouguer anomalies and altitude values could be used for studying the behaviour of the Moho surface and for determining its depth (Andreev, 1958;

Woolard, 1969a; Demenitskaya and Belyaevsky, 1969). Hence, a quantitative evaluation of the available geophysical data is clearly needed.

A gravity anomaly over a large topographic high, must be compensated by a mass deficiency at depth. This is necessary to offset the excess mass that forms the topography at the surface. Thus, for features in isostatic equilibrium, mass deficiency (lower density material at the base of the crust) occurs beneath regions having high topography; whilst a mass excess (higher density material at the base of the crust) occurs beneath regions of topographic depression. Within the earth, this accommodation is largely achieved through undulations in the Moho discontinuity or simply the Moho.

The Moho is the boundary between the earth's crust and mantle. It is also referred to as that level in the earth's crust, where the P wave velocity increases rapidly or discontinuously to a value between 7.60 and 8.60 km/s. Thus mantle material of high density lies within about 10 km (i.e shallow Moho depth) beneath the deep ocean areas of the world to compensate for the thickness of water which has low density relative to a continental crust. Conversely, the Moho lies at great depths of 40 to 60 km beneath high mountain ranges; and close to 30 km beneath continental plains at low elevation.

In this work the isostatic behaviour of the Main Ethiopian Rift and the adjacent plateaus will be investigated using the following methods.

1. Computation of the isostatic Moho depth map according to the Airy-Heiskanen model of isostatic compensation (Fig. 29).

2. Computation of mass distributions along the seismically controlled 2-D density models, summed up to different depth levels.

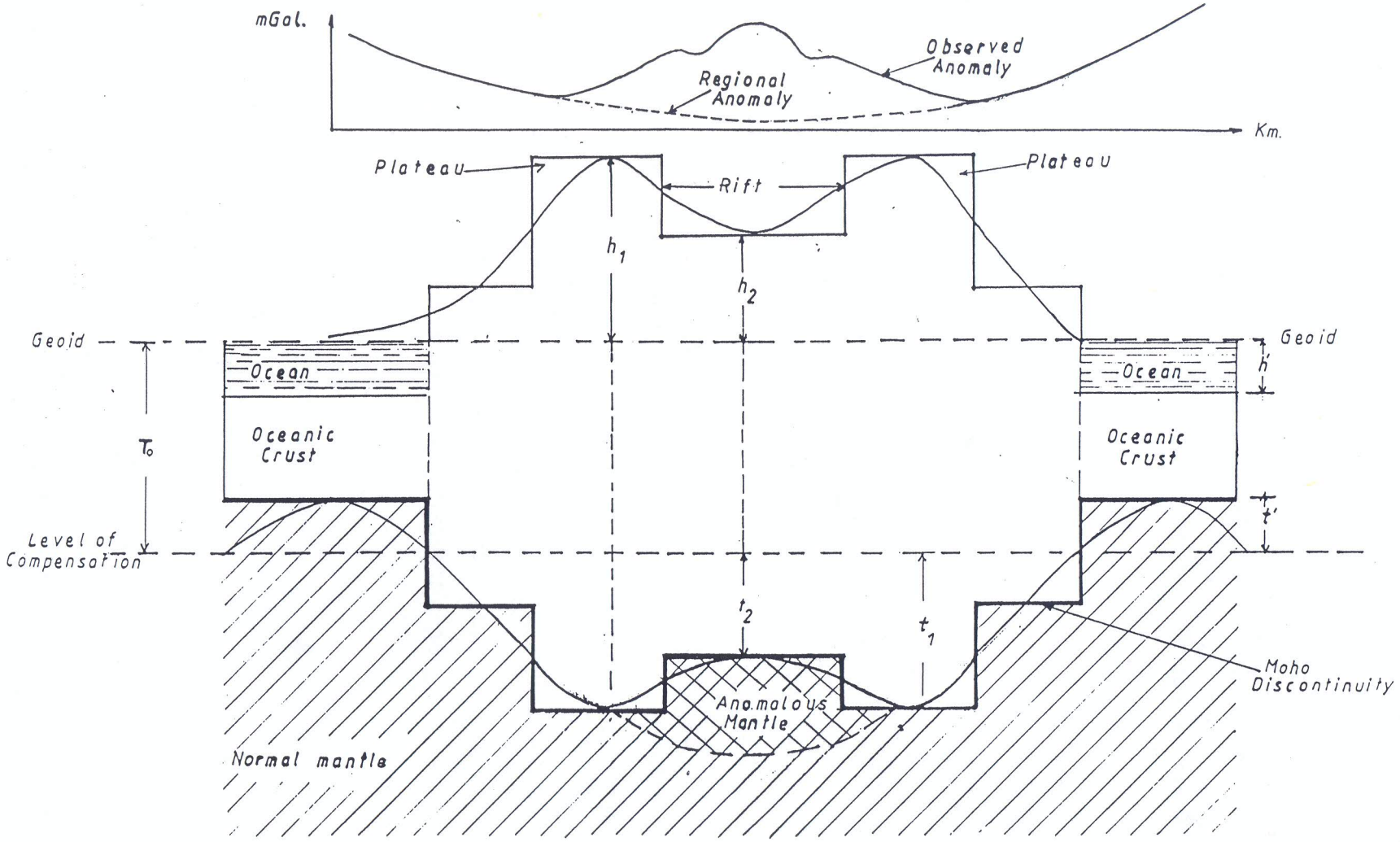

Figure 29: Schematic diagram of the Airy-Heiskanen Isostatic model used for the computation of Moho depth in the Main Ethiopian Rift and the adjacent plateau regions.

6.3 Isostatic Moho-depth map of the Main Ethiopian Rift and the adjacent plateaus.

The isostatic Moho-depth map was computed to check the regional isostatic trend of the Main Ethiopian Rift and the adjacent plateaus, according to the Airy-Heiskanen model of compensation (Fig.29). The parameters used in the calculations were defined according to the seismic results and the 2-D gravity models described earlier. The seismic results and the 2-D gravity models reveal that the normal mantle beneath the Western Plateau lies at a depth of 38-42 km.

The mean crustal thickness "Normal crust", T_0 (zero elevation) was taken to be 25 km for the plateaus, 20 km for the rift valley. A density contrast of 0.40g/cm^3, between the upper mantle density (ρ_{UM} = 3.35g/cm^3) and the mountain root zones (ρ_R = 2.95g/cm^3) was used in the calculations. Isostatic compensation was assumed to occur locally. This means that flexuring of the crust in the vicinity of a load is neglected (i.e. the crust has zero lateral strength). A mean density of (ρ_T = 2.67g/cm^3) was used for the topographic masses.

Using these parameters and assumptions, the mean elevations h_i within a 10000mx10000m grid were converted into root zone depths (t_i) and added to the mean crustal depth T_0 to obtain the depth of the Moho (T_M).

$$T_M = T_0 + t_i \qquad (14)$$

where

$$t_i = h_i\, \rho_T/(\rho_{UM}-\rho_R) \qquad (15)$$

Elevations ≥ 2000m were taken to correspond to the plateaus and those of < 2000m to the rift.

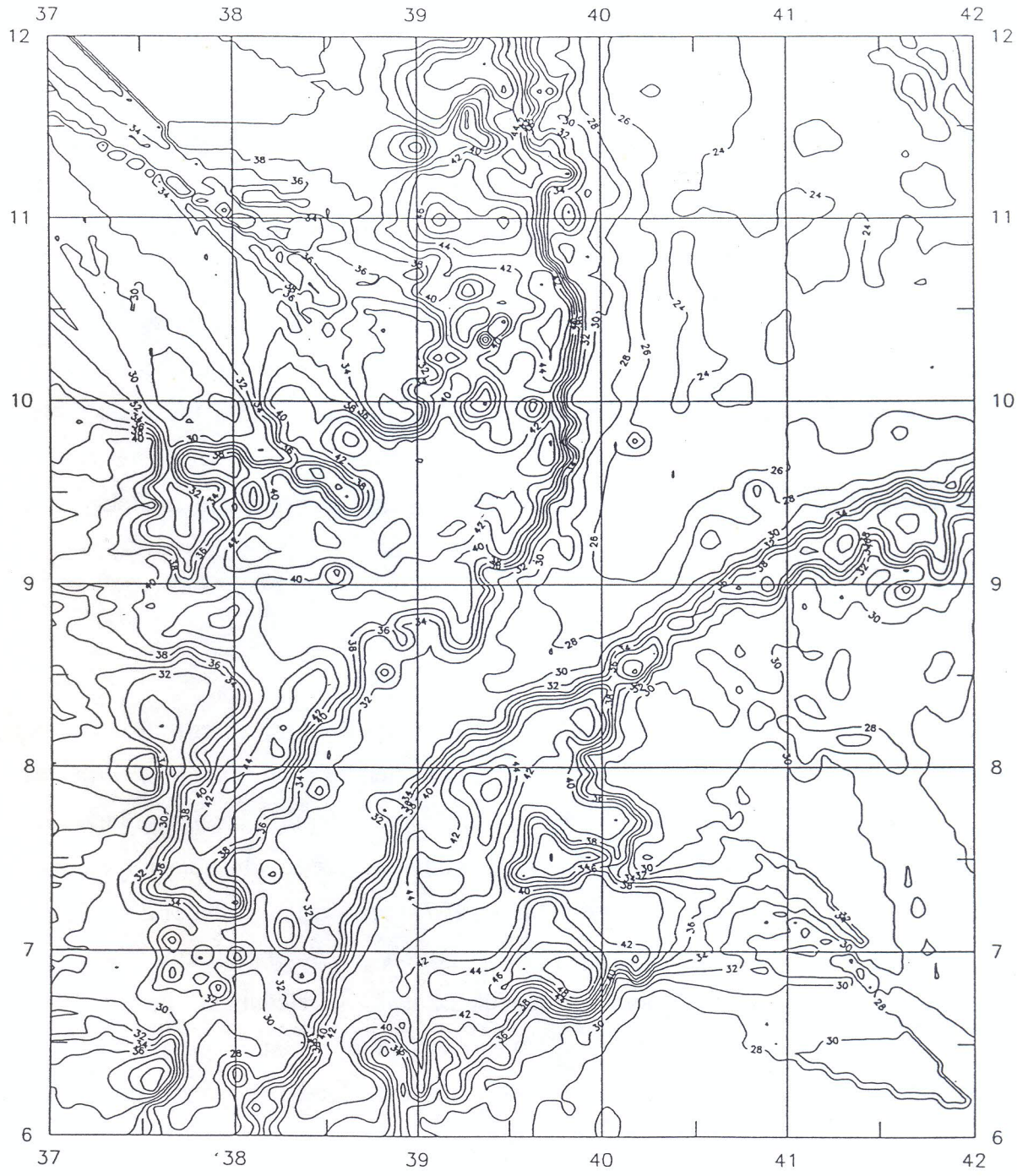

Figure 30: Isostatic Moho depth map of the Main Ethiopian Rift and the adjacent plateaus. The thickest crust is found in both the Western and the Eastern plateaus at the gravity minima. The Moho reaches a maximum of 46km beneath the high mountains of the Western plateau and 50km depth beneath those of the Eastern plateau. A steep gradient on the escarpments defines the transition of the Moho from both the Western and Eastern plateaus towards the rift eventhough it looks less steep on the Eastern side. In the central part of the Main Ethiopian Rift the Moho is at a uniform depth of 30 km, suggesting that the topography of the rift volcanoes has no response at this depth. The junction of the Main Ethiopian Rift and the Afar depression is marked by a Moho depth of 24km. Furthermore the signature of the Moho map clearly defines the location and orientation of the most prominent structures (the rift and the plateaus) in the region.

Fig.30 depicts the calculated map. The map reveals the following main features. The Moho depth in the most western part of the Western Plateau in the area considered is 28 km. It increases towards the center of the plateau and reaches a maximum value of 46 km beneath the highly elevated regions north and south of the Addis Ababa district. At the latitude of Addis Ababa (9^0N) the Moho attains an approximately constant value of 40 km from east to west until the rift escarpment is reached and this magnitude is comparable with the seismically determined Moho. On the Eastern plateau the Moho reaches a maximum depth of 50 km beneath the Batu mountain range. On both the Eastern and Western Plateaus, the locations of Moho depth maxima correspond to Bouguer gravity minima.

6.4 Mass distributions along the 2-D gravity models

Under the ideal conditions assumed for isostatic equilibrium, all crustal columns exert equal pressure at some depth. The crustal column extending above sea level with elevation h has a mass equal to that of the compensating mass at depth. This assumption was used in the gravity model calculations. To determine the degree to which each model attained isostatic balance, mass distributions (Makris, 1978) were calculated along each profile, at the profile points and summed up per cm^2 at 20, 30, 40, 50 and 60 km depth. The mass of the topography at each point, was calculated using its elevation value and the mean crustal density 2.67 g/cm^3. The model was considered isostatically balanced at a level where the total mass per cm^2 along the entire profile attained an approximate constant (the mean value of the sums at each profile point) value.
The results of these computations are discussed below for each model.

6.4.1 Profile AA (Chefa - Meteka - Hirna)

This profile begins at the Western Plateau ($\varphi=11^0$00'N, $\lambda=39^0$45'N) and runs across the northern end of the Main Ethiopian Rift and extends well into the Eastern Plateau. It thus crosses the three major tectonic units in the region.

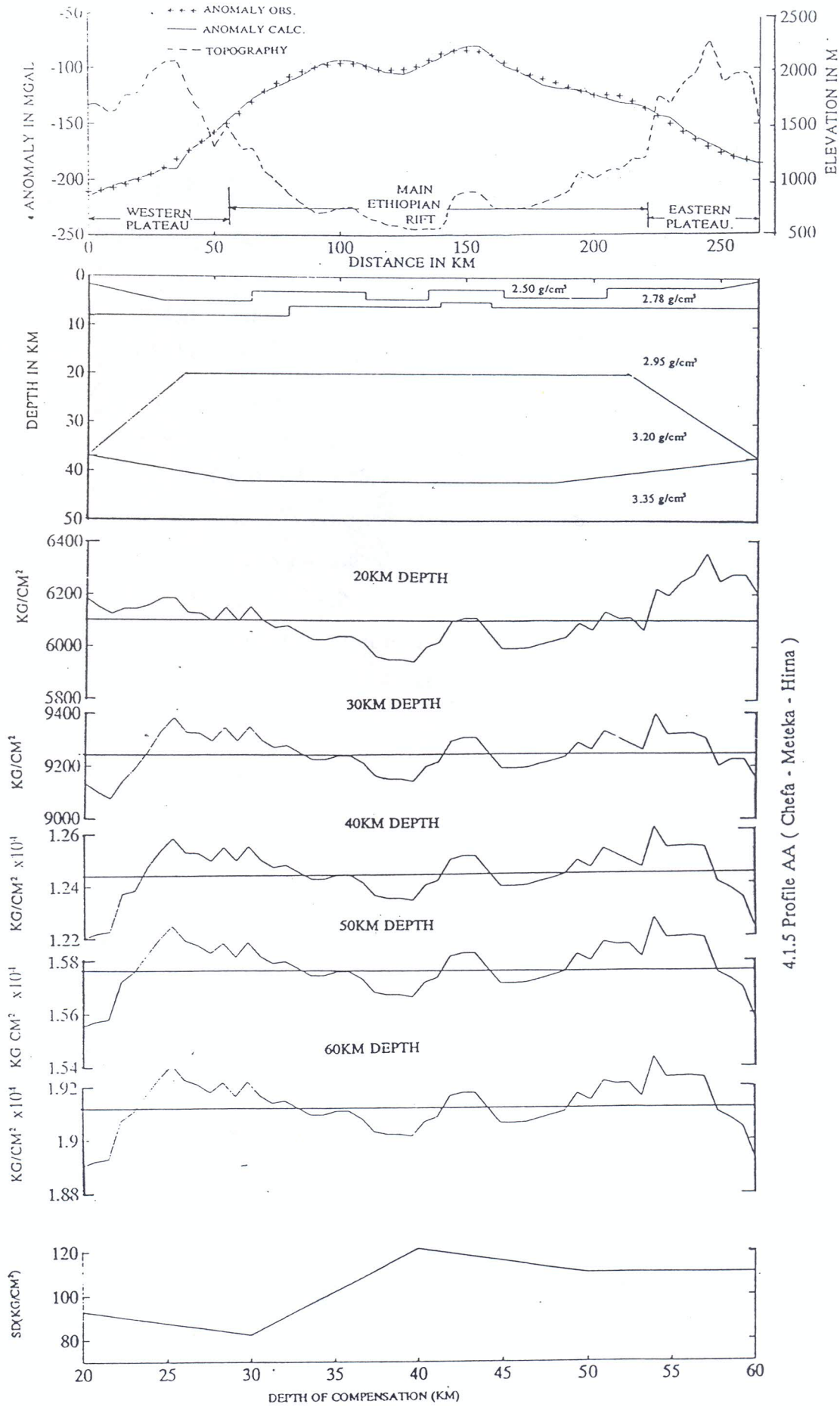

Figure 31: 2-D crustal model obtained from gravity data constrained by seismic observations, the mass distribution curves (pressure of the masses) at 20, 30, 40, 50, 60km depths and a plot of the various depths versus the standard deviation (SD) about the mean at each depth along profile AA. The mass distribution curves indicate the isostatic behavior of the model at different levels. Isostatic equilibrium is first apparent at the 30km depth as can be seen from the plot of depth versus SD curve. The crust reaches isostatic balance at the 50 and 60km depth (ie. constant SD) levels.

The mass distribution curves shown in Fig. 31 indicate the isostatic behaviour of the model at different depth levels. The mass distribution curve at the 20 km depth shows that the plateau regions have more mass than the rift zone the magnitude being higher on the Eastern plateau. The high topography of the plateau areas seem to be producing the excess mass. There is therefore undercompensation in the plateau regions and overcompensation in the attenuated sections of the crust beneath the rift. At 30 km depth the rift has gained more mass due to the quantity of anomalous mantle material at this level. Thus the surplus mass of the plateaus are partly balanced by the heavier material of the rift at this 30 km depth level indicating the model is isostatically balanced at this level.

A plot of the various depths versus the standard deviation (SD) about the mean of the sum of the masses shown in the same figure also shows that a minimum deviation is close to the 30 km depth indicating isostatic equilibrium is first apparent at this level. From the depth versus SD curve it can be seen that the model reaches isostatic balance at the 50 and 60 km depths (i.e constant SD).

6.4.2 Profile JJ (Debrebirhan - Dofan - Gelemso)

This profile (Fig. 32) also starts from the Western plateau and extends to the Eastern plateau across the rift. The crust beneath the Western and the Eastern Plateaus is 40 km. It thins to 23 km beneath the rift where there is a crustal attenuation due to the upward progression of the anomalous mantle.

The mass distribution curves for this model are similar in shape to those of profile AA. Thus, at the 20 km depth the plateau regions are undercompensated and the rift zone is overcompensated. This is because the high plateaus particularly the Western Plateau have more mass than the rift. The mass excess of the plateau regions are partly balanced by the mass due to the anomalous mantle at the 30, 40, 50 and 60 km depth levels.
The mass distribution curve at the 40 km depth, suggests that the model is tending towards isostatic balance. Isostatic equilibrium is reached at the 50 and 60 km depths. The depth versus standard deviation curve also demonstrates this same fact.

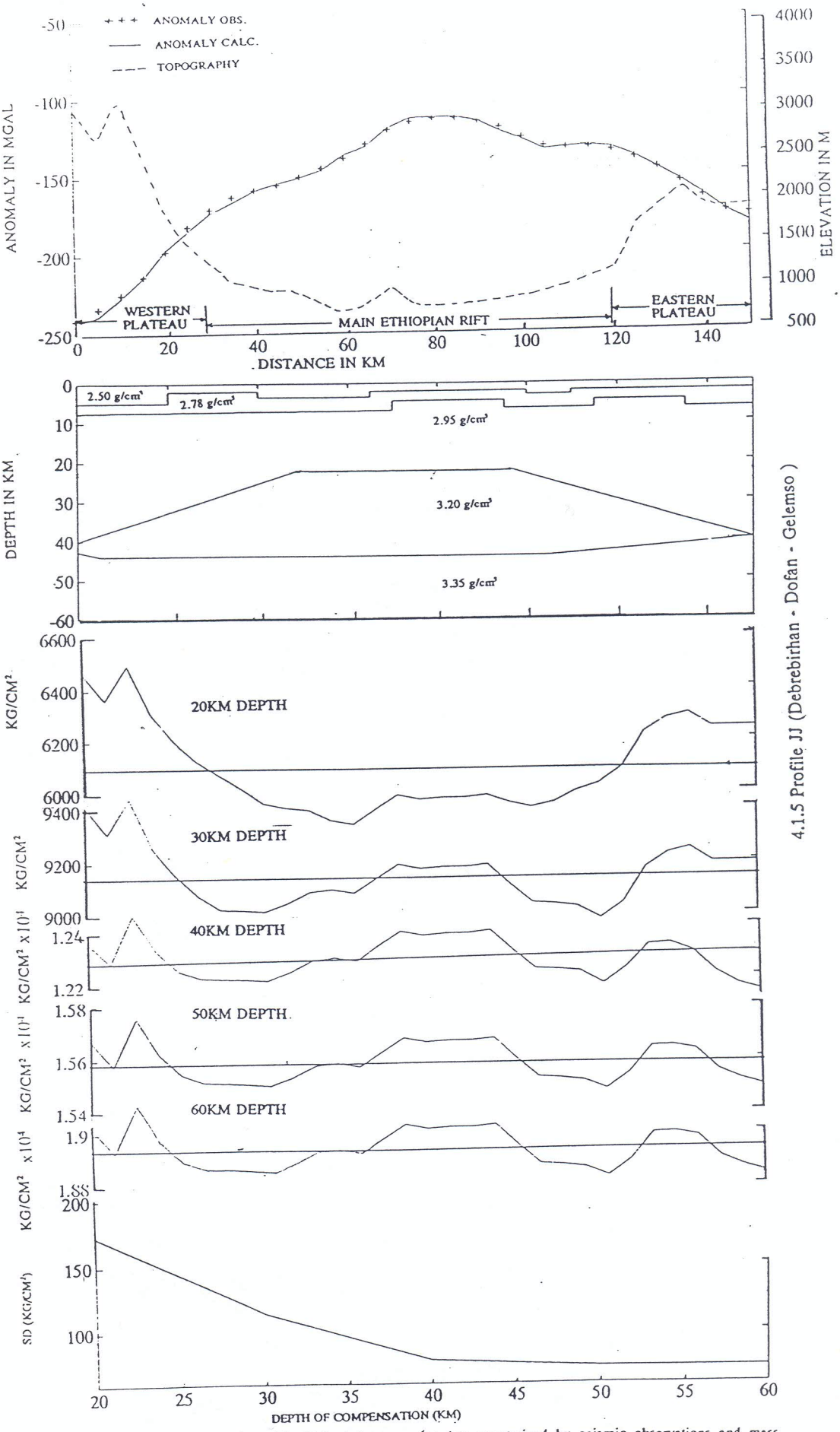

Figure 32: 2-D crustal model obtained from gravity data constrained by seismic observations and mass distribution curves (pressure of the masses) for 20, 30, 40, 50, 60km depths along profile JJ. The mass distribution curves indicate the isostatic behavior of the model at different levels. This model is balanced at the 50 and 60km depth levels.

6.4.3 Profile HH (Gebreguracha - Welenchiti - Ageresisay)

This profile (Fig. 33) begins well inside the Western Plateau at about the location of the gravity minimum shown in the Bouguer anomaly map (Fig. 18). It traverses the Main Ethiopian Rift and continues south east into the relatively less elevated Eastern plateau. As mentioned earlier normal continental crust of about 40 km thickness overlies the normal mantle beneath the Western Plateau. The gravity model shows that the crust below the Eastern Plateau is about 38 km thick.

As in the preceding model, the western plateau has more mass than the Main Ethiopian Rift and the Eastern plateau the 20 km depth. The total mass at the 30 km depth reveals an equipotential surface. However, the Western Plateau is still slightly overcompensated. The depth versus standard deviation (SD) curve shows that there is evidence of isostatic equilibrium close to 30 km depth. At this level the excess mass of the Western Plateau is balanced by the heavier crust of the Main Ethiopian Rift. The model reaches isostatic balance at the 50 and 60 km depths (i.e constant SD at these depths)

6.4.4 Profile MM (Guder - Koka - Diksis)

This profile is situated in the central part of the Main Ethiopian Rift. It extends from Guder on the Western Plateau to well inside the Eastern Plateau. The crust beneath the Western Plateau is 41 km thick and 40 km beneath the Eastern Plateau. The anomalous mantle beneath the rift reaches a depth of 30 km over a 100 km wide zone.

The mass distribution curves (Fig. 34) at the 20 km and 30 km depths show that the Plateau regions have excess mass as compared to the rift. At the 40 km depth the model indicates a tendency of isostatic balance the excess mass of the plateaus being compensated by the heavier crust of the rift at this level. Isostatic equilibrium is established at the 50 and 60 km depths. The equilibrium could be due mainly to the quantity of normal mantle at these levels. The depth versus SD curve also shows identical results.

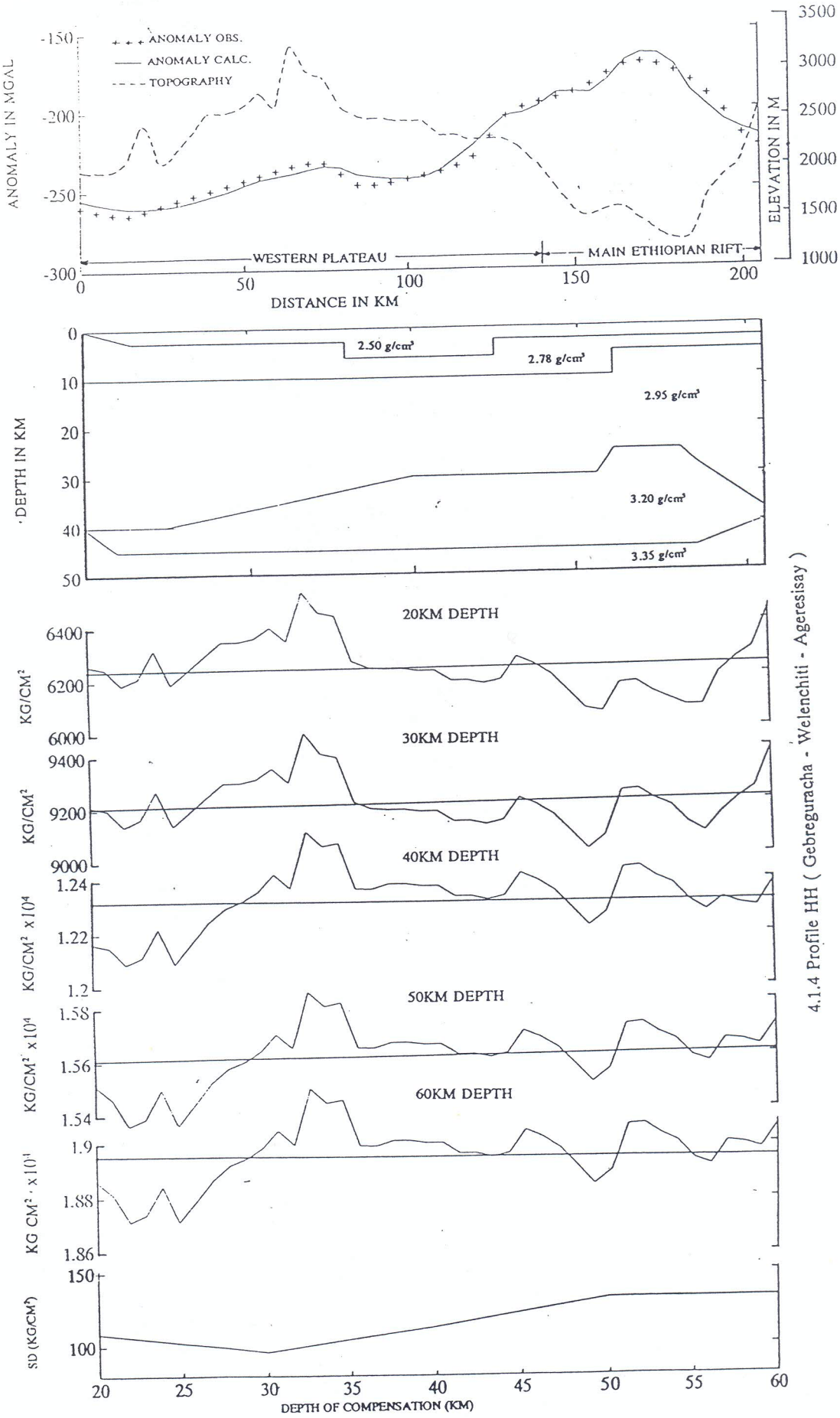

Figure 33: 2-D crustal model obtained from gravity data constrained by seismic observations, the mass distribution curves at the 20, 30, 40, 50 and 60km depths and a plot of depth versus standard deviation curves along profile HH. At the shallow depth (20km), the plateau areas attain excess mass due to their high topography in the region as compared to the rift. Isostatic equilibrium is first apparent at the 30km depth as can be seen depth versus standard deviation (SD) curve. This model reaches isostatic balance at the 50 and 60km depths (ie. constant SD at this depths).

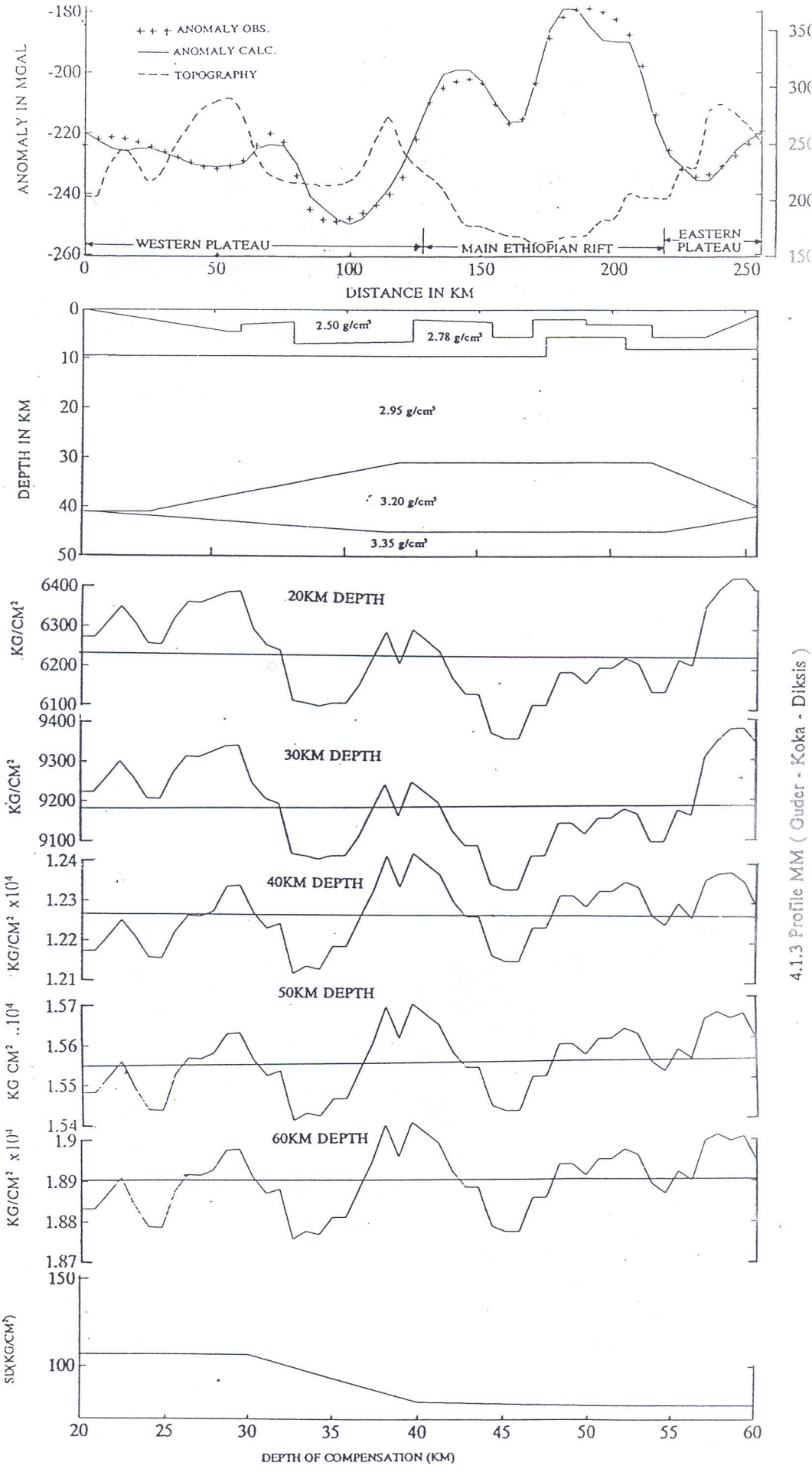

Figure 34: 2-D crustal model obtained from gravity data constrained by seismic observations, mass distribution curves at 20, 30, 40, 50, 60km depth levels and a plot of the various depth levels versus standard deviation about the mean of the mass distibutions at each depth along profile MM. The mass distribution at 40km depth reveals that the model is nearly in isostatic equilibrium. The crust reaches isostatic equilibrium at the 50 and 60km depth levels.

6.4.5 Profile SS (Hossaina - Bura - Adaba)

This profile crosses the Main Ethiopian Rift at the lakes region. The crustal thickness of both the Western and the Eastern plateaus along this profile is 40 km. The anomalous mantle beneath the rift lies at 30 km depth over a 100 km wide zone.

At the 20 and 30 km depths the Eastern Plateau has excess mass than the rift and the Western plateau as can be seen from the mass distribution curves in Fig. 35. The model reaches isostatic equilibrium at the 50 and 60 km depths. The plot of depth versus standard deviation curve also substantiates this argument.

6.4.6 Profile KK (Humbo - Abaya - Hagereselam)

This last profile is situated north of Lake Abaya. It starts in the vicinity of the Western plateau and extends to the Western escarpment of the Eastern Plateau across the rift. The crustal thickness along this profile is 30 km at its western end and 35 km at the eastern end. The anomalous mantle lies at a depth of 30 km over a 90 km wide zone.

The mass distribution curves (see Fig. 36) at all depths have similar pattern showing that the central zone of the rift has mass-deficients as compared to regions flanking the rift along this profile. A tendency of isostatic balance is evident at the 40 km depth mass distribution curve and the depth versus SD curve.

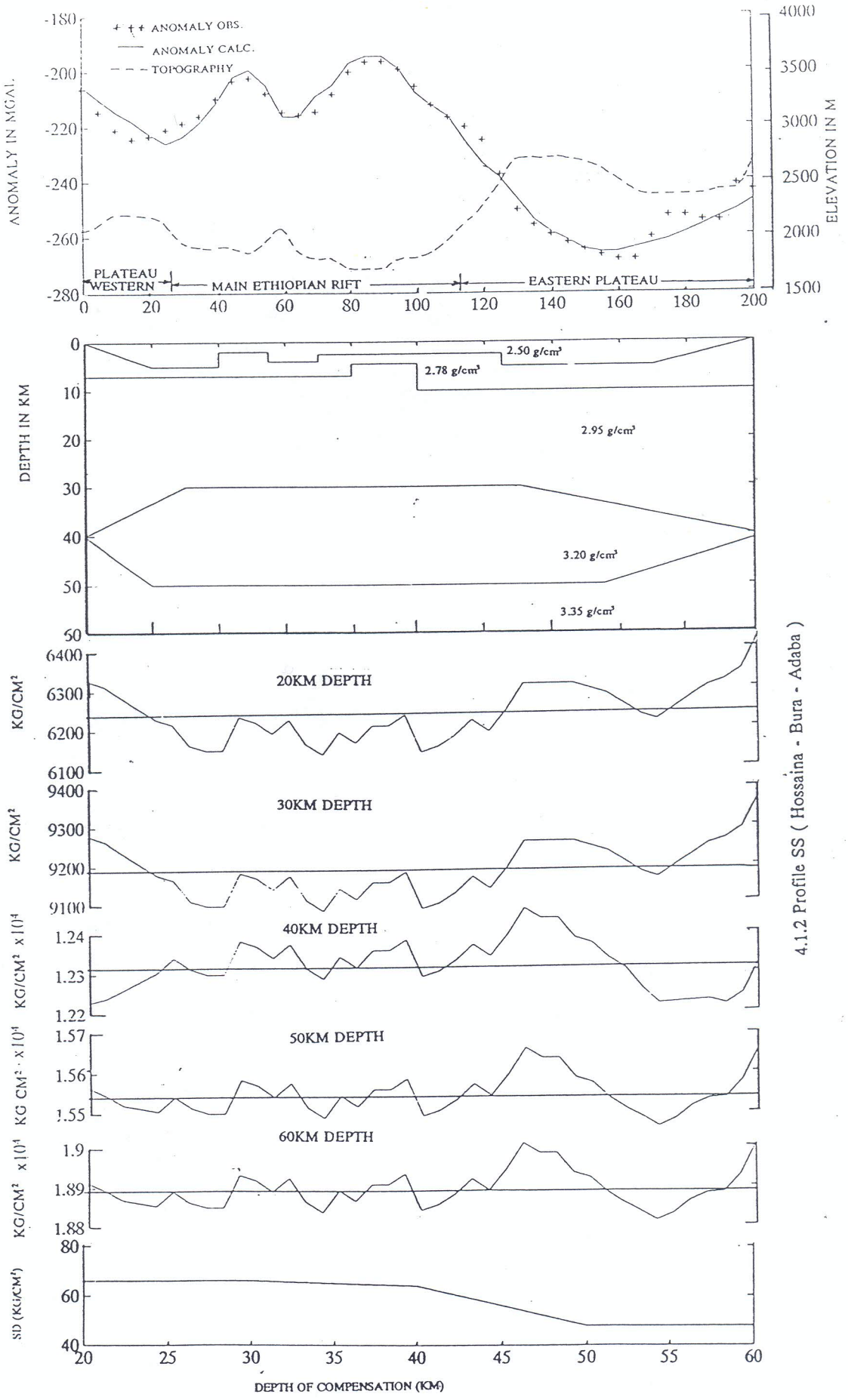

Figure 35: 2-D crustal model obtained from gravity data constrained by seismic observations, mass distribution curves for 20, 30, 40, 50, 60km depth levels and a plot of the various depths versus the standard deviation (SD) about the mean at each depth along profile SS. This model reaches isostatic equilibrium at the 50km depth level. Unlike the preceding models, the Western plateau indicates constant pressure at deep levels and even at shallow depths. This is due to the lower topography compared to the Eastern plateau at this latitude (7°N). The high mountains, on the Eastern plateau, on the other hand, show mass-excess which is also evident at the 60km depth.

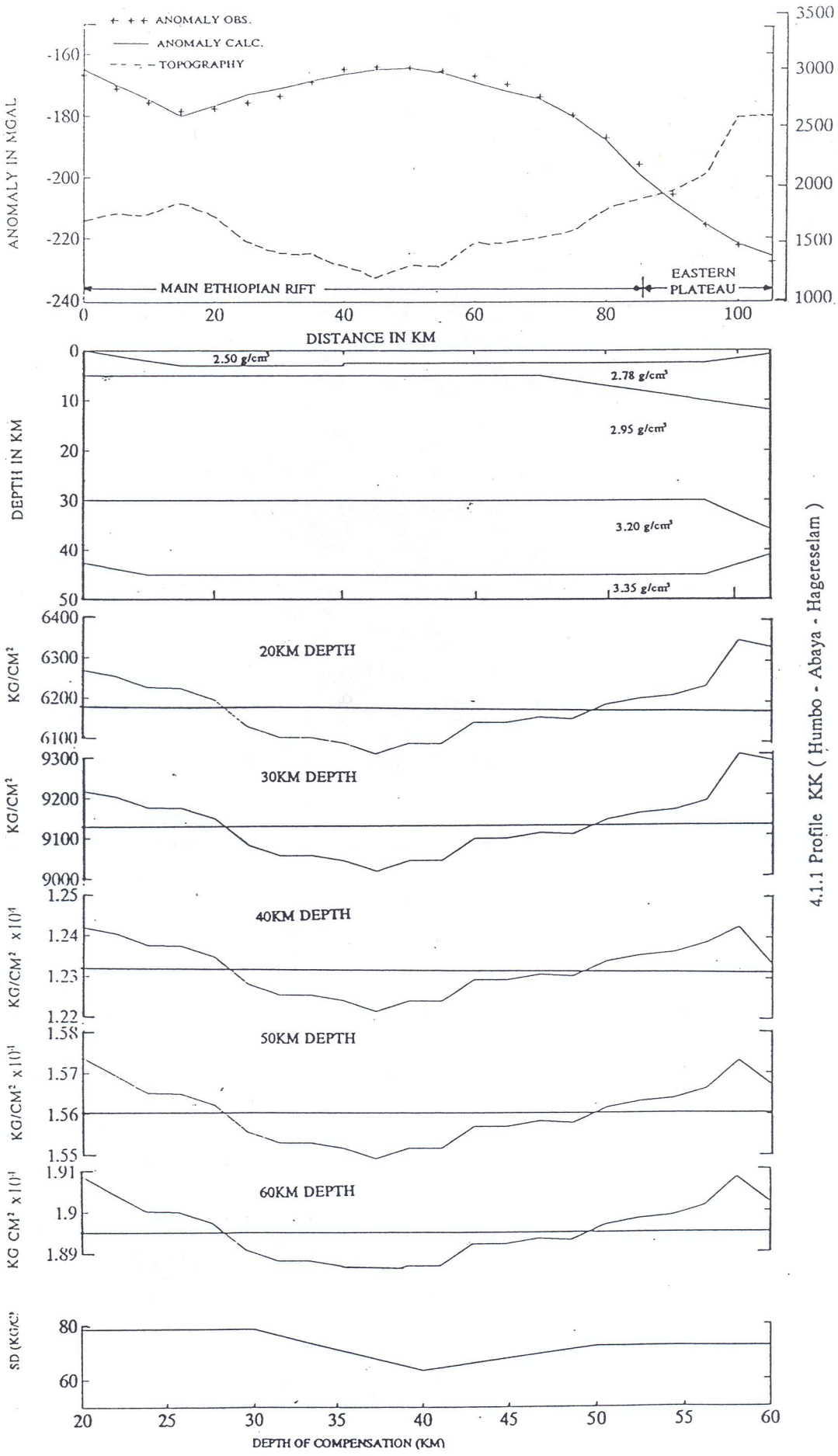

Figure 36: 2-D crustal model obtained from gravity data constrained by seismic observations, mass distribution curves and a plot of the various depths versus the standard deviation (SD) at each depth along profile KK. Evidence of isostatic equilibrium is first apparent at the 40km depth level. The 50 and 60km depth curves also show isostatic balance.

6.5 Geoid map of Ethiopia

In an attempt to supply additional data to study the process of rifting, geoid maps for Ethiopia were computed using the OSU89B and OSU91A geopotential models (Rapp et al., 1990; Rapp et.al., 1991). The resulting map derived from both models is given in Fig. 37. From both maps it is evident that the geoid is characterized by a northwestward increasing steep gradient on both the Eastern and the Western Plateaus. This steep gradient is disturbed beneath the rift, where the disturbance is more pronounced on the map derived from the OSU91A model due to the appearance of pockets of local anomalies. The appearance of local anomalies on the map derived from OSU91A model indicates that the OSU91A model is more detailed than the OSU89B model. It is reported that more terrestrial gravity data is added to OSU91A model (Rapp et al., 1991). On the Western Plateau, the geoid level on both maps rises to form a local maximum of amplitude 4.0 meters. Furthermore, both maps reveal that the geoid level decreases from the Western Plateau to the Eastern Plateau and then towards the Indian ocean, which is their essential characteristics. It is known that the Indian is associated with geoid undulation minimum.

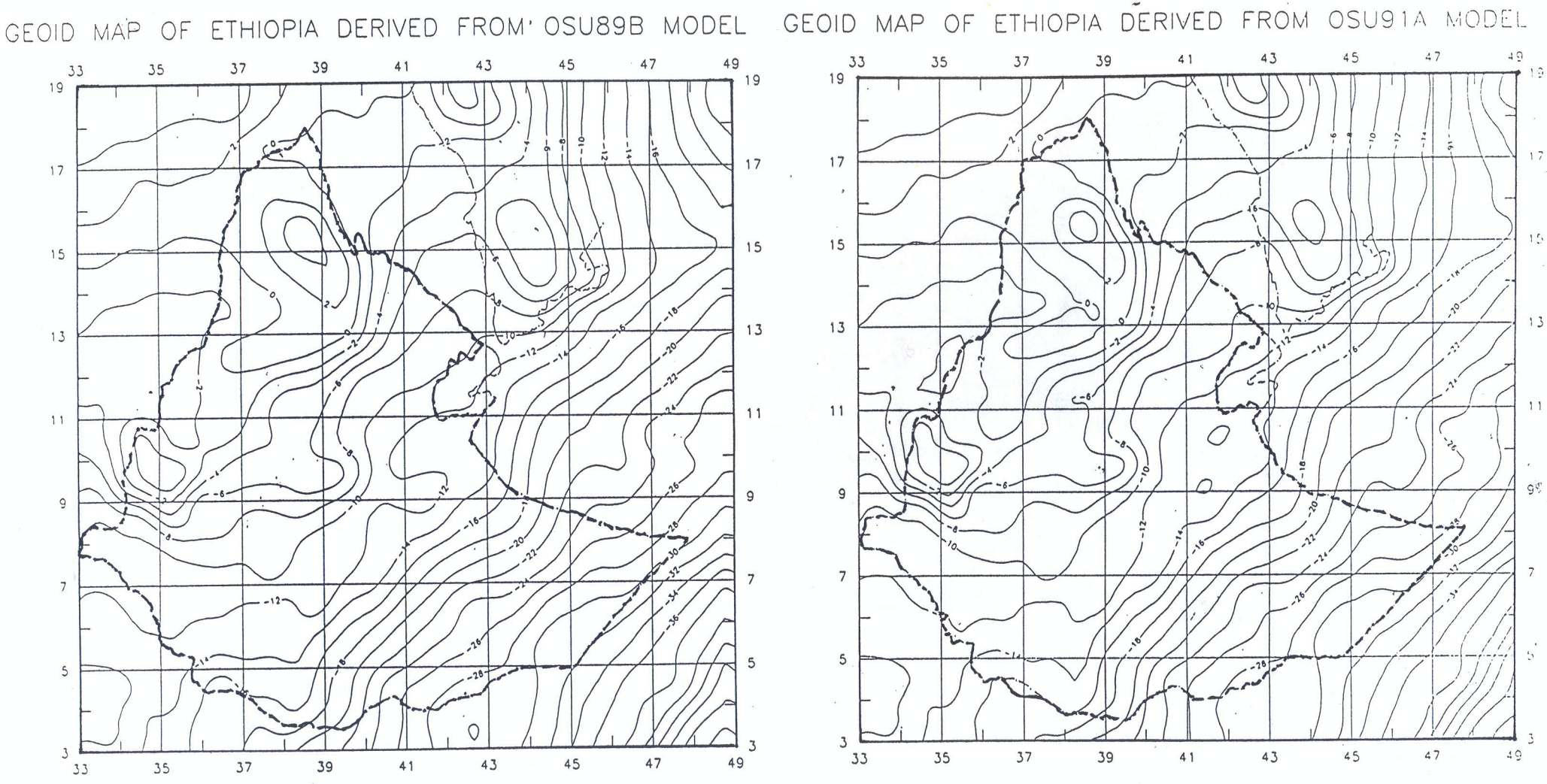

Figure 37: Geoid map of Ethiopia derived from OSU89B and OSU91A geopotential model in units of meters. From the two maps one can see that the OSU91A model is more detailed than the OSU89B one and shows some local anomalies.

6.6 Correlation between the gravity anomalies, Elevations, Moho-depth, and the Free-air anomalies in the Main Ethiopian Rift

6.6.1 Fundamental Terms

A quantity which is the result of a more or less random effect known and unknown influences, and the actual value of which cannot be determined exactly in advance, is considered to be a random variable (Pick, et al 1973). A random variable is always connected with a certain element, a certain property of which it expresses. Accordingly, gravity anomalies, elevations above sea level, Moho depth, geoid undulations and other geophysical quantities can be considered as random variables related to points $P(\varphi, \lambda)$ in a given region.

Let it be assumed that the random variables y_i, i = 1,2,...,m, are determined at points P_k, k = 1,2,...,n, and that each variable y_i can be expressed as a linear regression function of the remaining ones.

The numerical characteristics in correlation analysis are the mean values (moments of the 1st order)

$$\hat{y}_i = (1/n) \sum_k y_{ik} \tag{16}$$

and the covariances (mixed moments of the second order)

$$K_{ij} = 1/(n-1)\sum_k (y_{ik} - \hat{y}_i)(y_{jk} - \hat{y}_j) \tag{17}$$

For i = j the variance obtained is

$$\sigma^2_i = K_i = 1/(n-1)\sum_k (y_{ik} - \hat{y}_i)^2 \tag{18}$$

The correlation coefficient r_{ij} is computed by the relation

$$r_{ij} = K_{ij}/\sigma_i\sigma_j \tag{19}$$

This relation does not express in what ways the values of y_i change with respect to the values of y_j and vice versa. In the simplest case this dependence is expressed by regression lines

$$y_i = a + by_j \tag{20}$$

and

$$y_j = a' + b'y_i \tag{21}$$

As regards to computing the coefficients b and b', the following relations hold:

$$b = K_{ij}/\sigma^2_j \tag{22}$$

and

$$b' = K_{ij}/\sigma^2_i \tag{23}$$

The coefficients a and a' can be computed from the relations

$$a = \hat{y}_i - b\hat{y}_j \tag{24}$$

and

$$a' = \hat{y}_j - b'\hat{y}_i \tag{25}$$

The standard deviation

$$\sigma_{i(j)} = \sigma_i(1 - r^2_{ij})^{½} \tag{26}$$

is a measure of the scatter of y_i with respect to the regression line ($y_i = a + by_j$) and the standard deviation

$$\sigma_{j(i)} = \sigma_j(1 - r^2_{ij})^{½} \tag{27}$$

is a measure of the scatter of y_j with respect to the regression line ($y_j = a' + b'y_i$).

The fundamental relationships (formulas) derived above were used to make a correlation analysis between gravity anomalies, elevation, Moho depth and geoid undulations in order to understand the nature of their relationship.

6.6.2 Fundamental relationships

It is well known that the depths of the Moho discontinuity (Moho) can be determined using deep seismic sounding (DSS) experiments (seismic Moho) and the Airy-Heiskanen isostatic model (Isostatic Moho) in a region. In order to obtain an idea on how this boundary surface varies, it is a common practice to determine its relationship with Bouguer gravity anomalies and other quantities like, for instance, the geoid undulation as well. Moreover, it is recommended that the geoid is a significant parameter for the prediction of the shape of the Moho discontinuity (Čolič et al., 1988). In the analysis of geoid undulations, a relationship is discovered between the variation of the geoid and the Moho in the Alps region (Wolf,1971). Accordingly, a rise in the geoid is coupled with a subsidence of the Moho.

In order to study the relationship between the different parameters considered the following regression analysis was made.

6.6.3 The correlation between Bouguer anomaly and elevation

A correlation analysis between elevation (h) and Bouguer anomalies (Δg) were computed for the observed gravity points in the study area and outside it as shown in Fig. 38. This correlation analysis gave the regression equation $\Delta g = -54.317 - 0.078h$ mGal for h in metres. Δg and h are negatively correlated with a correlation coefficient of -0.845, which is quite significant. It is also noted from the plot that the linear correlation in the rift is stronger than on the elevated areas (plateaus).

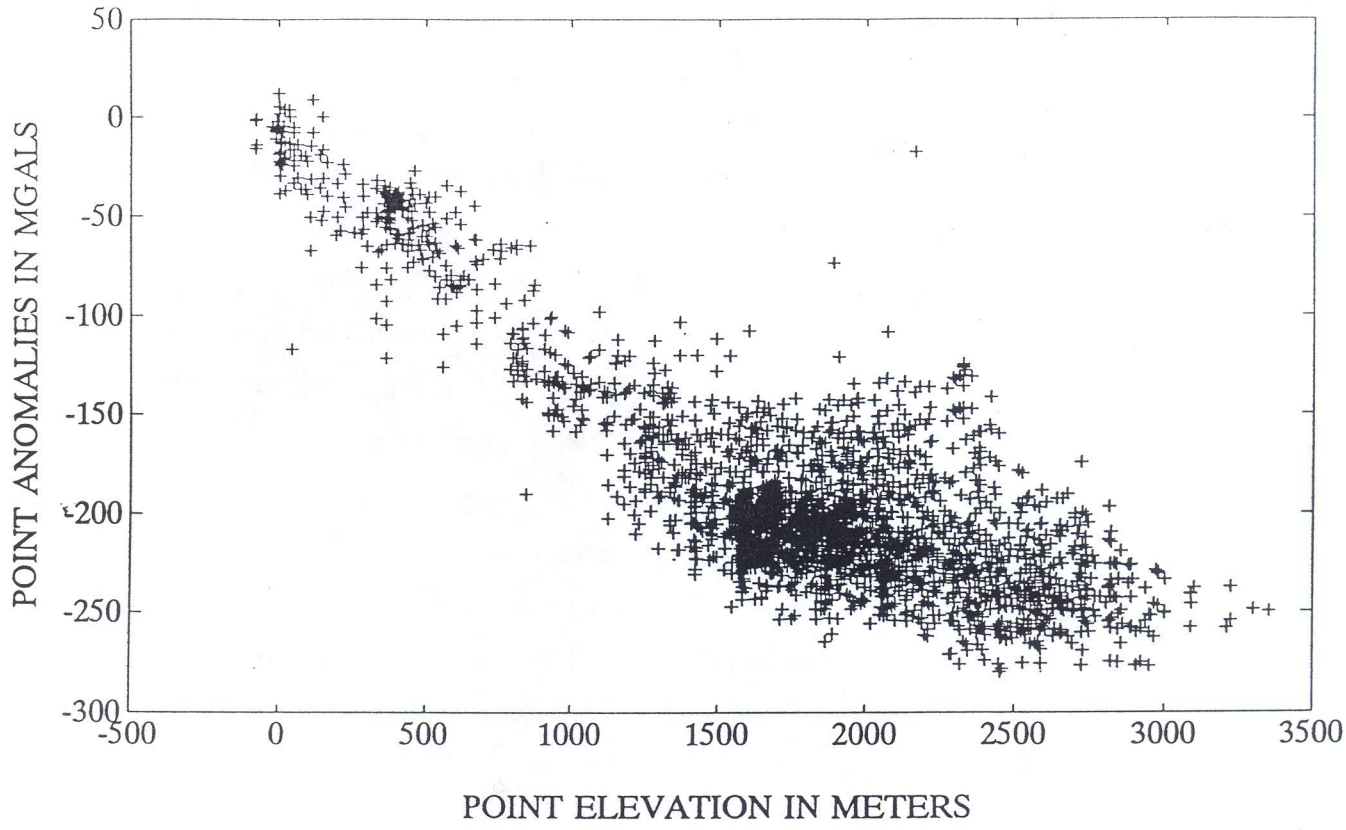

****

ANALYSIS OF CORRELATION BETWEEN ELEVATION AND BOUGUER ANOMALY

Total number of data pairs : 3544

		ELEVATION X	ANOMALY Y
Minimum values	:	-77.000	-280.300
Maximum values	:	3355.000	12.000
Average values	:	1741.866	-190.142
Estimated standard deviations	:	611.217	56.407
Correlation coefficient	:		-.845

Linear regression analysis of type: Y=a+b*X

		a	b
Estimated parameters	:	-54.317	-.078
Standard errors	:	91.129	.049
Unit-weight standard error	:		30.170

****

Figure 38: Correlation analysis between elevation (h) in meters and Bouguer anomalies (Δg)in mGals computed for the observed gravity points in the study area and outside of it.

6.6.4 The correlation between Moho depth and Bouguer anomalies

The correlation analysis between Moho depth (T_M) and Bouguer anomaly (Δg) is made for gravity points in the study area and outside it. This correlation gave the empirical relation $\Delta g = (213.966 - 11.67T_M)$ mGal for T_M in km. The data points considered here are the same as those considered for the correlation analysis between h and Δg. This computation indicates that Δg and T_M are also negatively correlated with a correlation coefficient of r = -0.845. As in Fig. 38, the correlation is found to be stronger in the rift than on the plateaus. Note that the correlation coefficients between the Bouguer anomaly and elevation is identical with that between the Moho depth and the Bouguer anomalies computed here. This is due to the fact that the Moho depth is derived from a linear function of elevation (cf. Eqs. 14 and 15).

In spite of the fact that data for this empirical relationship in the studied region may be insufficient, the obtained results could give an indication to the possibility of predicting Moho depths T_M by means of Bouguer anomalies Δg.

6.6.5 The Correlation between free-air anomaly Δg_F and elevation

From the plot of elevation versus free-air anomalies, the lower and the higher elevations seem to have different correlations, the higher elevations being significantly positively correlated with the free-air anomalies (Fig. 40). However, the computation results reveal that the correlation between Δg_F and h is not significant and subsequently the over all linear regression may be questionable. For both regression parameters a and b the standard errors exceed the estimated parameter values.

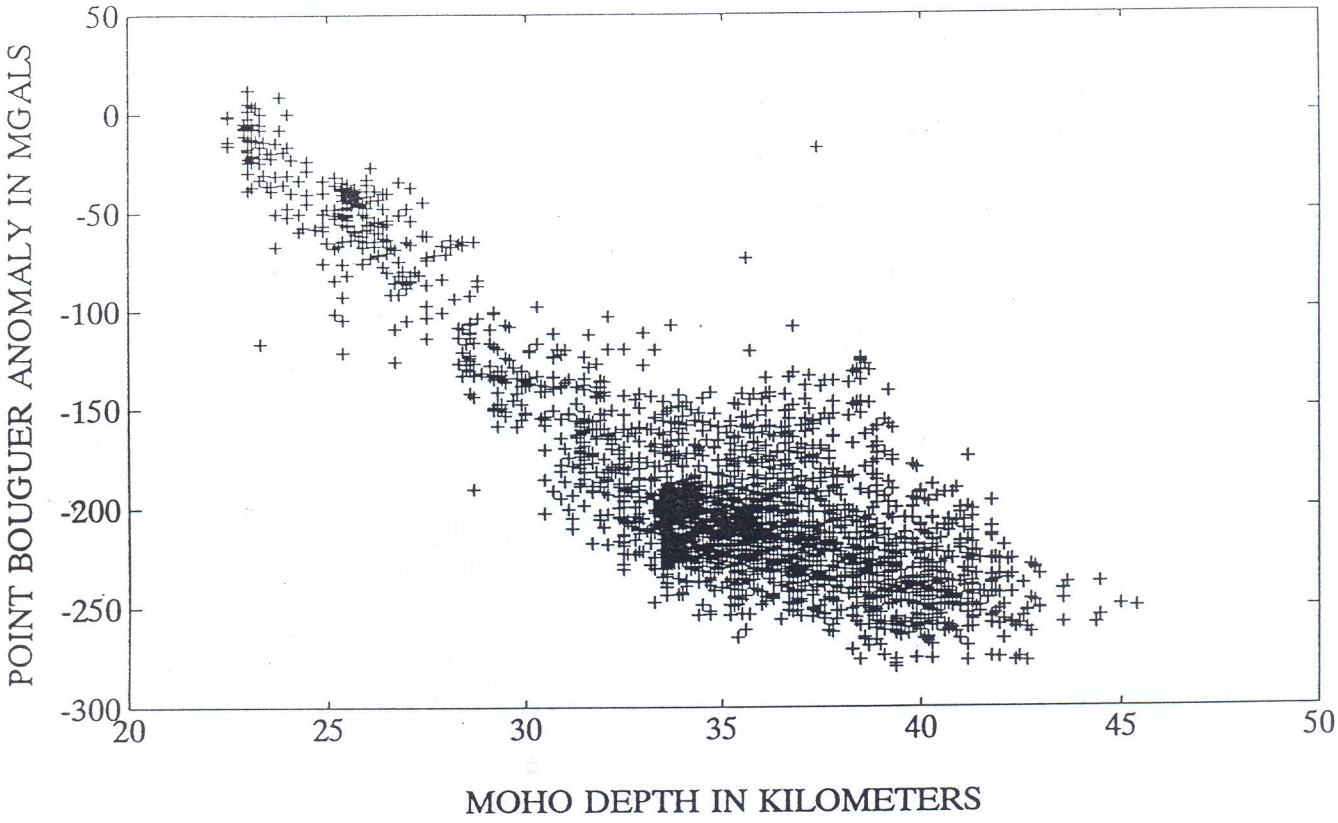

****

ANALYSIS OF CORRELATION BETWEEN MOHO DEPTH AND BOUGUER ANOMALY

Total number of data pairs : 3544

	MOHO DEPTH X	ANOMALY Y
Minimum values :	22.500	-280.300
Maximum values :	45.400	12.000
Average values :	34.627	-190.142
Estimated standard deviations:	4.083	56.407
Correlation coefficient :		-.845

Linear regression analysis of type: Y=a+b*X

	a	b
Estimated parameters :	213.966	-11.670
Standard errors :	257.814	7.394
Unit-weight standard error :		30.187

****

Figure 39: The correlation analysis between moho depth (T_M) and Bouguer anomalies (Δg) computed for gravity points in the study area and areas adjacent to it.

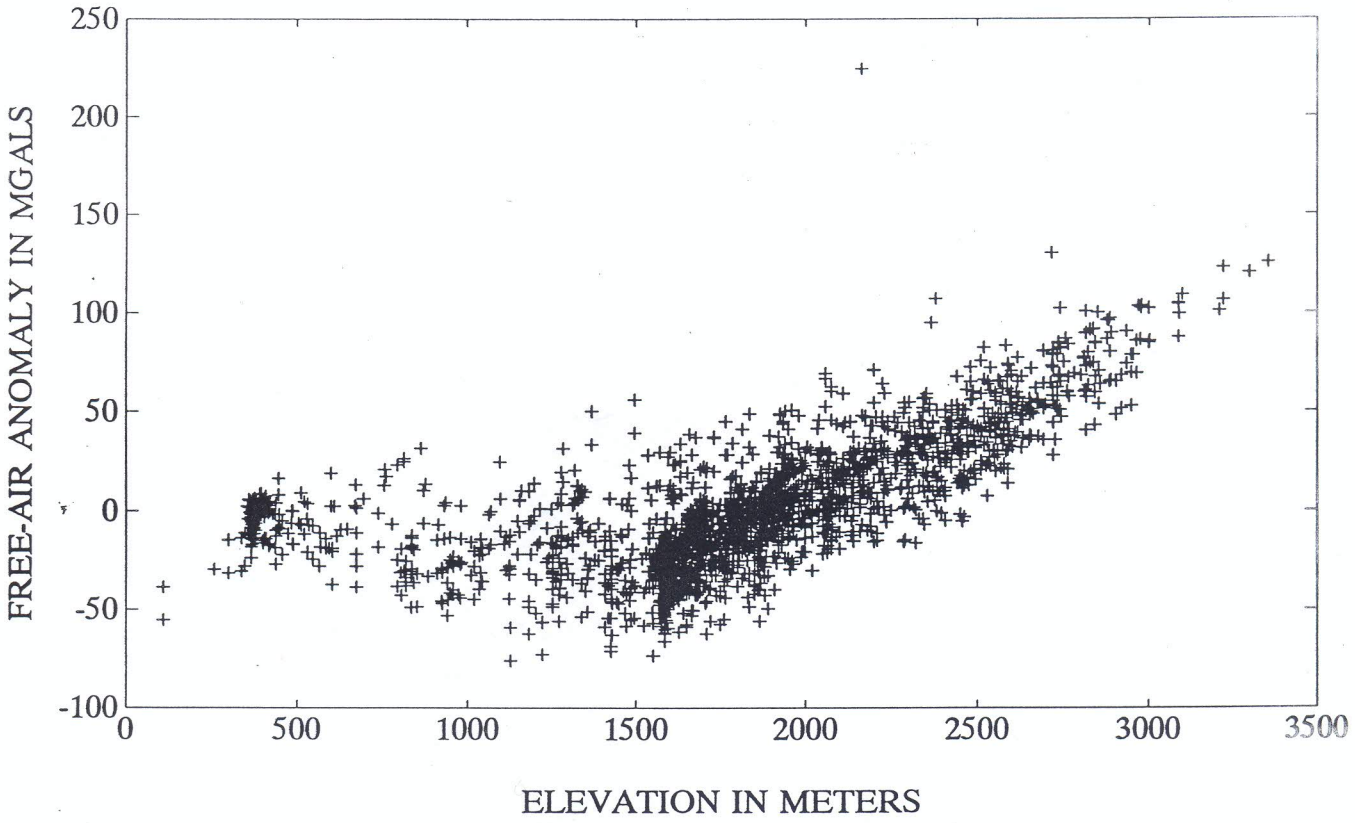

****

Analysis of correlation between elevation and free-air anomaly

Total number of data pairs	:	2971
	elevation	Free-air an
Minimum values	: 108.000	-76.300
Maximum values	: 3355.000	224.700
Average values	: 1731.943	-.675
Estimated standard deviations	: 592.578	31.049
Correlation coefficient	:	.548

Linear regression analysis of type: Y=a+b*X

		a	b
Estimated parameters	:	-50.428	.029
Standard errors	:	80.225	.044
Unit-weight standard error	:		25.967

****

Figure 40: The correlation between Free-air anomaly Δg_F and elevation h.

Chapter 7.

Seismicity studies

7.1 Seismicity of Ethiopia and the Horn of Africa

Historical records of the last six centuries and recent instrumental observations reveal that there have been continuous earth tremors in Ethiopia and the Horn of Africa (Gouin, 1979). These have sometimes been accompanied by outbursts of volcanic activity. Evidence of these tectonic events are shown by highly dissected surface geology. The geological features are expressed by complicated patterns of faults, which are often scaled in thousands of meters. These geologic features indicate that the process of rifting date back to the fissuring the Nubian swell. This rifting process created the Ethiopian (Afar and the Main Ethiopian Rift), the Red Sea and the Gulf of Aden Rifts. Rifting in northeastern Africa started 30 million years ago (Gass, 1970a,b). The manner how this rifting process occurred is outlined as follows.

The earth's crust was uplifted by a lithothermal system of forces which were generated by a stationary hot spot in the underlying mantle (Gass, 1970a,b). These forces passed the threshold breaking point, thus causing the crust to fissure along axes of maximum uplift. Following this, background seismic and volcanic activity accompanied the crustal readjustments to the vertical forces of alternate updoming and subsidence. Three major epirogenic episodes are identifiable during these 30 million years (Gass, 1970a,b; Mohr, 1971a,b). Earthquake and volcanic activity are therefore common in northeastern Africa, a fact that stems from the geological location of the region. The northeastern sector of Africa, which includes Ethiopia, borders the main oceanic boundary between the major tectonic plates of Africa and Arabia. It also straddles the so called " a failed rift" that marks the incipient breaking away of the East African minor continental plate from the rest of the African continent. The contiguous major oceanic boundary is identified by the Gulf of Aden and Red Sea rifts. The "failed rift" is the Ethiopian rift valley (the Afar Depression and the Main Ethiopian rift) southwardly prolonged by the East African rift system (Gouin, 1979).

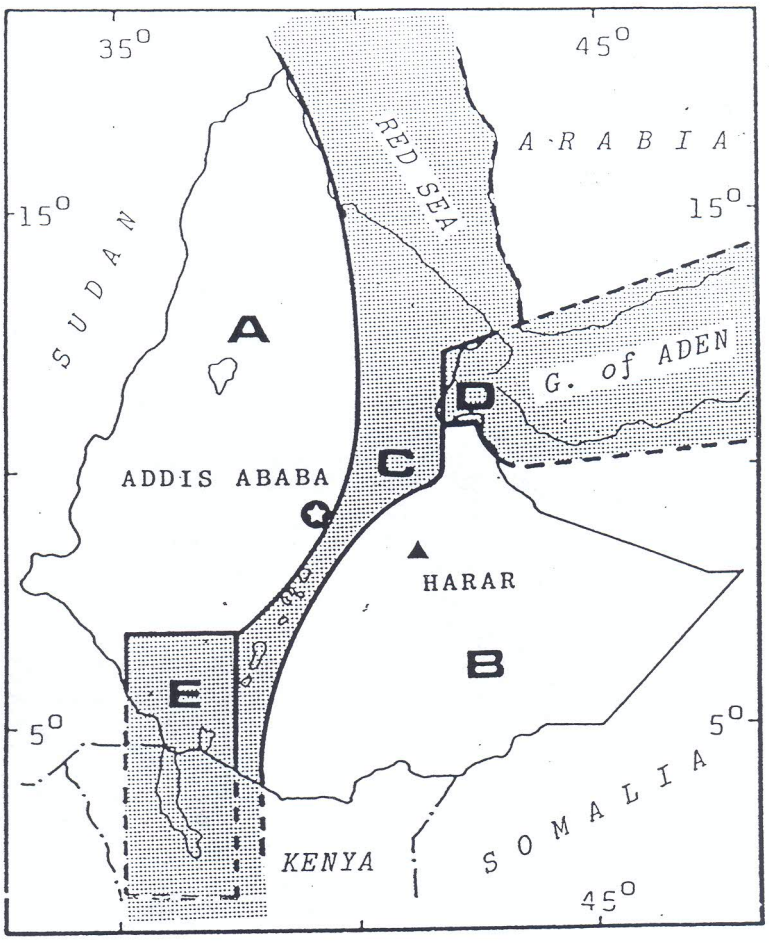

Figure 41: The natural subdivision of Ethiopia and the Horn of Africa into five distinct structural units or seismic regions. (After Gouin 1979)

Seismic events in Ethiopia and the Horn of Africa (Fig. 41) are grouped into five zones (zones A, B, C, D and E). The zoning is made according to the regions which naturally emerged from the breaking up of the African segment of the Nubian swell: the two highland or plateau regions and the rift units that dissected them (Gouin, 1979).

Zone A comprises the Western Plateau (Ethiopian Plateau). Zone B includes the entire South-eastern Plateau (Somali Plateau), whilst Zone C consists of the Main Ethiopian rift, Afar and the southern Red Sea. Zone D is defined by the western sector of the Gulf of Aden and Zone E the Gemu-Gofa and Turkana (Rudolf) rifts. The plateau-rift escarpments, which are geologically structural parts of the rifts are included in Zones A and B rather than Zone C because more than 90% of the seismic and volcanic activity are connected with the rifts (Gouin, 1979). The divisions, in general, are mainly influenced by the locations of the seismic effects on society rather than by geological norms.

distribution of epicenters (Fig. 44) reveals that the Ruwenzori seismic region between Lakes Edward and Albert as well as the northern end of Lake Tanganyika are the main earthquake zones of the region. On the other hand, the most active zones of the Eastern Rift are the Lake Nyasa district lying southeast of Lake Victoria, and the southern sector of the Eastern Rift (in northern Tanzania). The Spece Gulf and the Kavirongo rift structures located to the west of the Kenyan Rift are also seismically active. Furthermore, the seismicity map depicts the region lying between Lakes Albert and Turkana is an aseismic zone.

7.3 Conclusion drawn from the seismicity study

This review of the seismicity studies in Ethiopia and the adjacent areas confirms that most earthquake activity occurs within the rift system, indicating that this fault system is still developing. The seismically active zones are marked by cluster of earthquake epicenters, recent volcanic activities, geothermal activities, steep gravity gradients and local positive gravity anomalies.

Chapter 8

Discussions, Conclusions and Recommendations

8.1 Discussions

Before summarizing the results of this study thus far for the Main Ethiopian Rift including southern Afar, it is necessary to mention briefly what is known about the rift and its neighbouring regions.

Very little refraction seismic information is available concerning the crustal structure the MER to the south. It is known that the Turkana rift is underlain by an anomalous upper mantle with a velocity of 7.48 km/s from the refraction seismic experiment of Griffith (1972). Along this profile the lower crust is penetrated by a narrow belt of anomalous mantle to a depth of 20 to 22 km. Further south in the Kenyan Rift the anomalous mantle is mapped at a depth of 35 km (KRISP85 experiment results). These results demonstrate a thickening of the crust along the rift axis towards the Kenyan dome. Further north of the Turkana rift along the rift axis in Ethiopia, the 2-D gravity models computed in this study indicate that the crust thickens to 30 km in the central part of the MER. The thickening is consistent with the regional gravity data. Gravity values increase (negatively) from > -100 mGal around southern Turkana to about -200 mGal near Lake Naivasha (center of Kenyan dome) southwards along the Kenyan rift and to about > -195 mGal in the central part of the MER (at about latitude 7^0N) along the rift axis in Ethiopia.

Makris et.al (1969,1970) have published papers on crustal and upper mantle models from gravity measurements across the northern sector of the MER and the Afar Depression. These models show a thinning of the crustal layers from south to north and an intrusion of upper mantle material beneath the rift. There is a fair agreement with the concept that, north to south, in Ethiopia, we proceed from the oceanic crust of the central Red Sea Graben to the major crustal thinning with some oceanic crust at Erte Ale in the Afar (Makris,1972) and to the WFB - the axis of the Main Ethiopian Rift.

A glance at the NASA gravity map (Fig. 28b) shows that the magnitude of the gravity anomalies associated with these features decrease from the Red Sea through Afar to the central part of the MER. The development of the positive gravity anomalies seem to be dependent on the extent to which the anomalous mantle has developed.

Over the Gulf of Aden and Red Sea, the positive gravity anomaly is much more pronounced and here the thickness of the anomalous mantle is correspondingly larger. Further south, in Ethiopia, the axis of the MER is transferred to the Turkana Rift and finally to the Kenyan Rift. The Turkana Rift has a major positive anomaly (-100 mGal) comparable to the gravity values of the Afar area (Fig. 28b). In contrast to the Turkana positive anomaly (-100 mGal) the Kenyan Rift has a broad negative anomaly (-200 mGal) comparable with the gravity values in the central part of the MER along the rift axis (at about latitude 7^0N).

On the basis of the axial gravity anomaly positiveness as indicating the development and amount of intrusive activity (i.e progression towards new crust), the MER might be considered as an intermediate to the Turkana Rift and the Afar Depression. This fact suggests that the gravity data could be viewed as indicating a more advanced rift stage in the Turkana Rift and the Afar Depression relative to the Main Ethiopian and Kenyan Rifts.

From the foregoing analysis of the gravity data, the prominent point that can be highlighted is the correlation between gravity trends and structures of the rift system (Fig. 18 (a)). It has been observed that the axes of positive anomalies, are associated with the rift floor and belts of synclinal structures. The negative axes, on the other hand are associated with the uplifted regions and belts anticlinal structures.

On either side of the rift normal continental crust has been deduced from earthquake data (Bram and Schmelling, 1975; Bonjer et al., 1970; Herbert and Langston, 1985), seismic refraction data (Berckhemer et al., 1975; Khan et al., 1987) and also from gravity observations (Wohlenberg, 1975). Definite oceanic crust is known from the Gulf of Aden extending to the Gulf of Tadjura and about 40 km inland (Courtillot, 1980). This is clearly illustrated by the seismicity maps (Fig. 43 & 44). Oceanic crust is also known in the Red

Sea central trough, which extends up to the Farasan Islands in the east (Mooney et al., 1985). The crustal structure of Afar, as obtained from the refraction seismic profiles (Fig. 5) departs from normal continental crust in both thickness and velocity depth distribution in the crust and upper mantle. The profiles reveal that an upper crust with a velocity 6.10 to 6.20 km/s has been observed on all profiles. It is however thinner than normal when compared with the thickness of the upper crust in profile I on the Western Plateau (18 to 20 km). The total crustal thickness in Afar is less than that of continental crust, being over 20 km in most parts of the area. However, one should note that even in the north, near Dallol, where the crustal thickness is reduced to 14 km, a 6.10 km/s upper crust is still present.

The crustal structure of the Djibouti area (Ruegg, et al., 1975) is similar to the rest of the Afar, having a granitic layer overlying a 6.80 km/s lower crust (referred to upper mantle by Ruegg). This layer overlies a low velocity (7.10 to 7.40 km/s) upper mantle. Ruegg (1975) noted a higher than usual Poisson's ratio of 0.28 to 0.38 compared to 0.25 to 0.26 for old oceanic and continental crusts. Searle (1975) found a high V_p/V_s (Poisson's) ratio across the Afar Depression. These results indicate a partially melted upper mantle material.

The maps of earthquake epicenters (Figs. 43 & 44) illustrate that seismic activity in East Africa is mainly related to the major rift structures. In Ethiopia, for instance, most epicenters cluster along the plateau-rift transitions and along the axial zones of recent faulting (WFB).

The mass distribution curves computed along the crustal density models in the studied region demonstrate undercompensation in the plateau areas and overcompensation in the depression at shallow depths

The study suggests that compensation of the Ethiopian and Kenyan topographic domes are due, at least in part, to crustal thickening. The study also suggests that there are significant variations in the crustal structure along the rift axis.

8.2 Conclusions and Recommendations

The gravity data presented will play an important role in an interdisciplinary interpretation, in which all available geoscientific information of recent and future work in the Ethiopian Rift system are gathered.

The crustal structure of the Main Ethiopian Rift has been interpreted using the seismic refraction profiles obtained for the rift zones in Ethiopia and Kenya, the existing geological and seismicity information of the region and constraints generated from the new Bouguer anomaly map, free-air anomaly map, isostatic Moho-depth map and geoid undulation map of the study area constructed for this purpose.

The main conclusions of this study are:

The review of seismicity studies in the Ethiopian Rift and the associated highlands confirms that most activity occurs within the rift system, indicating that this fault system is still developing. The majority of earthquake occurrences are concentrated within the transition zone (plateau-rift escarpments) of isostatic imbalance, and are limited within crustal depths (23-33 km). This is demonstrated in the map of epicenters and the trend of mass distribution curves calculated along the seismically controlled crustal density models at shallow depths in these areas.

The measured gravity field and other related field quantities i.e the isostatic Moho depth map and the geoid computed for the region of the Main Ethiopian Rift seem to be sensitive indicators of the tectonic and geologic structures in the region.

Analysis of gravity and seismic refraction data indicates that the Main Ethiopian Rift and the rift zone of East Africa in general is underlain by a dense mantle derived material (anomalous mantle) in the lower crust. Other continental rifts show similar phenomena.

Between the southern end of the Main Ethiopian Rift and the Afar Depression the line of maximum crustal attenuation trends NNE-SSW. The gravity trends (positive and negative anomaly axes) observed in the region also align themselves along this line of maximum crustal attenuation.

Crustal models for all the gravity profiles indicate that the lower crust has been replaced by a zone of denser material (anomalous mantle) beneath the rift. The computed models show that the quantity of the anomalous material decreases from south to north.

- The crust is thinner beneath the central zone than under the flanking basements, and this would correspond to zones of high density intrusives. In the MER the centers of these intrusives culminate in the vicinity of the silicic volcanic centers of the WFB.

- The central positive anomalies are found to be associated with the axial zones of recent faulting (WFB), volcanism, and geothermal and seismic activity.

- Seismicity studies show that earthquake activity in East Africa is mainly related to the major rift structures. Their occurrences are concentrated within the transition zone (plateau-rift escarpments) of isostatic imbalances, and are limited within crustal depths (shallow depth earthquakes). This is demonstrated in the map of epicenters and the trend of the mass distribution curves calculated along the seismically controlled 2-D crustal density models at shallow depths in these areas.

In view of these conclusions the following suggestions for further work are made:

Without doubt further refinements of the observations, and consequently of the interpretations, can be made.

- Additional geophysical work such as refraction seismic, together with more detailed studies of the gravity field will provide better data for quantitative interpretations.

Gravity coverage of the gap between the MER and the Kenyan rifts will provide a valuable data for a further analysis of the crustal structure beneath the two rift systems.

Appendices

Appendix A. Continental rifts

An account of continental rifts including their arrangement and development is fully discussed by Milanovsky (1972). The following brief discussion is mainly taken from his work to give the reader a general background knowledge about continental rifts and their development.

Rift zones are regions where the crust is stretched and thinned. An upper mantle with density lower than the normal mantle lies beneath these regions. The most distinctive feature of a rift is a relatively narrow graben, which is often step faulted with deep normal faults and uplifted margins. These zones are usually characterised by high seismicity, magnetic anomaly bands, high heat flow and volcanism. Rift zones have been recognised as being globally continuous.

Three main types of rift zones are briefly described below.

1. Intraoceanic (oceanic) rifts; the axial graben of these rifts are bordered by oceanic crust.

2. Intracontinental (continental) rifts; the rift floor as well as its shoulders are of continental crust. The crust here is usually thinned.

3. Intercontinental rifts; Where the graben has oceanic crust whilst its shoulders are of continental crust. Examples are the Red Sea, Gulf of Aden and the Gulf of California.

Continental rifts may be subdivided into (i) rift zones of platforms and (ii) rift zones of young folded blocks.

(i) Rift zones of platforms: These are defined by single axial grabens with alkaline volcanism, frequently associated by carbonites. They are usually connected with old basement rocks whose history is normally varied and complex. The grabens often take the trend of the basement structures. They may also adjust to them, thus producing geniculate, zig-zag or en-echelon fault patterns.

Platform rifts may further be subdivided into; (a) rift zones of arch-volcanic type and (b) crevice type rifts.

(a) Arch-volcanic rifts: are characterised by the following. Intense and long volcanic activity is present in these zones. The igneous rocks are basic and the intermediate lava flows of highly alkaline nature. Volcanism is associated with uplift and arching. 1-2 km deep grabens, often with branched rifts, form along their axial parts. The arching is associated with Bouguer anomaly minima, which may be caused by melting in the lower crust-upper mantle interface. The axial grabens are defined by narrow Bouguer anomaly maxima (Girdler et al, 1969). Examples are the Ethiopian and the Kenyan rifts (Milanovsky, 1969, Baker and Wohlenberg, 1971, Mohr, 1968)

(b) Crevice type rifts: Incontrast to arch-volcanic rifts, crevice type rifts exhibit little volcanism (eg. Lake Tanganyika, the Upper Rhine graben), or no volcanism (Lake Baikal). Local volcanic centers exist only on the flanks (no volcanism in the axial areas). Volcanism normally occurs after the formation of the graben. The grabens of this group are very deep (eg. Lake Albert, 2-3 km, the upper Rhine graben, 3-4 km, and the Lake Baikal graben, 5-6 km). Marginal uplift zones are narrower, and sometimes absent. Most are normal faulted and connected with horizontal extension. Horizontal displacements sometimes occur, which may greatly exceed that of the extension (eg. the Levant rift). The grabens are seismically active. They are defined by negative Bouguer anomalies, due to the thickness of unconsolidated sediments. Heat leakage is concentrated along narrow fissure zones, rather than in the formation of large magma chambers, as in arch-volcanic type rifts.

(ii) rift zones of young folded belts. In contrast to platform rifts, these zones are formed after the completion of the geosynclinal cycle. They consist of a series of parallel grabens which are separated by narrow horsts. The topographical relief of these horsts are between 2000 and 5000m. Horizontal extension may be more than 1000 km, and may be accompanied by horizontal displacements (San Andreas rift). The formation of young folded type rifts was preceded and accompanied by intense eruptions of calc-alkaline magmas, which are both acidic and basic in nature. The zones overly a crust-mantle mix (cook, 1966), which later assume the characteristics of a more heated and plastic state of an orogenic era layer. Examples are the Basin-and-Range rifts of the western U.S.A (formed after a Mesozoic geosynclinal cycle), and the Early Mesozoic grabens of the west Siberian plate (formed after a Hercynian geosynclinal cycle).

Appendix B

Measured densities of rock samples collected from the central part of the Main Ethiopian Rift.

Sample No	Location or Depth (m)	Rock type and shape	Dry Density σD(g/cm³)	Wet Density σW(g/cm³)	Part. Density σp (g/cm³)	Porosity φ
1	47-49	Rhyolite lava: Sub-rounded to angular.	2.40	2.48	2.61	0.08
2	149.4-149.8	Rhyolite lava: Sub-rounded to angular.	2.32	2.41	2.53	0.08
3	200-201	Rhyolite lava flat angular.	2.53	2.58	2.65	0.04
4	300-302.2	Silicic Breccia: Moderately altered	1.72	2.00	2.38	0.28
6	" "	subrounded to angular.	1.57	1.85	2.17	0.28
8	500.2-502.6	Vitric crystal weakly	1.73	2.07	2.61	0.34
9	602-604	welded tuff: moderately altered subrounded to angular.	1.77	2.08	2.56	0.31
10	700-702.7	Basalt: highly altered subrounded to angular.	2.56	2.64	2.79	0.08
11	750.8-752.7	Basalt highly altered subrounded to angular.	2.44	2.53	2.69	0.10
12	850-851.5	Basalt highly altered flat angular.	2.54	2.64	2.84	0.11
13	950-951.5	Basalt highly altered subrounded to angular.	2.51	2.62	2.83	0.11
15	1050-1051.5	Basalt breccia highly altered subrounded to angular.	2.3	2.54	2.83	0.16
16	1150-1153	Basalt breccia highly altered subrounded to angular.	2.30	2.48	2.79	0.18
18	14491.1-1450.6	Basalt mod. altered subrounded to angular.	2.85	2.87	2.91	0.02

- Densities and Porosities of LA-3 Core Samples and Surface Samples Aluto-Langano Geothermal Field, Ethiopia.

Sample No	Location or Depth (m)	Rock Type and Shape	Dry Density σD(g/cm³)	Wet Density σW(g/cm³)	Part. Density σp (g/cm³)	Porosity φ
19	1549.75-1551.6	Basalt highly altered subrounded to angular.	2.50	2.60	2.78	0.10
20	1650-1651	Basaltic ash: Mod. altered silicified, S. to A.	2.56	2.65	2.79	0.08
21	1778.8-1779.08	Ignimbrite: Sl.altered highly Porph. S. to A.	2.53	2.56	2.61	0.03
22	1921.92-1922.52	Rhyolite: Sl. altered, Sl. Porph. S. to A.	2.48	2.53	2.62	0.05
23	2000-2000.9	Ignimbrite: Sl. altered, Sl. Porph. S. to A.	2.52	2.55	2.61	0.04
24	2117.9-2120.6	Ignimbrite: altered vitric rounded	2.35	2.42	2.54	0.08
E6	N7°33'E38°41'	Weakly welded tuff: lenticular, vit, crystal S. to A.	1.60	1.92	2.35	0.32
E12	*FSSELL	Ignimbrite: Cryst., flow bonded, S. to A.	2.29	2.37	2.49	0.08
E13	"	Ignimbrite highly porph. cryst., S. to A.	2.29	2.41	2.60	0.12

*FSSELL = from Scarp South-East of Lake Langano.

S. to A. = subrounded to angular, Sl.= slightl

DEPTH (m)	ROCK TYPE	$\bar{\sigma}D$	σp	$\bar{\sigma}w$	σw(S.D.)	$\bar{\phi}$	ϕ(S.D.)
47-201	Aluto peralkaline rhyolite lava..	2.42	2.60	2.49	0.09	0.07	0.02
201-604	Aluto and other silicic breccias and weakly welded tuffs.	1.68	2.43	1.98	0.10	0.31	0.03
604-1651	Bofa basalts	2.52	2.81	2.62	0.11	0.10	0.05
1651-2120.6	Tertiary ignimbrites and rhyolites	2.41	2.58	2.47	0.08	0.07	0.03

- Mean Densities and Porosities, with their Standard Deviation

S.D. = Standard Deviation

DENSITY AND POROSITY OF SOME SURFACE ROCK SAMPLES IN THE SOUTHERN LAKES DISTRICT, RIFT, (ETHIOPIA)

SAMPLE NO	ROCK TYPE	AREA/GRID COORDINATE	WET DENSITY ( ) (10^3Kg/m^3	DRY DENSITY ( ) (10^3Kg/m^3	PARTICLE DENSITY ( ) (10^3Kg/m^3	POPOSITY ϕ
1	Biotite-granite basement, equigranular holo crystalline	Kella (443250E,913115N)	2.60	2.59	2.62	1
2	Biotite-granite equigranular and holo crystalline	Kella (443250E,913115N)	2.59	2.56	2.59	1
3	Quartzite basement (equigranular)	(443050E,913350N	2.41	2.29	2.60	12
4	Quartzite basement (equigranular)	(443050E,913450N)	2.54	2.51	2.59	3
5	Fossiliferous limestone overlying the basement (Jurassic (?))	(442600E, 913300N)	2.68	2.67	2.70	1
6	Dolerite dyke intrusion overlying the basement.	(442600E,913300N)	2.67	2.65	2.69	1
7	Dolerite dyke intrusion diabasic texture	(342275E,679900N)	2.89	2.87	2.93	2
8	Trap basalt (micro crystalline)	(342900E,679300N)	2.64	2.63	2.66	1
9	Trap basalt	(341900E,689850N)	2.92	2.91	2.94	1
10	Ignimbrite (Lithic-crystal tuff)	N-E LA_2 2km	2.09	1090	2.35	19

DENSITY AND POROSITY OF SOME SURFACE ROCK SAMPLES IN THE SOUTHERN LAKES DISTRICT, RIFT, (ETHIOPIA)

SAMPLE NO	ROCK TYPE	AREA/GRID COORDINATE	WET DENSITY ( ) ($10^3 Kg/m^3$)	DRY DENSITY ( ) ($10^3 Kg/m^3$)	PARTICLE DENSITY ( ) ($10^3 Kg/m^3$)	POPOSITY ϕ
11.	Ignimbrite Crystal tuff	Hunesa	2.39	2.27	2.58	12
12	Aluto pumiceous Ignimbrite (Lithic crystal tuff)	Aluto	1.7	1.32	2.13	38
13	Awaroftu Ignimbrite pumiceous lithic tuff (little welded)		1.95	1.7	2.27	25

- mass measurement was done using a Mettler balance with reading accuracy of $\pm$ 0.02g
- low pressure vessel (20mm Hg) was used for saturating the rocks with water; drying temperature of 70°c in an oven.

References

Alemu, A., 1983. Crustal Modelling from Gravity Data in the Ethiopian Rift. M.Sc. Thesis. Addis Ababa University.

Alemu, A., 1988. Gravity Field Interpretation Over the Main Ethiopian Rift. Proceedings of the 6th International Symposium "Geodesy and Physics of the Earth", Potsdam, Part II, pp. 99-115.

Alemu, A., Sjöberg, L.E., 1990. Gravity Field Interpretation and Crustal Model Studies in the Main Ethiopian Rift. Presented at the Third International Symposium on Recent Crustal Movements in Africa. 8-16 December 1990, Aswan, Egypt.

Andreev, B.A., 1958. Gravity anomalies and thickness of the earth's crust. Dokl. Akad. Nauk SSSR, 199 (2).

Asfaw, L.M., 1990. Implication of shear deformation and earthquake distribution in the East African Rift between 4^0N and 6^0N. Journal of African Earth Sciences, 10: (4) 745-751.

Asfaw, L.M. and Kebede, F., 1981. An earthquake swarm from the northern part of the Wonji Fault Belt and the state of seismicity of the rest of the Ethiopian Rift. Proc. First Int. Symposium on recent crustal movements in Africa. In: A.M. Wassef (editor), 86-103.

Baker , B.H. and Wohlenberg, J.,1971. Structure and Evolution of the Kenya Rift Valley. Nature, 229: 538-542

Baker, B.H. and Mitchell, J.G.,1976. Volcanic stratigraphy and Geochronology and the Kedong-Olorgesaile Area & the Evolution of the South Kenya Rift Valley. J. Geol. Soc. London 132: 467-484.

Behle, A., Makris, J, Baier, B. and Delibassis, N., 1975: Salt thickness near Dallol (Ethiopia) from seismic reflection measurements and gravity data; in A. Pilger (editor), The Afar Symposium, Stuttgart, Vol. I, pp. 156-157.

Belayneh, M., 1983. Petrology, chemistry and physical properties of core samples from well LA-3 Aluto-Langano geothermal field, Ethiopia. Geothermal Institute, University of Auckland, NZ.

Berckhemer, H., Bair B., Bartelsen, H., Behle, A., Burkhart, H., Gebrande, H., Makris, J., Menzel, H., Miller H. and Vees, R., 1975: Deep seismic soundings in the Afar region and the highlands of Ethiopia; in A.Pilger (editor), The Afar Symposium, Stuttgart, Vol. I pp. 66-79.

Beyth, M., 1986. 'Smooth' and 'rough' propagation of spreading in the southern Red Sea - Afar depression region: Geological survey of Israel, Jerusalem.

Birch, F., 1961. The velocity of compressional waves in rocks to 10 kilobars. Part II: Journal of Geophysical research; vol. 66; pp. 2199-2223

Bjerhammar, A., 1973. Theory of errors and generalized matrix inverses. Elsevier Scientific Publishing Company, Amsterdam

Bonjer, K.P., Fuchs, K. and Wohlenberg, J., 1970. Crustal structure of the East African Rift system from spectral response ratios of long period body waves. Z. Geophys., 36: 287-297.

Bram, K. and Schmelling, B.D., 1975: Structure of the crust and upper mantle beneath the Western rift of East Africa, derived from investigations of near earthquakes. In: A. Pilger (editor), The Afar Symposium, Stuttgart, vol. I, pp 138-143.

Brown, C. and Girdler, R. W., 1980. Interpretation of African Gravity and Its Implication for the Breakup of the continents. JGR, 85: B11, 6443-6455.

Castro, L. and Oddone, E., 1909. La citta e il clima di Addis Ababa. Boll.Soc. Sism. cItal. (Italy), Roma.

Courtillot, V., 1980. Opening of the Gulf of Aden and Afar by progressive tearing. Physics of the earth and planetary interior, vol. 21, pp. 343-350

Čolić, K., Vučetić, N. and Petrovvić, S., 1988. The geoid and the Moho discontinuity. 6th International Symposium " Geodesy and Physics of the Earth", Potsdam; Published in Akademie der Wissenshaften der DDR, Veröffentlichungen des Zentralinstituts fur Physik der Erde, No. 102 vol.II, pp 168-179.

Demenitskaya, R.M., and Belyaevesky, N.A., 1969. The relation between the earth's crust, surface relief and gravity field in the USSR.

Di Paola, G.M., 1972. The Ethiopian Rift Valley (between 7^0 and $8^0 40'$ lat. north). Bull. Volc. 36: 517-560.

Di Paola, G.M. and Berhe, S., 1979. The Kella horest: A hitherto unknown Precambrian crystalline basement in the Ethiopian Rift Valley (preprint).

Ewing, W.M. and Heezen ,B.C.,1956. Some Problems of Antarctic Submarine Geology, Monogr. AGU, 1: 75-81.

Fairhead, J. D. and Girdler, R. W., 1970. The seismicity of the Red Sea, Gulf of Aden and the Afar triangle. Phil. Trans. Roy. Soc. Lond., A.267: 49-74

Gass, I.G., 1970a. The evolution of volcanism in the southern area of the Red Sea, Gulf of Aden and Ethiopian rifts. Philos. Trans. R. Soc
. Lond. A. Maths. Phys. Sci. (England), A267, 369-381.

Gass, I.G., 1970b. Tectonic and magmatic evolution of the Afro-Arabian dome. In: Tarling, T.H., and Runcorn, S.K., (editors), African magmatism and tectonics. Edinburg, Oliver & Boyd Ltd. 285-300.

Gass, I.G., 1972. The role of lithothermal systems in magmatic and tectonic processes. Journal of earth sciences, Leeds, Vol.8, part 2, pp. 261 - 273.

Girdler, R.W.,1958. The Relationship of the Red Sea to the East African Rift System. Q. J. Geol. Soc. Lond., 114: 79-105.

Girdler, R.W., Fairhead, J.D., Searle, R.C. and Sowerbutts, W.T.C., 1969. The Evolution of Rifting in Africa, Nature, 224: 1178-1182.

Girdler, R.W. and Sowerbutts, W.T.C., 1970. Some Recent Geophysical Studies of the Rift System in East Africa, J. Geomagn. Geoelectr., 22: 153-163.

Griffiths, D. H., 1972: Some comments on the results of a seismic refraction experiment in the Kenya rift; Tectonophysics, vol. 15, pp 151-156.

Gouin, P., 1970. Seismic and gravity data from Afar in relation to surrounding areas. Philos. Trans. Roy. Soc. Lond. Ser. A, 267: 339-358.

Gouin, P., 1979. Earthquake history of Ethiopia and the Horn of Africa. International Development Research Centre Public. 118e, Ottawa, 258 pp.

Gouin, P. and Mohr, P.A., 1964. Gravity Traverses in Ethiopia (first interim report) Bull. Geophys. Obs. Addis Ababa, 7: 185-239.

Gutenberg, B., and Richter, C. F., 1941. Seismicity of the earth. Geol. Soc. of Amer. Bull. (USA), special paper No. 34, 121p.

Hammer, S., 1939. Terrain corrections for gravimeter surveys. Geophysics, Vol. 4, No. 3, p.184.

Hattori, S. 1974. Regional distribution of "b" values in the world. Bull. Intern. Inst. of Seismology and earthquake engineering (Tokyo), 12: 39-58.

Heiskanen, W.A. and Moritz, H., 1967. Physical Geodesy, Freeman, San Fransisco.

Henkel, H., Lee, M.K., Lund, C-E. and Rasmussen, T. 1990. An integrated geophysical interpretation of the 2000 km Fennolora section of the Baltic shield. Geological Survey of Sweden, Uppsala.

Herbert, L. and Langston, C. A.,1985. Crustal thickness estimates at AAE (Addis Ababa, Ethiopia) and NAI (Nairobi, Kenya) using P-Wave conversions. Tectonophysics, 111, 299-327.

Hubbert, M.K.,1948. A Line-Integral Method of computing the gravimetric effects of Two-Dimensional Masses. Geophysics 215-225.

Hunegnaw, A., 1989. Gravity and electrical resistivity sounding applied in geothermal exploration in the northern part of the Main Ethiopian Rift. Masters Thesis, University of Leicester, England.

Khan, M. A. and KRISP working group, 1987. Structure of the Kenyan Rift from seismic refraction (KRISP). Nature, 325: 239-242.

Karnik, V., 1969. Seismicity of the European area. Part 1. D. Reidl Publ. Co., Dordrecht, Holland.

Kazmin, V., 1972. Geological map of Ethiopia. Ethiopian Geological Survey Ministry of Mines, Addis Ababa Ethiopia.

Kazmin, V. and Berhe, S., 1978. Geology and Development of the Nazret area. Ethiopian Institute of Geological Survey.

Lepine , J.C., Ruegg, J.C. and Steinmetz, L., 1972. Seismic profiles in the Djibouti area. In: R.W. Girdler (Editor), East African Rifts. Tectonophysics, 15(1/2): 59-64.

Lloyd, E.F.,1977. Geological Factors Influencing Geothermal Exploration in the Langano Region, Ethiopia. Privately circulated report, 73pp.

Maasha, N. and Molnar, P., 1972. Earthquake fault parameters and tectonics in Africa. J. Geophys. Res., 77: 5731-5743.

Maguire, P.K.H. and Long, R.E., 1976. The Structure on the western flank of the Gregory rift. Part I. The crust Geophys. J.R. Astron. Soc., 44: 299-311.

Makris, J., 1978. Some geophysical considerations on the geodynamic situation in Greece. Tectonophysics 46: 251-268.

Makris, J., Menzel, H., Zimmermann, J., Bonjour, K.-P., Fuchs, K. and Wohlenberg, J., 1969. Crustal and Upper Mantle Structure of the Ethiopian Rift Derived from Seismic and Gravity Data. Z. Geophys. 36: 387-391.

Makris, J., Thiele, P. and Zemmermann, J., 1970. Crustal Investigation from Gravity Measurements at the Scarp of the Ethiopian Plateau. Z. Geophys., 36: 299-311.

Makris, J., Menzel, H., Zimmermann, J. and Gouin, P., 1975. Gravity Field and Crustal Structure of North Ethiopia. In: A. Pilger and A. Rösler (editors), Afar depression of Ethiopia. Stuttgart (Schweizerbart), 1: 135-144.

Makris, J. and Ginzburg, A., 1987. The Afar Depression: Transition between continental rifting and sea floor spreading. Tectonophysics, 141: 199 - 214.

McCall, G., J., H., 1968. The five caldera volcanoes of the central rift valley, Kenya; Proceedings of the Geological Society of London: No. 1647; pp 54-59.

McCall, G., J., H.; Baker, B., H.; Walsh, J., 1967. Late Tertiary and quaternary sediments of the Kenya rift valley. In: Bishop, W.,and Clark, J., D. (editors); Background to evolution in Africa; Chicago, University of Chicago Press; pp 191-220.

McConnel, R.B., 1967. The East African Rift System. Nature, 215: 578-581.

McKenzie, D.P., Davies, D., and Molnar, P., 1970. Plate tectonics of the Red Sea and East Africa. Nature, 226: 243-248.

Mohr, P.A., 1960. Report on Geological Excursion through Southern Ethiopia Bull. Geophys. Obs., Addis Ababa. 3: 9-20.

Mohr, P.A., 1962a. The Geology of Ethiopia. Univ. College Press, Ethiopia. 268P.

Mhor, P.A., 1962b. The Ethiopian Rift System. Bull. Geophys. Obs., Addis Ababa, 5: 33-62.

Mohr, P.A., 1966a. Chabbi Volcano (Ethiopia) Bull. Volcan. 29:797-816

Mohr, P.A., 1966b. Geological report on the Lake Langano and adjacent Plateau regions. Bull.Geophys. Obs., Addis Ababa, 9: 59-75.

Mohr, P.A., 1967. The Ethiopian Rift System. Bull. Geophys. Obs., Addis Ababa, 11: 1-65.

Mohr, P.A., 1971a. Tectonics of the Dobi graben region, Central Afar, Ethiopia. Bull. Geophys. Obs. Addis Ababa, 13: 73-89.

Mohr, P.A., 1971b. Outline tectonics of Ethiopia. UNESCO, Tectonics of Africa. p. 447-458.

Mohr, P:A.,1971c. The Ethiopian triple-rift junction in terms of plate tectonics. Bull. Geophys. Obs. (Ethiopia), 13: 1-18.

Mohr, P.A., 1972. Surface Structure and Plate Tectonics of Afar. Tectonophysics, 15 (1/2): 3-18.

Mohr, P.A., 1980. Geodynamic Evolution of the Afro-Arabian Rift-System. Accademia Nazionale Dei Lincel, TTI DEI Convengi Linccei 47. Roma.

Mohr, P.A, 1983. Ethiopian Flood Basalt Provience. Nature 303: 577-584.

Mohr, P.A and Wood, C.A., 1976. Volcano spacings and lithospheric attenuation in the Eastern Rift of Africa. Earth Planet. Sci. Lett. 33: 126-144.

Mohr, P.A., Mitchell, J.G. and Raynolds, R.G.H., 1980. Quaternary Volcanism and faulting at O'a Caldera, Central Ethiopian Rift. Bull. Volcanol., 43: 173.

Mohr, P.A. and Gouin, P., 1967. Gravity traverses in Ethiopia (third interim report). Bull. Geophys. Obs. Addis Ababa 10, 15-52.

Mooney, W.D., Gettings, M.E., Blank, H.R.and Healy, J.H., 1985. Soudi Arabian seismic refraction profile: A travel time interpretation of crustal and upper mantle structure. Tectonophysics, 111, 173-246.

Morelli, C., Gantar, C., Honkasalo, T., McConnell, R.K., Tanner, I.G., Szabo, B., Uotila, U. and Whalen C.T., 1971. The International Gravity Standardization Net 1971, IAG, 39 ter rue Gray Lussac, 75005, Paris.

Moritz, H., 1971. Geodetic Reference System 1967. Pub. No.3, Bulletin Geodesique, Paris.

Pick, M., Picha, J. and Vyskočil, V., 1973. Theory of the earth's gravity field. Academia Publishing House of the Czechoslovak Academy of Sciences, Prague

Oluma, B., 1989. The application of gravity and electrical resistivity serveys to geothermal exploration in the Main Ethiopian Rift. Masters Thesis, University of Leicester, England.

Nafe, I., E.; Drake, C. L., 1963. Physical properties of marine sediments; Hill (editor) The Sea; Interscience, 794-815.

Rapp, R. H., Palvis N. K., 1990. The development and analysis of geopotential coefficient models to spherical harmonic degree 360. Geophys. Res., 95, No. B13, pp 21,885-21911.

Rapp, R. H., Palvis, N. K., Wang, Y. M., 1991. High resolution gravity field models combining terrestrial and satellite data. XX General assembly of IUGG, Vienna, Austria.

Rasmussen, R. and Pederson L. B., 1979. End corrections in potential field modelling, Geophysical Prospecting 27, 749-760.

Rosendahl, B.R., 1987. Architecture of continental rifts with special reference to East Africa. Ann. Rev. Earth. Planet. Sci., 15: 445-503.

Rosendahl, B.R., Reynolds, P.M., Lorber, P.M., Burgess, C.F., McCill, J., Scott, D., Lambiase, J.J. and Derksen, S.J., 1986. Structural expressions of rifting: lessons from Lake Tanganyika, Africa. In Sedimentation in the African Rifts, Geological Society Special Publication No 25, 29-43.

Ruegg, J.C., 1975. Main results about the crustal and upper mantle structure in the Djibouti region (T.F.A.I). In: A. Pilger (Editor), The Afar Symposium, Stuttgart, Vol. I: 120-134.

Rykounov, L.N., Sedov, V.V., Savirna, L.A. and Bourmin, V.Ju., 1972. Study of microearthquakes in the rift zones of East Africa. In: R.W. Girdler (editor), East African Rifts. Tectonophysics, 15: 55-58.

Searle, R.C., 1970. Evidence of Gravity Anomalies for the Thinning of the Lithosphere Beneath the Rift Valley in Kenya. Geophys. Journal Roy. Astron. Society. 21: 13-31.

Searle, R.C and Gouin, P., 1972. A Gravity Survey of the Central Part of the Ethiopian Rift Valley. Tectonophysics. 15: 41-52.

Sjöberg, L. E., 1990. The best linear combinations of L1 and L2 frequency observables in the application of Transit/Doppler and GPS. Manuscripta geodaetica 15: 17-22.

Talwani, M., 1973. Computer usage in the computation of gravity anomalies, in computational physics, ed. by B. Alder, vol. 13, 343-389.

Talwani, M., Worzel, J.L. and Landisman, M., 1959. Rapid Gravity Computations for Two-Dimensional Bodies with an Application to the Mendocino Submarine Fracture zone. J. G.R., 64: 49-59.

Tazieff, H. and Varet, J., 1969. Signification tectonique et magmatique de L'Afar septentrional (Ethiopie). Rev. Geographie Phys. et Geologie Dynam., vol. 11, pp. 429-450.

Wolde, B., 1989. Cenozoic Volcanism and Rift development in Ethiopia. Department of Geology, Addis Ababa University, Ethiopia.

Wolf, H., 1971. Geoid und Mohorovičić-Diskontinuität. ZfV, Stuttgart, 96: 9,172-175,

Woolard, G.P., 1969a. Regional variations in gravity in the earth's crust and upper mantle. American Geophys. Union, Geophys. Monogr. 13: 320-341.

ROYAL INSTITUTE OF TECHNOLOGY
Department of Geodesy

KUNGL TEKNISKA HÖGSKOLAN
Geodetiska institutionen

RESEARCH REPORTS FROM THE DEPARTMENT OF GEODESY

FORSKNINGSRAPPORTER FRÅN GEODETISKA INSTITUTIONEN

TRITA GEOD

1001 Sjöberg, L.E.: Some Methods of Estimating Geoid Undulations by Least Squares Combination of Stokes' Formula and Geopotential Coefficients, November 1985

1002 Sjöberg, L.E.: A Comparison of Some Modification Methods to Stokes' Formula Using GEM 9 Potential Coefficients, November 1985

1003 Sjöberg, L.E. and Huaan Fan: Studies on the secular land uplift and long periodic variations of sea level around the coasts of Sweden, August 1986

1004 Sjöberg, L.E. and Huaan Fan: A comparison of the modified Stokes' formula and Hotine's formula in physical geodesy, November 1986

1005 Huaan Fan: A general model for the least squares adjustment and estimation, November 1986

1006 Galvenius, G.: Metoder och instrument för inmätning av underjordiska ledningar (Procedures and instruments for positioning of sub-surface pipes and cables) tillsammans med Svenska Kommunförbundet, November 1986

1007 Huaan Fan and L.E.Sjöberg: On the estimation of variance-covariance components with and without invariance in the Gauss-Helmert model, December 1986

1008 Torbjörn Cederholm: System för rationell hantering av lägesbunden information
Delrapport 1: Metoder för insamling av lägesdata - en översikt. Februari 1987
(Systems for efficient handling of spatially related data.
Part one: Data collection methods - an overview.)

1009 Petr Vanicek and L.E.Sjöberg: A note on vertical crustal movement determination techniques, February 1987

1010 Lars.E.Sjöberg and Huaan Fan: Experiences with the UNB land uplift modelling program using Swedish levelling and tide gauge data, March 1987

1011 Göran Galvenius: Metoder och instrument för inmätning av underjordiska ledningar. Teoretiska studier och fältförsök. 1988
(Procedures and instruments for measuring in positions of subsurface cables and pipes - Theoretical studies and field research.) 1988

1012 Torbjörn Cederholm: System för rationell hantering av läges bunden information
Delrapport 2: System för geodetisk datafångst. 1988
(Systems for efficient handling of spatially related data.
Part two: Field survey data collection system.) 1988

1013 Stig C Holmberg: Planning support facilities in geoinformatic systems; An environment for handling, visualizing and communicating Geo-information. September 1988

1014 Lars E Sjöberg, Huaan Fan and Erick Asenjo: Studies on the secular change of gravity in Fennoscandia, September 1988

1015 Huaan Fan and Lars E Sjöberg: First order terrain corrections to geopotential coefficients 00000 a numerical investigation, January 1989

1016 Göran Galvenius: Metoder och instrument för inmätning av underjordiska ledningar - Fortsatta studier, Januari 1989

1017 Erick Asenjo och Lars E Sjöberg: Tröghetspositionering - en överblick med tonvikt på utjämning av Ferranti-data, Inertial surveying a review with emphasis on the adjustment of Ferranti data, March 1989.

1018 Erik W Grafarend: The geoid and the gravimetric boundary value problem, August 1989.

1019 Huaan Fan: Geoid determination by global geopotential models and integral formulas (Doctoral Dissertation), August 1989.

1020 Egeltoft, Tomas: GPS-bestämning av stompunkter vid Husarviken
(Determination of control points at Husarviken with GPS), December 1989.

1021 Sjöberg, Lars E: Systematic tropospheric errors in geodetic positioning with the global positioning system, January 1989.

1022 Holmberg, Stig C: User's requirements in geoinformatic systems, February 1990

1023 Cederholm, Torbjörn, Larsén, J: GIS-terminologi. Terminologiprojektets insamlingsfas, Augusti 1990. GIS-terminology, collection phase.

1024 Sjöberg, Lars E: Contributions to the problem of modifying Stokes' formula, September 1990.

1025 Ming Pan: GPS orbit improvement, May 1991

1026 Alemu, Abera: The gravity field and crustal structur of the main Ethiopian rift, January 1992.